

1-2013

Preparation, Characterization and Catalytic Activity Study of Transition Metal Doped Porous γ -Alumina

Seham Nasser Al Hadrami

Follow this and additional works at: https://scholarworks.uaeu.ac.ae/all_theses

Part of the [Materials Science and Engineering Commons](#)

Recommended Citation

Al Hadrami, Seham Nasser, "Preparation, Characterization and Catalytic Activity Study of Transition Metal Doped Porous γ -Alumina" (2013). *Theses*. 693.

https://scholarworks.uaeu.ac.ae/all_theses/693

This Thesis is brought to you for free and open access by the Electronic Theses and Dissertations at Scholarworks@UAEU. It has been accepted for inclusion in Theses by an authorized administrator of Scholarworks@UAEU. For more information, please contact fadl.musa@uaeu.ac.ae.



United Arab Emirates University

Deanship of Graduate studies

M. Sc. Program in Material Science and Engineering

**PREPARATION, CHARACTERIZATION AND CATALYTIC
ACTIVITY STUDY OF TRANSITION METAL DOPED POROUS γ -
ALUMINA**

By

Seham Nasser Al Hadrami

Submitted to

United Arab Emirates University In partial fulfillment of the requirements
For the Degree of M. Sc. Material Science and Engineering

January 2013



United Arab Emirates University

Deanship of Graduate studies

M. Sc. Program in Material Science and Engineering

**Thesis Title: PREPARATION, CHARACTERIZATION AND
CATALYTIC ACTIVITY STUDY OF TRANSITION METAL DOPED
POROUS γ -ALUMINA**

Author Name: Seham Nasser Al Hadrami

Supervisors

Advisor :Dr. Abbas Khaleel Associate Professor Department of Chemistry Faculty of Science UAE University	Co-Advisor :Dr. Yaser E. Greish Associate Professor Department of Chemistry Faculty of Science UAE University
---	--

January 2013

Thesis of Seham Nasser Salem Nasser Al Hadrami

Title: **PREPARATION, CHARACTERIZATION AND CATALYTIC ACTIVITY
STUDY OF TRANSITION METAL DOPED POROUS γ -ALUMINA**

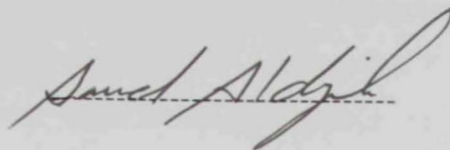
Submitted In Partial Fulfillment for the Degree of
Master of Material Science and Engineering

Chair of Examination Committee

Dr. Saud Aldajah

Mechanical Engineering Department

United Arab Emirates University



External Examiner

Dr. Ryan Richards

Associate Professor of Chemistry

Dept. of Chemistry and Geochemistry

Colorado School of Mines

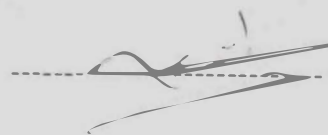
USA

Internal Examiner:

Dr. Nathir A. Al-Rawashdeh

Chemistry Department

United Arab Emirates University



Program Director (Material Science & Engineering)

Dr. Saud Aldajah

Mechanical Engineering Department

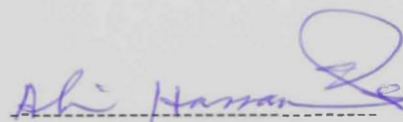
United Arab Emirates University



Associate Dean for Research & Graduate Studies

Dr. Ali Al-Marzouqi

United Arab Emirates University



January 2013

I-Acknowledgments

There can be no doubt that my advisor Dr. Abbas Khaleel was the key indicator of accomplishing my thesis successfully. Therefore, I would firmly appreciate his cooperation that will never be forgotten. Furthermore, I would highly thank my co-advisors Dr. Yaser Afifi for his kindness and patience in providing me with all support that I needed throughout the whole period of processing my thesis.

I cannot deny that my husband has also been very helpful by encouraging and intensifying me in order to reach a phenomenal success.

My family members and my kids did also play significant role in making me achieve this work done smoothly.

I must admit that I cannot forget all the help provided by the Department of Chemistry laboratory specialists and technicians (Mr. Bassam Hindawy and Dr. Mohamad Nawaz).

Lastly, special thanks to The Chemistry Department, College of Science and everyone contributed to make my thesis get done with substantial success.

II-Abstract

Transition-metal ions -doped γ -alumina composites with various dopant concentrations (Cr^{3+} , Fe^{3+} , Ce^{3+} , Zn^{2+} , Mn^{2+} , V^{2+} and Cu^{2+}) were prepared by straightforward template-free sol-gel method. They were characterized by XRD, FTIR, SEM, NMR and N_2 adsorption-desorption isotherm technique. The presence of dopant metal ions, generally, enhanced the gel formation and their behavior was dependent on the nature of the metal ion and its concentration. Certain ions, especially Fe^{3+} , resulted in rapid formation of a transparent gel upon hydrolysis. The presence of the acetylacetonate ions (acac) enhanced the condensation reactions in the sol-gel process and resulted in eventually unique textural properties of the calcined products including high surface areas, small particle size, homogeneous mesopores, and enhanced resistance to sintering especially at high dopant concentrations and elevated calcination temperatures.

The prepared doped γ -alumina powders were weakly crystalline at low dopant ion concentrations, 3%, and became completely amorphous at a concentration of 10%. The morphology of the particles was also dependent on the dopant concentration. While dopant concentration of 2% resulted in nano-particles with significant amount of inter-particle mesopores, 10% concentration led to significant aggregation into larger particles. The prepared doped γ -alumina as well as the undoped γ -alumina showed high surface areas ($377 \text{ m}^2/\text{g}$) and pore volumes (1.65 cc/g) which were largely dependent on the nature of the dopant metal ions and on their concentrations. While composites with low dopant concentration, 2 and 3%, exhibited surface areas and pore volumes comparable to those of undoped γ -alumina, a considerable decrease was associated with higher concentrations. The changes in textural properties were referred to the evident enhanced sintering associated with high dopant concentrations. Composites with low Cr^{3+} ion concentration, 0.75 and 2%, showed reversible thermochromism where their greenish yellow color changed to red upon calcinations at temperatures between 500 and 700 °C. Based on NMR results, occupation of tetrahedral sites by Cr^{3+} ions was preferred over octahedral sites at low Cr^{3+} concentrations. The composites showed unique textural properties comparable with those of high-surface-area porous γ -alumina, especially at low concentrations of Cr^{3+} .

The catalytic activity of the doped catalysts as well as that of undoped γ -alumina was studied over 1,2-dichloroethan (DCE) at 300°C using FTIR spectroscopy to monitor the reaction products. γ -alumina catalyst doped with Cu(II) and Cr(III) ions showed higher

conversion than undoped γ -alumina. The nature of the products was strongly dependent on the presence of dopant ions and on the type of dopant. While pure γ -alumina resulted, mainly, in the formation of C_2H_3Cl , Cu- and Cr-doped catalysts showed significantly stronger capability for deep oxidation of DCE to CO_2 on the account of C_2H_3Cl .

III-Table of Content

<u>Dedication</u>	1-2
<u>I-Acknowledgments</u>	4
<u>II-Abstract</u>	5-6
<u>III-Table of Content</u>	7
<u>IV List of Tables</u>	10
<u>V List of Figures</u>	11-15
<u>VI List of Abbreviations</u>	15
<u>VII. Chapter 1. Literature Review: Introduction about Alumina and modified alumina</u>	
1.1 Introduction	16
1.2 Physical and Chemical properties of Alumina	17
1.3 Common Classifications of Alumina	19
1.4 Characteristics of γ -Alumina	21
1.4.1 The textural properties of γ -Alumina	21
1.4.2 Surface active sites of γ -Alumina	22
1.4.3 Adsorption abilities of γ -Alumina	22-23
1.4.4 Thermal stability of γ -Alumina	25
1.5 Preparation of γ -Alumina	25-27
1.6 Factors that affect the textural, chemical and catalytic properties of γ -Alumina	29
1.6.1 Effect of Surfactant/ Template	29
1.6.2 Effect of Water Content	29
1.6.3 Effect of pH	30
1.6.4 Effect of solvent and acid catalyst	30
1.6.5 Effect of calcinations temperature	31
1.7 Modified γ -Alumina	32
1.7.1 γ -Alumina in mixed metal oxides	
1.7.2 Anions-doped γ -Alumina	33
1.7.3 Modified Alumina-based alkaline earth metals	35

1.8 Summary	36
<u>VIII. Chapter 2 . Highly porous transition-metal-modified γ-alumina: Effect of doping element and preparative conditions</u>	38
2.1 Introduction	38
2.2 The Experimental Procedure	41
2.2.1 Reagents and Materials	41
2.2.2 Preparative procedures	41
2.2.3 Characterization techniques	42
2.3. Results and Discussions	42
2.3.1 Formation of mixed oxides	42
2.3.2 Structure and Thermochromism of Al-Cr-x	46
2.3.3 FTIR spectroscopic characterization	49
2.3.4 Morphology characterization	51-54
2.3.5 The Effect of the Foreign Metal ions And the Precursor on the Gel Formation	55
2.3.6 Powder XRD of Al-Metal oxide systems	57
2.3.6.1 Composites with different metal ions	57
2.3.6.2 Effect of Metal ion Concentration on Crystallization	60
2.3.6.3 Effect of Metal ion Precursor on Crystallization	63
2.3.6.4 Thermal Stability of Metal doped γ -Alumina	66
2.3.7 Textural Properties by N_2 -adsorption	68
2.3.7.1 Textural properties of pure γ - Al_2O_3	68
2.3.7.2 Effect of Different Metal Dopants on the Textural Properties of γ -alumina	70
2.3.7.3 The Effect of Metal ion Concentration on Textural Properties of γ -Alumina	82
2.3.7.4 The Effect of the Metal ion precursor on the Textural properties of γ -Alumina	92
2.3.7.5 The Effect of Different Solvents on the Textural properties of doped γ -Alumina	99
2.3.7.6 The Effect of Acid catalysts on the Textural	102

properties of γ -Alumina	
2.3.7.7 Effect of Calcinations Temperature on the Textural properties of γ -Alumina	105
2.4 Conclusion	113
<u>IX. Chapter 3. Catalytic oxidation by transition-metal-doped γ-Al₂O₃: deep oxidation of 1,2-dichloroethane</u>	116
3.1 Introduction. γ -Alumina-based Material in Applications	116
3.1.1 Alumina in Medical Applications	116
3.1.2 Alumina in Separation and Chromatographic Applications	116
3.1.3 Alumina in Clean Energy Production	117
3.1.4 Alumina in Environmental Remediation	117
3.1.4.1 Alumina in Water Purification	117
3.1.4.2 Alumina in Air Purification	118
3.1.5 γ -Alumina-Supported Transition Metal Oxide for Oxidation of Chlorinated VOCs	120
3.1.6 γ -Alumina-Based Mixed Metal Oxides and Doped Alumina	121
3.1.7 Catalytic Oxidation of 1,2-Dichloroethane Over γ -Alumina	122
3.2 Objectives	122
3.3 Experimental Procedure	122
3.3.1 Materials and Catalysts Preparation	122
3.3.2 Catalytic Activity Study	122
3.4 Results and discussion	125
3.4.1 Qualitative Evaluation of The Catalytic Activity	125
3.4.2 Quantitative Evaluation of the Catalytic Activity	131
3.5 Conclusions	134
<u>X. References</u>	135-147
<u>XI. Title in Arabic</u>	148
<u>XII. Abstract in Arabic</u>	149
<u>XIII. Dedication in Arabic</u>	150

IV List of Tables

Table 1. Colors of the bulk mixed oxides vs. the colors of the corresponding single metal oxides. The color of pure γ -alumina is white.

Table 2. The ionic radii (pm) of the different metal ions in study, $r(M^{n+})$, in 6- and 4-coordination.

Table 3. BET surface area and pore characteristics of Al-M-2 after calcinations at 500 °C.

Table 4. BET surface area and pore characteristics of Al-M-3 after calcinations at 500 °C.

Table 5. BET surface area and pore characteristics of Al-M-5 after calcinations at 500 °C.

Table 6. BET surface area and pore characteristics of Al-M-10 after calcinations at 500 °C.

Table 7. BET surface area and pore characteristics of composites with different metal ions concentrations after calcinations at 500 °C.

Table 8. BET surface area and pore characteristics of Al-M-10 compositions after calcinations at 500 °C.

Table 9. BET surface area and pore characteristics Al-Fe-10 prepared from nitrate precursor in different solvents after calcinations at 500°C.

Table 10. BET surface area and pore characteristics of Al-Fe-10 prepared from nitrate precursor in the presence and in the absence of an acid catalyst.

Table 11. BET surface area and pore characteristics of Al-V-7.5 after calcinations at different temperatures.

Table 12. BET surface area and pore characteristics of Al-Cr-x after calcinations at different temperatures.

V List of Figures

Figure 1. The phase transition sequence of different types of alumina under thermal conditions

Figure 2. Surface of γ -alumina at high temperatures (a) and low temperatures (b).

Figure 3. 3D Atomic arrangement of a) four-five coordinated alumina b) six-coordination alumina.

Figure 4. Formation of Lewis acid and Lewis base sites on the surface of alumina after dehydration to OH groups

Figure 5. Adsorption ability of alumina compared to carbons and Ion exchange resins at low and high concentration.

Figure 6. Different functional groups on the surface of γ -alumina versus the adsorbed species adsorption over alumina.

Figure 7. General flow chart of sol-gel method to prepare porous alumina.

Figure 8. ^{27}Al -NMR spectrum of pure alumina compared with Al-Cr-0.75 and Al-Cr-5.

Figure 9. DRIFT spectra of different Al-Cr Oxide composites.

Figure 10. SEM micrographs of (a) Al-Cr-02 and (b) Al-Fe-02

Figure 11. SEM micrographs of (a) Al-Cr-05, (b) Al-Fe-05, and (c) Al-V-10

Figure 12. Powder XRD patterns of Al-M-10 of different metal ions versus $\gamma\text{-Al}_2\text{O}_3$.

Figure 13. Powder XRD patterns of Al-Cr-3, Al-Cr-10 versus $\gamma\text{-Al}_2\text{O}_3$.

Figure 14. Powder XRD patterns of Al-Ce-03, Al-Ce-10 versus $\gamma\text{-Al}_2\text{O}_3$

Figure 15. Powder XRD patterns of Al-Mn-03, Al-Mn-10 versus $\gamma\text{-Al}_2\text{O}_3$.

Figure 16. Powder XRD patterns of Al-Cr-10 from $\text{Cr}(\text{NO}_3)_3 \cdot 9\text{H}_2\text{O}$ and $\text{Cr}(\text{acac})$ versus $\gamma\text{-Al}_2\text{O}_3$

Figure 17. XRD patterns of Al-V -7.5 and calcinated at different temperatures versus the XRD pattern of pure alumina.

Figure 18. BJH pore size distribution of pure γ -Alumina.

Figure 19. N₂ adsorption-desorption isotherms of pure γ -Alumina.

Figure 20. N₂ adsorption-desorption isotherms of composites containing 2% and 3% of various metal ions.

Figure 21. BJH pore size distribution of all composites containing 2% and 3% of various metal ions versus alumina.

Figure 22. N₂ adsorption-desorption isotherms of composites containing 5% of various metal ions.

Figure 23. BJH pore size distribution of all composites containing 5% of various metal ions versus alumina.

Figure 24. BJH pore size distribution of all composites containing 10% of various metal ions versus pure alumina.

Figure 25. N₂ adsorption-desorption isotherms of composites containing 10% of various metal ions versus pure alumina

Figure 26. N₂ adsorption-desorption isotherms of Al-Zn-2, Al-Zn-3 and Al-Zn-10 versus alumina.

Figure 27. BJH pore size distribution of Al-Zn-2, Al-Zn-3 and Al-Zn-10 versus alumina.

Figure 28. N₂ adsorption-desorption isotherms of Al-Ce-3, Al-Ce-5 and Al-Ce-10.

Figure 29. BJH pore size distribution of Al-Ce-3, Al-Ce-5 and Al-Ce-10 versus alumina.

Figure 30. N₂ adsorption-desorption isotherms of Al-Mn-3, Al-Mn-5 and Al-Mn-10.

Figure 31. BJH pore size distribution of Al-Mn-3, Al-Mn-5 and Al-Mn-10 versus alumina.

Figure 32. N₂ adsorption-desorption isotherms of Al-Cu-3, Al-Cu-5, Al-Cu-10 and Al-Cu-20

Figure 33. BJH pore size distribution of Al-Cu-3, Al-Cu-5, Al-Cu-10 and Al-Cu-20 versus alumina.

Figure 34. N₂ adsorption-desorption isotherms of Al-Cr-0.75, Al-Cr-3, Al-Cr-5 and Al-Cr-10

- Figure 35.** BJH pore size distribution of Al-Cr-0.75, Al-Cr-3, Al-Cr-5 and Al-Cr-10 versus alumina
- Figure 36.** N₂ adsorption-desorption isotherms of Al-Fe-2, Al-Fe-3, Al-Fe-5 and Al-Fe-10.
- Figure 37.** BJH pore size distribution of Al-Fe-2, Al-Fe-3, Al-Fe-5 and Al-Fe-10 versus alumina
- Figure 38.** N₂ adsorption-desorption isotherms of Al-V-3, Al-V-7.55 and Al-V-10
- Figure 39.** BJH pore size distribution of Al-V-3, Al-V-7.55 and Al-V-10 versus alumina.
- Figures 40.** N₂ adsorption-desorption isotherms of Al-Cr-10 prepared from Cr(NO₃)₃ and from Cr(acac)₃.
- Figures 41.** BJH pore size distribution of Al-Cr-10 Al-Cr-10 prepared from Cr(NO₃)₃ and from Cr(acac)₃.
- Figures 42.** BJH pore size distribution of Al-Zn-10 prepared from ZnCl₂ and from Zn(acetate)₂
- Figures 43.** N₂ adsorption-desorption isotherms of Al-Zn-10 prepared from ZnCl₂ and from Zn(acetate)₂
- Figures 44.** BJH pore size distribution of Al-Cu-10 prepared from CuCl₂ and from Cu(acac)₂.
- Figures 45.** N₂ adsorption-desorption isotherms of Al-Cu-10 prepared from CuCl₂ and from Cu(acac)₂.
- Figures 46.** N₂ adsorption-desorption isotherms of Al-Fe-10 prepared from Fe(NO₃)₃ and from Fe(acac)₃.
- Figures 47.** BJH pore size distribution of Al-Fe-10 prepared from Fe(NO₃)₃ and from Fe(acac)₃.
- Figure 48.** The N₂ adsorption-desorption isotherm of Al-Fe-10 prepared in different solvents
- Figure 49.** BJH pore size distribution of Al-Fe-10 prepared in different solvents

Figure 50. The N₂ adsorption-desorption isotherm of Al-Fe-10 prepared in the presence and in the absence of an acid.

Figure 51 . BJH pore size distribution of Al-Fe-10 prepared in presence and in the absence of an acid.

Figure 52 . BJH pore size distribution of Al-V-7.5 at different calcinations temperatures.

Figure 53. The N₂ adsorption-desorption isotherm of Al-V-7.5 at different calcination temperatures

Figure 54. The N₂ adsorption-desorption isotherm of Al-Cr -0.75 prepared from Cr (acac)₃ and calcinated at different temperatures.

Figure 55. The N₂ adsorption-desorption isotherm of Al-Cr-5 prepared from Cr (acac)₃ and calcinated at different temperatures

Figure 56. BJH pore size distribution of Al-Cr -0.75 prepared from Cr (acac)₃ and calcinated at different temperatures.

Figure 57. BJH pore size distribution of Al-Cr -5 prepared from Cr (acac)₃ and calcinated at different temperatures.

Figure 58. Chemical structure for most common VOCs .

Figure 59. a) A photograph of the Experiment setup b) Schematic diagram of Experiment setup

Figure 60. FTIR spectra of the products of DCE oxidation over Al-Cr-3% at 300°C at different reaction times.

Figure 61. FTIR spectra of the products of DCE oxidation over Al-Cr-3, Al-V-3 and Al-Cu-3 at 300°C after 1hr of reaction.

Figure 62. FTIR spectra of the products of DCE oxidation over Al-Cr-3, Al-V-3 and Al-Cu-3 at 300°C after 2hr of reaction.

Figure 63. FTIR spectra of the products of DCE oxidation over Al-Cr-3, Al-V-3 and Al-Cu-3 at 300°C after 3hr of reaction.

Figure 64. FTIR spectra of the products of DCE oxidation over Al-Cr-3, Al-V-3 and Al-Cu-3 at 300°C after 4hr of reaction.

Figure 65. FTIR spectra of the products of DCE oxidation over Al-Cr-3, Al-V-3 and Al-Cu-3 at 300°C after 5hr of reaction.

Figure 66. % Conversion of DCE over undoped and doped γ -alumina containing 3% dopants at 300°C .

Figure 67. CO₂ an VC profiles after 5 h on stream at 300 °C over doped γ -alumina containing 3% dopants compared with undoped γ -alumina. The peak areas of both products were normalized using the area of the same peaks in the γ -alumina spectrum as a reference

VI: List of Abbreviations

Abbreviation	Full Name
BJH	Barett-Joyner-Halenda
BET	Brunauer-Emmett-Teller
XRD	Powder X-ray Diffraction
DRIFTS	Diffuse Reflectance Infrared Fourier Transform Spectroscopy
SEM	Scanning Electron Microscope
NMR	Nuclear Magnetic Resonance
FTIR	Fourier Transform Infra-Red Spectroscopy
1,2-DCE	1,2-Dichloroethane
VC	Vinyl Chloride
CO ₂	Carbon Dioxide
ASB	Aluminim tri-sec-butoxide
acac	Acetylacetonate ions
CVOCs	Chlorinated Volatile Organic Compounds
COCs	Chlorinated Organic Compounds

VII. Chapter 1. Literature Review: Introduction about Alumina and modified Alumina

1.1 Introduction

Aluminum (Al) is the most third abundant element, after oxygen and silicon presents in the earth crust and is richly found in rocks such as feldspars and micas. Due to its low density and high resistivity to corrosion, aluminum metal is extensively used in diverse industrial applications ranging from aerospace industry, transportation and structural materials.

The oxide of aluminum is called Aluminum oxide or Alumina (Al_2O_3) and it had been known and used by human beings for many centuries. Many evidences have shown that Babylonians and Egyptians had used the native alumina in medicine and in dyes as early as 2000 B.C. Around 5300 B.C archeologists in northern Iraq found that pottery was first made from clays containing aluminum silicate. In 1875, the French chemist Le Chatelier was the first one who prepared pure alumina by thermal decomposition of aluminum salts and by sintering bauxite with soda. The worldwide alumina chemicals industry had started by Charles Martin Hall in the United States and Paul Heroult in France in 1886, and the current annually world production capacity of alumina is almost 40 million tones. Due to its unique chemical and physical properties, wide variety of alumina products are being commercialized today. For example, alumina is used as an insulating material in many applications because it has low electrical conductivity and high thermal coefficient value. In addition, alumina is used as a catalytic material because of its high surface area, mechanical strength and thermal stability. There are other common products that contain alumina in different forms such as: toothpaste, plastics, paper, paint, industrial ceramics, electronic substrates, refractories, catalysts, abrasives, polishing compounds, selective adsorbents and many others [1].

In this chapter, we will discuss the main physical and chemical properties of alumina, its main classifications, some important characteristics of γ -alumina, different preparation methods of γ -alumina, the factors that affect the textural, chemical and catalytic properties of γ -alumina, some important applications of γ -alumina and later we will introduce the importance of modified alumina and alumina mixed oxide.

1.2 Physical and Chemical properties of Alumina

Alumina is a white crystalline powder which has melting point at 2040°C and boiling point at 2977°C, thus it is stable at elevated temperatures. Its specific gravity is 3.7 - 4.0 g/cm³, it has low solubility in water, however, it adsorbs water vapor very fast. Alumina composes from Oxygen ions (O²⁻) bonded to Al cations (Al³⁺) and they have various atomic arrangements in lattice structure which produce seven different crystallographic phases which are: (δ, γ, α, η, κ, θ and χ) based on the pressure and the temperature. Naturally occurring alumina minerals exist as: gibbsite (Al(OH)₃)

The phase transition of each alumina phase under thermal processing of gibbsite, bayerite, boehmite and diasporite is illustrated in (Figure 1); noting that transformation between these phases depends on precursor and thermal treatment. At room temperature, alumina adsorbs water H₂O on its surface via Al³⁺ cations and Oxygen ions O²⁻, forming hydroxyl (OH⁻) groups [2,3]. The most important and common alumina phases are: α-Al₂O₃ and γ-Al₂O₃. The α-Al₂O₃ prepared by heating aluminum hydroxides is a finely divided powder constituted by micrometer sized particles. Moreover, α-Al₂O₃ has many uses in traditional and advanced ceramics. γ-alumina is a very special material and is widely used in the industry as catalysts and adsorbents. In terms of their crystal structure, alpha phase has hexagonal close-packed structures in which aluminum ions fill two-thirds of the octahedral sites, while gamma phase occurs in a cubic spinel structure but converts readily to the alpha phase at high temperatures [4].

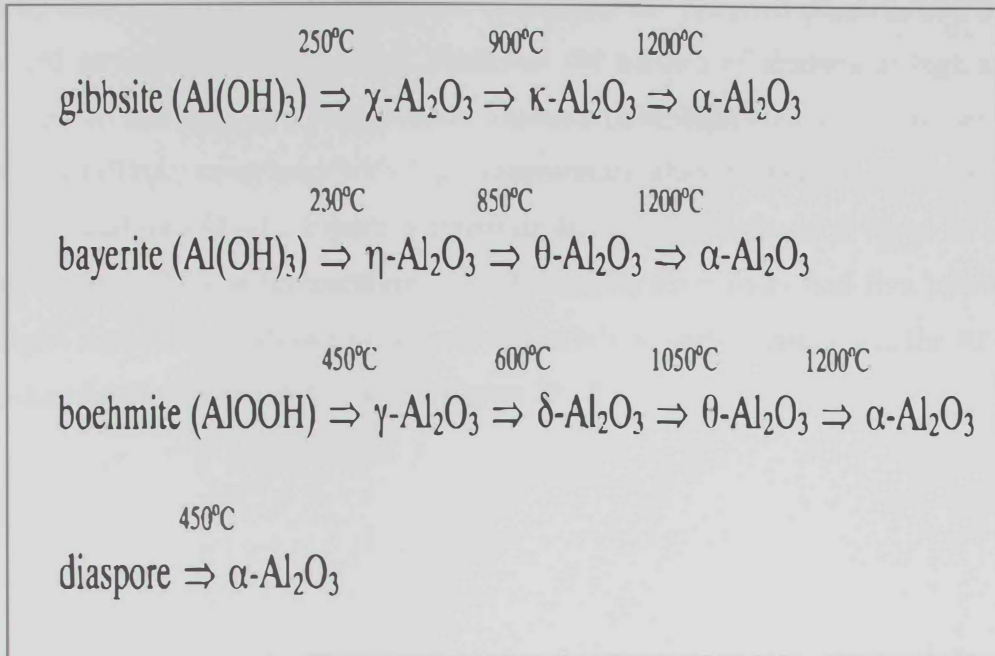
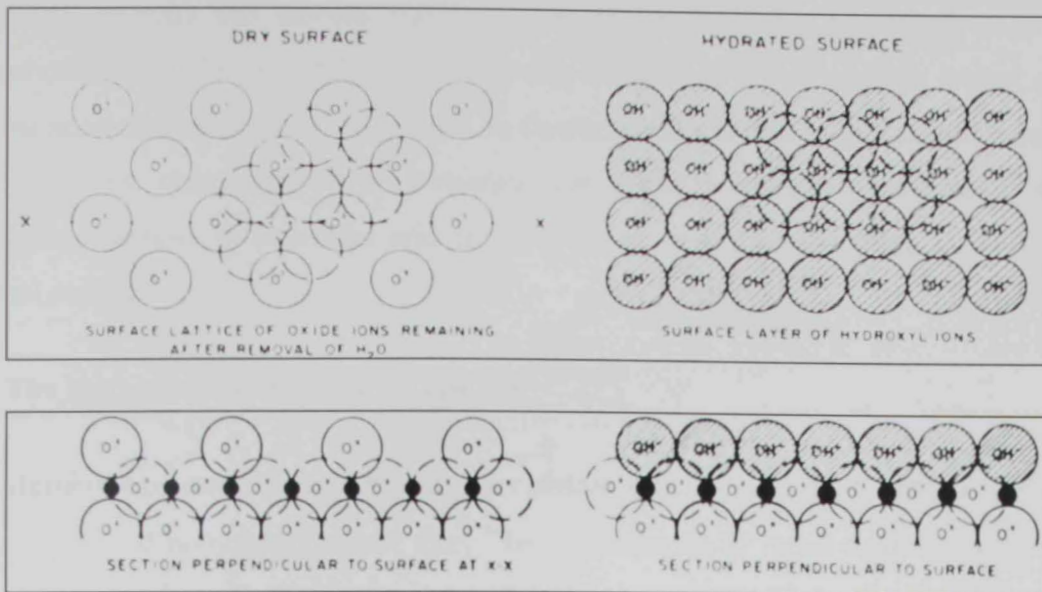


Figure 1. The phase transition sequence of different types of alumina under thermal conditions [3].

1.3 Common Classifications of Alumina

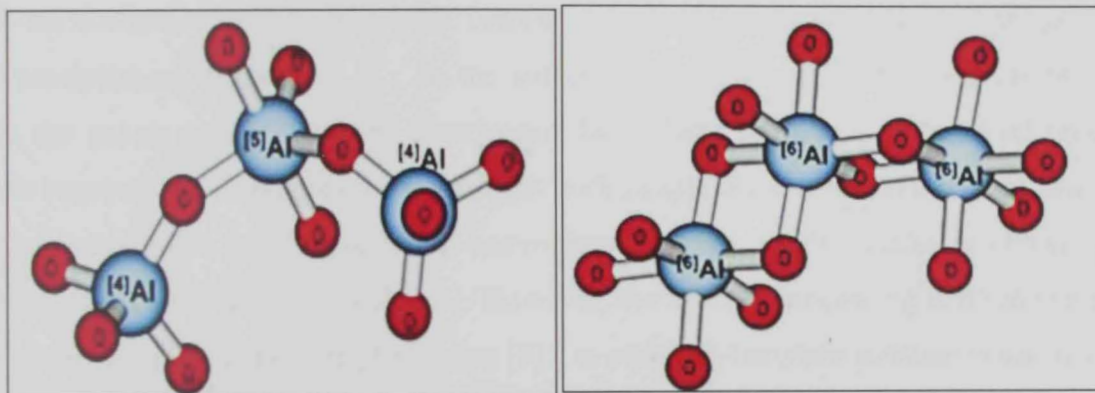
Alumina can be classified either as A) hydrous and non-hydrous alumina or as B) high and low temperature alumina based on its thermal stability. At high temperature ($> 1000^{\circ}\text{C}$), alumina is nearly anhydrous, and they are characterized by hexagonal close-packed oxygen lattices. Whereas, at low temperature alumina are partially hydrated and are obtained by dehydration at temperatures not below 600°C . They are characterized by cubic close-packed oxygen lattices. Figure 2 illustrates the surface of alumina at high and low temperatures. In addition, low temperature alumina have high catalytic activities due to their low crystallinity compared with high temperature alumina phases which have high degree of crystallinity [2-4]. Figure 3 illustrate the Al-O coordination types at low and high temperatures. At low temperature, the Al cations form four- and five coordination with Oxygen ions (O^{2-}) as shown in (Figure 3a), while at high temperature; the Al cations form six-coordination with oxygen ions, Figure 3b [5].



(a)

(b)

Figure 2. Surface of γ -alumina at high temperatures (a) and low temperatures (b).



(a)

(b)

Figure 3. 3D Atomic arrangement of a) four-five coordinated alumina b) six-coordination alumina

1.4 Characteristics of γ -Alumina

γ -Alumina exhibits high surface area and porosity, strong surface acidity, good mechanical strength and thermal stability. Therefore it is widely employed in different applications especially in catalysis. Due to the importance of alumina in nature and its growing applications, the need to modify its characteristics is one of great importance. The most important characteristics of γ -alumina that effect is overall performance are: 1) Textural properties, 2) Structure and surface active sites 3) Adsorption ability and 4) Thermal stability.

1.4.1 The textural properties of γ -Alumina

γ -Alumina possesses unique textural properties that include; high surface area, high pore volume and homogenous pore size. The performance of metal oxides as catalysts or catalyst supports largely depends on its morphology and textural properties. Mesoporous materials are particularly important as they offer the advantage of avoiding the pore plugging that often occurs in microporous solids. Therefore, the preparation of porous alumina with defined and controllable porous structure has been of great importance. The textural properties of γ -alumina are largely dependent on the employed preparative method and conditions [3]. Several synthetic strategies have been developed to obtain porous high-surface-area alumina. The most common synthetic routes are based on sol-gel [4,6] and precipitation methods [7,8]. In the sol-gel process, the method of solvent removal from the gel is very critical and determines the textural properties of the final product. While supercritical drying results in aerogels with unique textural properties including high surface areas and total pore volumes, conventional drying usually results in xerogel with lower surface areas and pore volumes. However, the xerogel processing is often preferred due to the low cost and easier processing [9]. In addition, template substances and organic additives have been widely used in the sol-gel synthesis to obtain stable mesoporous alumina [6,8,9]. On the other hand, alumina prepared by precipitation in aqueous solutions usually exhibits lower surface areas and pore volumes as compared with the sol-gel-prepared counterparts [10,11]. For example, in one study [12], the surface area of γ -alumina prepared by precipitation method was 170.8 m²/g. Whereas in another study [13] high surface area ~ 358 m²/g were achieved for alumina prepared through sol-gel method.

1.4.2 Surface active sites of γ -Alumina

In applications that include catalytic reactions, surface acid-base sites play key roles. These sites include O^{2-} , Al^{3+} and OH^- . Active alumina can be considered as possessing both Lewis and Bronsted acidic and basic sites which are considered to be the main source of catalytic activity of alumina [2]. Hydroxyl groups on alumina surface act as Bronsted acid sites. However, the removal of H_2O (from OH groups) from the surface of alumina by heating is an important step for the establishment of alumina catalytic activity [2,3]. Removal of H_2O (OH groups) creates unsaturated anions (O^{2-}) and cations (Al^{3+}) [3]. The dehydration of two neighboring OH^- ions from the surface of alumina lead to formation of strained oxygen bridge that behaves as Lewis base while exposed Al^{3+} behaves as Lewis acid sites as shown in Figure 4. These sites significantly determine the catalytic activity of alumina [2,3,14-16]. Adsorption or chemisorptions of materials over alumina surface are results from an interaction of the adsorbed substance with Al^{3+} cations as electron acceptor (Lewis acid) and/or OH^- anions as electron donor, Lewis base [2].

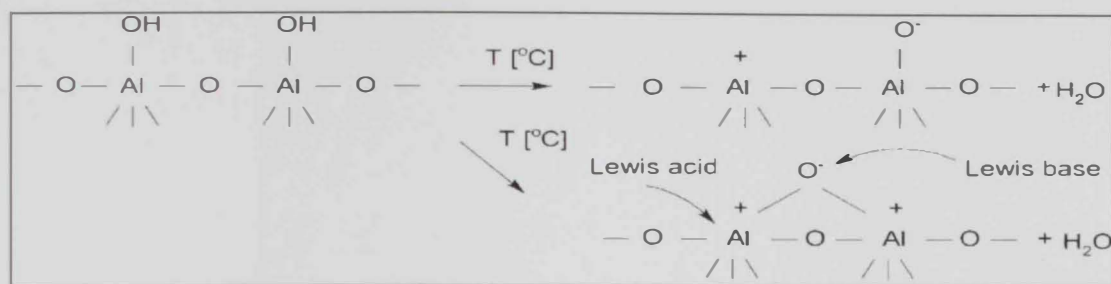


Figure 4. Formation of Lewis acid and Lewis base sites on the surface of alumina after dehydration to OH groups

1.4.3 Adsorption abilities of γ -Alumina

For many years, Activated carbons from different origins have been the major part of adsorbents that are widely applied for adsorption of toxic materials. For example, activated carbon was previously used for removal of lead (II) from wastewater. Nowadays, alumina is commonly used for adsorption and separation of trace amounts of harmful elements due to its unique textural properties and the presence of distinctive active sites. There are two steps involved in the adsorption process on alumina. The first step is diffusion of particles from bulk solution to the surface of alumina. The second step involves the formation of bonds between adsorbate and alumina surface sites [2]. The two

reasons which made the alumina to be very distinctive over other materials such as carbon and ion-exchange resins are; first, it is particularly good at removing very small quantities of substances from a bulk stream. However, other materials become competitive at higher concentrations as shown in Figure 5 [1]. The second reason is that alumina selectively removes different species present in water stream [1]. Figure 6 illustrates general outline of species as they are defined by

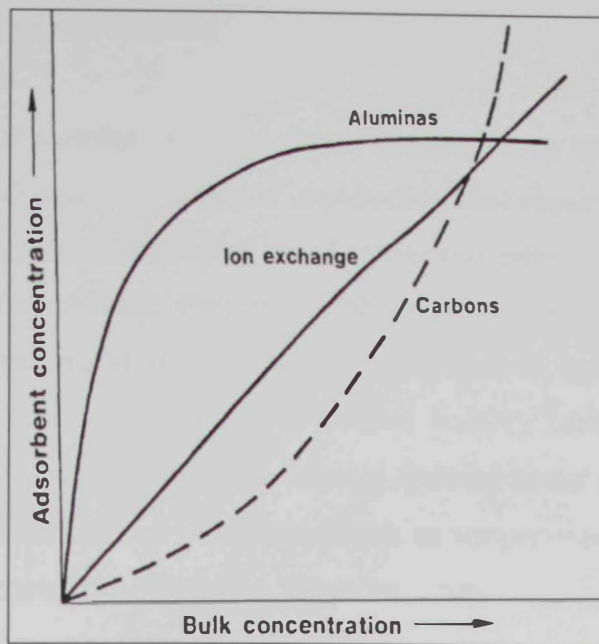


Figure 5. Adsorption ability of alumina compared to carbons and Ion exchange resins at low and high concentration [1]

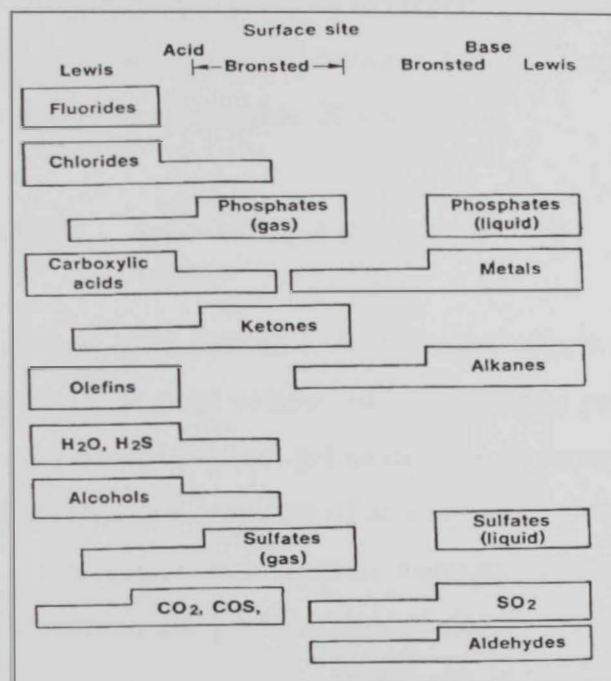


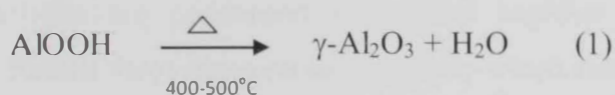
Figure 6. Different functional groups on the surface of γ -alumina versus the adsorbed species adsorption over alumina [1]

1.4.4 Thermal stability of γ -Alumina

Thermal stability of alumina is an important characteristics which make it the most useable material in industrial and catalytic applications that require high temperatures in some reactions such as catalytic conversation of automotive emission and high temperature catalytic fuel conversions. These conditions require more stable catalysts in terms of resistance to transformation and to structural damages. Even though, noble metal catalysts show high catalytic activity, they have low thermal stability besides their high cost. γ -Alumina, in contrast, is significantly more suitable material under severe conditions [17]. However, phase transformation of γ -alumina occurs as temperature increases, which also affect its surface structure [18]. Therefore, there are many ongoing studies on modifying alumina in order to enhance its thermal stability as well as its surface chemical activity.

1.5 Preparation of γ -Alumina

There are different well established methods to prepare γ -alumina. The old conventional method involved heating boehmite (AlOOH) between 400-500° (reaction 1), which usually produces γ -alumina with surface areas below 200 m^2/g [19].



However, sol-gel method is considered to be the most effective technique to prepare alumina with high surface area, pore volume and homogenous pore size distribution. In addition, Some other advantages of the sol-gel method are its versatility and the possibility to obtain high purity materials, the provision of an easy way for the introduction of trace elements, allowance of the synthesis of special materials. In addition, it offers better control over synthesis conditions and purity of the sample.

The majority of the reported work based on xerogel processing, including studies that employed template molecules, resulted in surface areas below 300 m^2/g and pore volumes in the range of 0.2-0.8 cc/g [20-22]. In a recent study, it was found that γ -alumina can be prepared in significantly higher surface areas and pore volumes via straightforward sol-gel synthesis from aluminum alkoxides under non-acidic and template-free conditions [22].

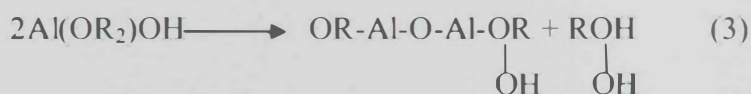
The sol-gel method is based on the phase transformation of a sol obtained from metallic alkoxides or organometallic precursors. This sol which is a solution containing particles in suspension is polymerized at low temperature, in order to form a wet gel. The solvent is removed by drying the gel and the next step is a proper heat treatment. Sols are dispersion of alumina colloidal particles in a solvent. A gel formation is a process that involves forming a rigid of network pores of submicrometer dimensions and polymeric chains whose average length is greater than micrometer [23-25].

Sol-gel preparation of Alumina involves five general steps:

- 1- Dissolving an alkoxide such as Aluminum Isopropoxide (AIP) or Aluminum Secondary Butoxid (ASP) in a suitable solvent at defined pH to prevent precipitations followed by Hydrolysis of the alkoxide precursor to form pseudoboehmite according the following reaction (2) :



- 2- Gelation of the solution of colloidal particles where the alumina intermediate colloidal particles are condensed and linked together through polymerization reactions to form a three-dimensional network, which results in an increase in the viscosity, reaction (3):



- 3- Aging which involves maintaing the gel for a period of time from hours to days while polymerization or gelation process continues along .
- 4- Drying, which involves removing the solvent from the interconnected pore network by conventional evaporation or supercritical drying that a voids the solid-liquid interfaces.
- 5- Dehydration and densification or calcinations is the last treatment process of gel and it occurs by heating the porous gel at high temperatures to remove any excess liquids and to stabilize the alumina. During this process the surface area , a phase

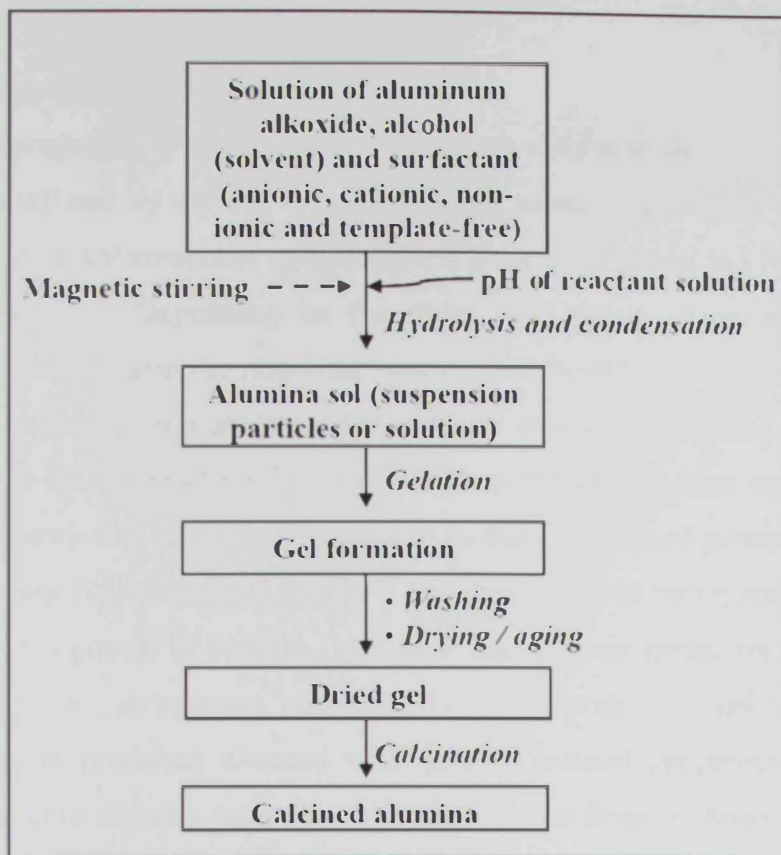


Figure 7. General flow chart of sol-gel method to prepare porous alumina.

1.6 Factors that affect the textural, chemical and catalytic properties of γ -Alumina

The final textural properties of calcined γ -alumina depend strongly on various preparative conditions and parameters including, the presence of a surfactant, water/Al ratio, pH, solvent, and calcinations temperature [25, 30-33].

1.6.1 Effect of Surfactant/ Template

The textural properties of mesoporous alumina are similar to the mesoporous silicates, and they can be tailored by varying the type and size of surfactant agent employed during the synthesis. Surfactant composes of hydrophilic polar head group and hydrophobic non-polar hydrocarbon tail. Depending on the polar head group of surfactants, they are classified into anionic, cationic, non-ionic and non-surfactants. However, the interaction between surfactant and aluminum precursor is not as strong as silica and exhibit unstable porosity. This is a major drawback for alumina. Thus, researchers have exerted significant efforts on the selection of surfactants employed in the synthesis of porous alumina as the pore directing agent [25]. Jagadis C.Ray [34] prepared series of mesoporous alumina from ASB using selected groups of anionic, non-ionic and cationic surfactants and they found that anionic surfactant in aqueous solution produced thermally unstable alumina while cationic surfactants produced alumina with greater textural properties. Qian liu [35] obtained mesoporous alumina with mesoporous structure from boehmite sols using non-ionic surfactants as structure directing agent.

1.6.2 Effect of Water Content

Water plays an important role in the hydrolysis reaction of aluminum precursor. To obtain porous alumina [36]. Low water content tends to slow down the hydrolysis rate of aluminum source, however fast hydrolysis rate in high water concentration results in uncontrolled phase separation of surfactant and aluminum precursor. Kim et al. [37] used water as initiating solvent for the hydrolysis of aluminum alkoxide during the terminal reaction step. Water was slowly added into stearic acid and aluminum tri-sec-butoxide which dissolved into sec-butanol mixture, to form white colloidal sols. They found that adding excess water into the solution did not improve the formation of mesoporous

alumina, but it likely decreased the pore uniformity and produced incomplete condensed alumina structure. These results were in agreement with other's work [38].

1.6.3 Effect of pH

The hydrolysis and condensation process in the synthesis of alumina is strongly dependent on the pH of reaction medium. At pH values around the isoelectric point (IEP) of alumina (pH = 7–8), the predominant alumina species in the solution is Al(OH)_4^- . At pH < IEP, $\text{Al(H}_2\text{O)}_6^+$ cations are mainly presents. pH > IEP, deprotonation of water occurs, forming $[\text{Al(OH)(H}_2\text{O)}_5]^{2+}$ ions that can produce dimeric or polymeric intermediates. Alumina exhibits a high affinity for anionic species such as I^- , ClO^- , Br^- , Cl^- , IO_3^- , F^- . With further increase of the solution pH, more deprotonation of water takes place and AlO_2^- species form. Alumina displays a high affinity for wide range of cations such as Mg^{+2} , Ca^{+2} , Sr^{+2} , Ba^{+2} , Cu^{+2} , Pb^{+2} , Ni^{+2} , Cd^{+2} . At pH values in the range (4–8), precipitation of Al hydroxide takes place, often as a poorly ordered solid phase, that is transformed by ageing into crystalline aluminum hydroxide (Al(OH)_3) or oxide hydroxide (AlOOH), depending on the pH and temperature [25,39]. The pH also influences the charge of the inorganic precursor species and surfactant head groups which affect their mutual interaction [40].

Valange et al. [40] reported that ordered mesostructure of alumina with high surface areas (670-810 m^2/g) were obtained in the pH 6-7 of synthesis medium. However, it was also reported that the synthesis of mesoporous alumina is better to be carried out at pH close to 7 due to low curvature of rippled alumina sheets which will lead to form microporous sturcture at pH <7. The interactions between surfactant molecule and alumina sheets would be weakened by increasing the pH value since the positive charge on the alumina sheets is decreased and a charge balance matching cannot be provided [25]. In a recent study, it was found that γ -alumina can be prepared in significantly highe surface areas and pore volumes via straightforward sol-gel synthesis from aluminum alkoxides under non-acidic and template-free conditions [22].

1.6.4 Effect of solvent and acid catalyst

The textural properties of alumina were found to depend on the solvent and the presence or absence of the acid catalyst. In one recent study [22], aluminum isopropoxide was dissolved in different alcoholic solvents (1-butanol, 2-propanol, 2-butanol, tert-butanol and toluene) and it was found that alumina obtained in 1- butanol exhibited the highest

surface areas, $\sim 500 \text{ m}^2/\text{g}$, and very narrow distribution of the observed mesopores, between 4 and 10 nm. Hydrolysis reaction of aluminum isopropoxide dissolved in alcoholic solvent was also carried out under acidic and non-acidic conditions. It was found that the textural properties of alumina prepared from aluminum isopropoxide in alcoholic solvents in the absence of an acid catalyst were higher than the ones prepared under acidic conditions. The effect of the acid catalyst was referred to its role in enhancing the precursor solubility besides its role in increasing the rate of hydrolysis on the account of the rate of condensation. Rajan Bosco [26] carried out a study on physical and textural properties of alumina that were prepared under different basic conditions, ammonia/alkoxide mole ratio. It was found that decreasing (ammonia/alkoxide) mole ratio to solvent mole ratio ($\text{H}_2\text{O}/\text{Isopropylalcohol}$) resulted mesoporous alumina with lower surface area. While, increasing ($\text{H}_2\text{O}/\text{Isopropylalcohol}$) mole ratio to (ammonia/alkoxide mole ratio) resulted in microporous and mesoporous alumina with higher surface area.

1.6.5 Effect of calcinations temperature

Once the mesostructure of material is synthesized, the surfactant and water should be removed in order to generate the desired pore structure. Hence, Dehydration or calcination process is an important step in removing water and surfactant to obtain γ -alumina, in order to generate a good catalyst support and to improve the thermal stability of alumina which can stand for high temperature reactions [18]. Generally, the elimination of water and removal of surfactant, as well as alumina phase change upon calcination generate significant amount of pores and internal surface area with increasing of the calcination temperature. The aluminum atoms inside the structure would be rearranged and resulting miscellaneous pore coalescence to create thick pores wall and broad pore diameter [41]. This elimination process of surfactant and the release of water content from alumina gel should be controlled properly or otherwise, the mesostructure of the alumina will be disordered. Micropores were observed in alumina calcined below 400°C and high surface areas ($\sim 600\text{m}^2/\text{g}$) were obtained [9, 42].

The phase transformation from pseudoboehmite to pure γ -alumina was found to be only complete when the calcination temperature increased up to 550°C . The micropores disappear as the temperature increased. Micropores in the alumina framework collapse owing to crystallization of γ -alumina phase as the calcination temperature increases [43]. In general, increasing of calcination temperature from 400 to 1100°C results in alumina

with larger pore size due to the collapse of pore structure regardless of alumina source and surfactant [44]. However, the surface area and the pore volume usually decrease when the temperature is increased [45-47]. This phenomenon suggests that alumina micelles tend to aggregate into large particles when heated at higher temperature due to the combination of sintering and phase transformation [9,48]. The different phases of transition aluminas subsequently follow the changes from γ -boehmite to the final γ -alumina, as illustrated in Figure (1).

1.7 Modified γ -Alumina

1.7.1 γ -Alumina in mixed metal oxides

Active alumina is a multifunctional material with various surface active sites. Engineering the alumina to contain advantageous surface functionalities and to become thermally stable material is fast becoming science and is a powerful tool in designing of selective adsorption sites. Several attempts have been made to improve the efficiency of alumina by modifying it with other ions such as sulfur, phosphorus, chlorine, alkaline-earth elements and transition metal ions [49].

One of the ways to modify the characteristics of γ -alumina and to enhance its performance in catalysis is to dope it with foreign elements, especially metal ions, resulting in a type of bulk mixed oxides. Mixed oxides can be very interesting materials due to the unique advantages that they can offer compared with their corresponding single metal oxides. Very often, they exhibit modified textural properties, enhanced thermal stability, and catalytic activity [50,51].

Many methods have been used to synthesize metal-doped alumina, especially the coprecipitation and sol-gel. Significant number of studies have been reported on attempting to enhance the alumina properties by doping alumina with different transition metal ions such as Fe^{+3} , Cr^{+3} , Ce^{+3} , V^{+3} . For instance, Loretta Soraro [52] and others used chromia and chromim-doped alumina pillared clay for vapor phase deep oxidation of methylene chloride as CVOCs material at temperatures between 300-400 °C. They have shown that the catalytic activity increased with Cr ions content, and they referred that to the presence of acid sites located on chromial pillar.

Other researchers [19] prepared two mesoporous alumina samples (one was doped with Fe ion, and the other without Fe ion) using the sol-gel method, and these samples were

tested as catalysts for trichloroethylene combustion. It was found that the crystallite size for the alumina catalyst doped with Fe ions was smaller than the crystallite size of pure alumina and the doping delayed the stabilization of γ -alumina with respect to temperature. In addition, the catalyst with Fe ions doping had better catalytic activity than the pure alumina catalyst in the temperature range between 100°C to 450°C. Furthermore, they concluded that alumina catalyst doped with Fe ions introduced an effective area of micropores that helped in better performance than the pure alumina catalyst in the abatement of chlorinated VOC.

A.P. Ferreira, D. Zanchet [53], studied the effect of the CeO_2 content on the surface of γ - Al_2O_3 and the structural properties of CeO_2 - Al_2O_3 mixed oxides prepared by sol-gel method. The precursor of Al_2O_3 showed a structure of boehmite $\text{AlO}(\text{OH})$ and its crystallinity decreased slightly with increasing the Ce(III) ion content. M.Crisan [54] and others prepared Manganese doped alumina via sol gel method, and they found that Mn doped alumina showed enhanced catalytic activity in ozone decomposition process. Christian phlitsch [55] prepared Chromium doped alumina films via sol-gel method for surface temperature sensor application. I.Khedher [56] prepared Vanadium doped alumina pillared catalysts for epoxidation of trans-2hexan-1-ol and it was found that doping alumina with Vanadium ions increased catalytic activity.

J. Sanchez Valente [57] investigated the role of zinc doped in alumina prepared via sol-gel method for reduction in Fluid catalytic cracking FCC process. They found that 12% of Zn exhibited the highest surface area and pore volume, however, the surface area decreased as zinc content increased due to increasing of spinal phase of alumina. In another study, Hongmei Huang [58] studied the effect of zinc-doped alumina prepared via incipient wetness impregnation method on the catalytic activity in COS hydrolysis reaction ($\text{COS} + \text{H}_2\text{O} = \text{CO}_2 + \text{H}_2\text{S}$). They found that deactivation period of zinc-doped alumina decreased compared with pure alumina. Yuji Torikai [59] prepared alumina doped with different metals including Cu^{+2} , Fe^{+3} , Co^{+2} , Cr^{+3} , Ni^{+2} , Zn^{+2} and V^{+2} via incipient wetness impregnation method, and it was found that Cu and Co increased the catalytic activity of alumina for the selective reduction of NO with ethane.

1.7.2 Anions-doped γ -Alumina

One of the ways to modify the characteristics of γ -alumina is by adding ions such as Sulfur, Phosphorus, Chlorine. Addition of sulfur ions to alumina produces sulfated

alumina. Researchers found that sulfate ions cover the shell of colloidal particles which prevented the aggregation of sol particles [60]. Thus, sulfate ions help to control crystallization into bohemite and prevent the colloidal particles from aggregations. In one study [61] sulfated alumina with different sulfur content were used for Isobutane /butane alkylation and it was found that increasing sulfur content up to 14%wt led to an increase in the selectivity and catalytic activity of alumina. However, further increase in sulfur content reduces the catalytic activity, the pore volume and the surface area of alumina.

Fluorinated alumina was found to have high catalytic activity. Jianchao Xia [62] and others used fluorinated alumina for production of dimethylether and they found that F ions enhances catalytic activity of alumina up to certain content. When alumina was loaded with more fluoride ions, it showed lower surface area and weaker acidity. Similarly, the addition of Phosphorous ions on the surface of alumina was also found to enhance the alumina catalytic activity. Jun Wang and others [63] examined the effect of addition of phosphorous ions on the textural properties and the acidity of alumina. They found that phosphorous ions improved the stability of alumina by modifying acid-base surface properties. In addition, it delayed the phase transition of alumina from gamma to alpha. Also they found that Phosphorous ions decreased the number of Lewis acid sites. In another study, Phosphorous ions were introduced during the formation of alumina gel, and it was found that addition of phosphate could effectively improve thermal stability and textural properties of alumina [64].

The addition of chlorine ions on the surface of alumina has also been found to enhance the catalytic performance of γ -alumina catalysts. G. Celt [65] prepared chlorinated alumina by reacting γ -alumina with gaseous CCl_4 or HCl for alkylation of isobutene. They found that chlorination using CCl_4 was inefficient for the reaction, whereas using HCl was able to catalyze the reaction at temperatures as low as 273 K because HCl interacted with particular Lewis acid sites on alumina surface and created strong Bronsted sites that are required for catalytic alkylation.

Among other ions that have been also frequently studied for γ -alumina modification are La^{3+} , Ce^{4+} , Ba^{2+} , Y^{3+} and Zr^{4+} which have resulted in modified properties of γ -alumina [53,66-68]. Lanthanum oxide, La_2O_3 , has been reported to be one of the best inhibitors of sintering in alumina [67]. Similarly, yttria-doped alumina showed enhanced thermal stability, less surface area loss upon calcination, and delayed crystallization [68]. In a

recent study, γ -alumina-supported Ni catalysts, for reforming processes, was reported to show less Ni sintering and C deposition upon doping with ions such as Cs, Mg, Fe, Ce, and La [69]. There is also a special interest in Fe and Cr-doped γ -alumina for various catalytic applications [70].

1.7.3 Modified Alumina-based alkaline earth metals

Several studies reported that γ -alumina can be modified by doping with alkaline earth elements. For instance, one study [71] reported that alkaline metals have been demonstrated as active promoters in numerous heterogeneous catalysts. Therefore, alumina-supported manganese was doped with K and it was found that the catalytic oxidation of aromatic alcohol increased when K was introduced. Sylvie [72] attempted to shift the phase transition of alumina towards higher temperature by doping sol-gel prepared alumina by alkaline earths or lanthanides (Mg, Ce, Ba, La, Pr) using impregnation process and it was found that there was direct influence of the doping element on the structure of alumina. The obtained composites showed an increase in surface area where 1% Al-Mg and 1.4 % Al-Ce showed surface area of 180 and 163 m^2/g , respectively, as compared with pure Al_2O_3 which was (130 m^2/g). However, it was found that the introduction of alkaline earth's (Mg, Ba) in alumina resulted, generally, in better specific surface area than doping with lanthanide elements such as Ce and La. They also concluded that low contents of doping element are sufficient to increase the thermal stability of alumina especially when Ba was used. Furthermore, Tania Montanaria [73], studied adsorption of CO , CO_2 and NO_x over alumina with different loadings of potassium acetate. It was found that light doping resulted in weak adsorption of CO_2 as bicarbonate species and NO_2 as bidentate nitrates, while heavy doping resulted in the adsorption of CO_2 as bidentate carbonates and NO_2 as polydentate nitrate species. Srinivasan [74] and co-workers studied the role of sodium on the catalytic behavior of alumina on dehydration of isopropanol. They found that added Na impurities modified the catalytic behavior of alumina and affected the hydroxyl groups and adsorbed pyridine.

While numerous studies have been reported on surface doped γ -alumina, few studies have been reported on sol-gel preparation of transition metal-aluminum bulk mixed oxides. In addition, few studies have been reported on template-free sol-gel preparation of mesoporous doped γ -alumina without the use of an acid catalyst [75]. In the present study, powders of γ -alumina doped with several transition metal ions were prepared via template-

free sol-gel method in the absence of an acid catalyst. The gel formation and the textural properties of the calcined powders versus the nature of the dopant ions and their concentrations were studied are discussed in chapter 2.

1.8 Summary

Alumina is a widely used material for its promising chemical, physical, and mechanical properties. In addition, due to its high surface area and chemical activity; γ -alumina has been used extensively as a catalyst or catalyst support. The strong catalytic activity of γ -alumina results from the active sites present on its surface. These sites include hydroxyl groups (OH^-) which act as Brønsted acid, (O^{2-}) which act as Lewis base and Al^{3+} which acts as Lewis acid. There are several factors that affect chemical, physical and catalytic properties of alumina including the type the preparative method, the pH of starting solutions, calcination temperature, and the presence of additives.

The most common γ -alumina preparative methods are based on sol-gel and precipitation processes. Each method has its own advantages and disadvantages. However, the sol-gel method usually results in unique homogeneous textural properties. In addition, it allows some control over the final pore size and the surface area.

Alumina has been used in a variety of applications including medicine, chromatography, production of H_2 fuel, and cleaning of waste water from toxic materials. In addition, it is extensively used as a catalyst or catalyst support for many different reactions such as conversion of methanol to DME, combustion of hydrocarbons compounds, and catalytic purification for the exhaust of vehicle. However, these catalytic reactions require high temperatures and for this reason enhancing physical properties and thermal stability of transition alumina is of primary industrial interest. Generally, the catalytic reactivity and the stabilization of alumina can be promoted through modifying alumina by doping it with foreign elements such as anions (F, Cl, P, S) or with alkaline-earth metals. However, modified alumina and alumina based-mixed oxides can result in materials with interesting properties due to the unique advantages that they can offer compared with their corresponding single metal oxides. Very often, they exhibit modified textural properties, enhanced thermal stability, and catalytic activity. Few studies have been reported on template-free sol-gel preparation of mesoporous doped γ -alumina without the use of an acid catalyst. In the present study, powders of γ -alumina doped with several transition metal ions were prepared via template-free sol-gel method in the absence of an

acid catalyst. The gel formation and the textural properties of the calcined powders versus the nature of the dopant ions and their concentrations were studied.

VIII. Chapter 2 . Highly porous transition-metal-modified γ -Alumina: Effect of doping element and preparative conditions

2.1 Introduction

Aluminum oxides are important materials that have been widely studied and employed in various applications due to unique textural, chemical, and mechanical characteristics [76]. Their applications included catalysts, catalyst supports, ceramics, and oxidation/reduction resistant coatings. Due to their wide applications, aluminum oxides continue to attract the attention of researchers worldwide in efforts to modify their fabrication aiming at improved chemical and mechanical properties. γ -Alumina, in particular, usually exhibit high surface area and porosity, strong surface acidity, good mechanical strength, and thermal stability. Therefore, it has been employed widely in the field of catalysis. It is an active catalyst by itself for several important reactions such as dehydration of methanol to dimethyl ether [77,78] and degradation of volatile organic compounds [79].

The performance of metal oxides, in general, as catalysts or catalyst supports largely depends on their crystalline structure and textural properties. Besides the role of the surface area, the pore structure plays an important role in the catalytic activity. Mesoporous materials are particularly important as they offer the advantage of avoiding the pore plugging that often occurs in microporous materials. Therefore, the preparation of porous alumina with defined and controllable porous structure is of great importance. The attempts to prepare mesoporous alumina started immediately after the invention of mesoporous molecular sieves by Mobil in early 1990s which provided solutions to the limitations of zeolite-based microporous molecular sieves.

The textural properties of alumina are largely dependent on the employed preparation method and conditions. Several synthetic strategies have been developed to obtain porous high-surface-area alumina. The most common synthetic routes are based on sol-gel [9,80] and precipitation methods [81,82]. In the sol-gel process, the method of solvent removal from the gel is very critical and determines the textural properties of the final product. While supercritical drying results in aerogel with unique textural properties including high surface areas and total pore volumes, conventional drying usually results in xerogel with

lower surface areas and pore volumes. However, the xerogel processing is often preferred due to the low cost and easier processing [9]. On the other hand, alumina prepared by precipitation in aqueous solutions usually exhibit lower surface areas and pore volumes as compared with the sol-gel-prepared counterparts [81-83].

Template substances and organic additives have been typically used in the sol-gel synthesis to obtain stable mesoporous alumina [34,80,84]. An extensive work has been reported on xerogel alumina prepared under various preparative conditions using neutral, anionic and cationic templating surfactants [34,76]. The final textural properties have been found to depend on the starting solution pH, water/Al ratio, the type of surfactant, the solvent/Al ratio, the aging period of the gel, and more importantly on the method of drying the gel [85-88]. The majority of the reported work based on xerogel processing resulted in surface areas below 400 m²/g and pore volumes in the range of 0.2-0.8 cc/g. In some studies, non-surfactant organic molecules such as triethanolamine were used as a template [89]. In a recent study, mesoporous γ -alumina was prepared using different saccharide molecules as templates where the textural properties of the obtained alumina were dependent on the molecular size of the saccharide template [90]. These preparative methods resulted in alumina of relatively low surface areas and pore volumes in the range of 150-300 m²/g and 0.2-0.6 cc/g, respectively. In another study, polystyrene spheres and a block co-polymer were used as dual templates to produce γ -alumina with ordered meso- and macropores [91]. However, the surface area and the pore volume after calcinations at 500 °C were also low, 167 m²/g and 0.26 cc/g respectively. In a recent study, it was found that γ -alumina can be prepared in high surface areas and uniquely high pore volume via straightforward sol-gel synthesis from aluminum alkoxides under non-acidic conditions in the absence of surfactants [79]. Besides the relatively homogeneous mesoporosity, the obtained alumina showed a noticeable macroporosity which varied depending on the preparative conditions.

One of the ways to modify the characteristics of alumina as a catalyst support as well as a catalyst to enhance its catalytic activity is to dope the alumina lattice with foreign ions especially metal ions forming mixed oxides. Bulk mixed oxides are very interesting materials due to the unique advantages that they can offer compared with the corresponding single metal oxides. Very often, they exhibit modified textural properties, enhanced thermal stability, and catalytic activity [92]. Doping of γ -alumina may also improve its selectivity in reactions. Therefore, these systems are important classes of

materials for a wide variety of applications including ceramics, optics, electronics, lasers and catalysis [93].

Among the ions that have been frequently studied for γ -alumina modification are La^{3+} , Ce^{4+} , Ba^{2+} , and Zr^{4+} which have resulted in retarding the sintering and delaying the phase transformation of γ -alumina [53,94]. Lanthanum oxide, La_2O_3 , has been reported to be one of the best inhibitor of sintering in alumina [95]. Similarly, yttria-doped alumina showed enhanced thermal stability, less surface area loss upon calcination, and delayed crystallization [94]. In a recent study, γ -alumina-supported Ni catalysts, for reforming process, was reported to show less Ni sintering and C deposition upon doping with ions such as Ca, Mo, Mg, Ce, and La [96]. Numerous examples are reported in the literature and significant work is undergoing aiming at fabricating more robust and efficient γ -alumina materials for various applications. In addition, there is a special interest in Fe and Cr-doped alumina as solid solutions with improved mechanical and catalytic properties [97].

The traditional ceramic methods that are used to prepare binary or more complex aluminum oxides involve physical mixing of the powders of the oxides (or oxide precursors) and sintering at high temperatures for extended reaction times. These reaction conditions are necessary to promote solid state diffusion since physical mixing is limited to the micron scale. Therefore, chemical routes to the synthesis of mixed metal aluminum oxide powders and ceramics are increasingly being adopted. The most widely employed methods are the sol-gel based techniques due to their versatility and atomic level homogeneity.

While numerous studies have been reported on doping alumina, few studies have been reported on sol-gel prepared transition metal-aluminum bulk mixed oxides. In addition, systematic studies on the additives' effect on various properties of alumina especially textural properties as well as correlations with preparative conditions are few. Furthermore, the homogeneity of the mixed oxide has been always a concern as segregated oxide of the foreign ion may form. These facts are the main driving force behind the present work which aims at optimizing straightforward sol-gel route for homogeneous γ -alumina doped with various transition metal ions.

2.2 The Experimental Procedure

2.2.1 Reagents and Materials

Chemicals including Aluminum tri-sec-butoxide (ASB), $\text{Cr}(\text{NO}_3)_3 \cdot 9\text{H}_2\text{O}$, 2-propanol, Cr(III) acetylacetonate ($\text{Cr}(\text{acac})_3$) Aluminum tri-sec-butoxide, $\text{MnCl}_2 \cdot 9\text{H}_2\text{O}$, $\text{Zn}(\text{CH}_3\text{COO})_2 \cdot 2\text{H}_2\text{O}$, ZnCl_2 , CuCl_2 , $\text{CuC}_{10}\text{H}_{14}\text{O}_4 \cdot \text{H}_2\text{O}$, $\text{Fe}(\text{NO}_3)_3 \cdot 9\text{H}_2\text{O}$, VCl_3 , $\text{Ce}(\text{NO}_3)_3 \cdot 6\text{H}_2\text{O}$, 2-propanol, methanol, toluene and 1-butanol of purity > 97% were purchased from Aldrich and were used without further purification.

2.2.2 Preparative procedures

γ -Alumina doped with metal ions including V(III), Fe(III), Cr(III), Mn(II), Cu(II), Ce(III) and Zn(II) were prepared via sol-gel method. The aluminum precursor was ASB while the precursor of the dopant metal ions were metal nitrate, metal acetate, or metal acetylacetonate precursor. In a typical experiment, an example of Al-Cr composite, 6 ml (0.023 mol) of ASB was dissolved in 200 ml 2-propanol and the desired amount of the chromium nitrate precursor was dissolved in 50 ml 2-propanol separately. Methanol was used as the solvent for $\text{Cr}(\text{acac})_3$ precursor. The Cr precursor solution was then added to the ASB solution and the mixture was stirred for 20 minutes. While stirring, 2.0 ml (0.11 mol) of distilled water was added drop wise to the mixture which was stirred for 4 more h and aged for 16 h in a covered beaker. The solvent was removed from the gels by evaporation at around 80 °C. The obtained powders were then dried in an oven at 120 °C for 1 hour before calcinations at 350 °C and 500 °C for 1 h and 5 h respectively. γ -Alumina was prepared via the same procedure without the other metal. While 2-propanol was used as the solvent for all precursors, VCl_3 , $\text{Cu}(\text{acac})_2$ and $\text{Zn}(\text{CH}_3\text{COO})_2 \cdot 2\text{H}_2\text{O}$ were dissolved in methanol. Composites with different compositions were prepared and the formula Al-M-X will be used to represent the composites where "M" refers to the dopant metal ions and "X" refers its molar concentration calculated as $(M/M+\text{Al}) \cdot 100$.

It was observed that different metal and metal ions precursors had an effect on the gelation process. While generally a colloidal gel was observed after the addition of water and after aging, some precursors resulted in a turbid gel upon mixing the solutions of the two precursors before the addition of water. These precursors include metal acetate and metal acetylacetonate produced which a turbid colloidal gel after mixing them with alumina precursor solution and before addition of H_2O .

2.2.3 Characterization techniques

Powder X-ray diffraction (XRD) analyses were obtained using a Philips PW/1840 diffractometer (40 kV, 25 mA) with Cu-K α radiation, $\lambda = 1.542 \text{ \AA} = 1.542 \text{ \AA}$. Data was collected in the 2θ angle range of 20-80 degrees at a rate of 2 degrees/min. SEM micrographs were obtained using an EFI Quanta-200 scanning electron microscope.

Diffuse reflectance infrared Fourier transform spectra (DRIFTS) were collected in the 4000-400 cm^{-1} range at 4 cm^{-1} resolution using a Shimadzu IR-Affinity-1 spectrometer. The DRIFTS accessory, from Pikes Technologies, was equipped with a heated cell for in-situ studies with the capability of heating to temperatures as high as 900 °C. The samples were prepared in KBr powder mixtures, 10% by mass. A background spectrum was recorded for KBr at 25 °C after pretreatment at 150 °C under nitrogen flow, 10 ml/min. The samples were then heated under the same N $_2$ flow to 400 °C at a rate of 10°/min and were soaked for 20 min before spectra were recorded.

N $_2$ adsorption studies at 77 K for surface area and porosity measurements were conducted on a Quantochrome Autosorb-1 volumetric gas sorption instrument. Samples were degassed at 150 °C for one hour before measurements. The surface area was obtained by the Brunauer-Emmett-Teller (BET) method and the pore size distributions were determined by Barrett-Joyner-Halenda (BJH) model from the desorption branch of the N $_2$ isotherms.

2.3. Results and Discussions

2.3.1 Formation of mixed oxides

The formation of mixed oxides and the effect of the doping ion on the characteristics of the final composite depend largely on the method of preparation. The traditional preparation of mixed metal oxides involves physical mixing and solid state reactions of parent oxides or oxide precursors followed by high temperature treatment for extended reaction times. However, sol-gel methods have been widely employed as an alternative due to lower processing temperatures, versatility, and homogeneity of the final product properties. In addition, sol-gel routes usually result in composites with unique textural properties. One of the problems associated with the preparation of mixed metal aluminum oxides from alkoxides is the fact that alkoxides can have different hydrolysis rates leading to phase segregation in the gels. Therefore, in the present study we used common

inorganic salts of the dopant ions, which besides their chemical stability, are cost effective. In addition, we avoided the use of the commonly used acid catalysts that are usually used to enhance the hydrolysis and condensation during the gelation process. The non-acidic conditions would result in slower gelation of the aluminum hydrolyzed species which would, in turn, result in thorough and more homogeneous mixing of the aluminum precursor with the other metal ions. The different physical characterization studies of the prepared doped alumina indicated well dispersion of the foreign metal ions in the alumina matrix. In addition, the final calcined products exhibited unique textural properties comparable with those of γ -alumina alone. Furthermore, various metal ions and different metal ion precursors resulted in different behavior during the gelation process and different characteristics of the final products indicating different modes of interaction of the metal ions with the alumina network. In addition, the homogeneous colors obtained for the solids after calcinations and the thermochromism observed for some ions, as discussed below, is an evidence of the homogeneous incorporation of the metal ions in the alumina matrix. Table I shows the colors of the calcined composites and the color of the corresponding single metal oxides.

Table 1. Colors of the bulk mixed oxides vs. the colors of the corresponding single metal oxides. The color of pure γ -alumina is white.

M^{n+}	M^{n+} (%)	M^{n+} Precursor	The mixed oxide	Single metal oxide
Cr^{+3}	0.75	nitrate	Greenish-yellow	dark green powder
	2	nitrate	Greenish-yellow	
	3	nitrate	Pale yellow	
	5	nitrate	Yellowish-green	
	10	nitrate	Yellowish-green	
	5	acac	Light green	
	10	acac	Light green	
Fe^{+3}	2	nitrate	Orange	Reddish brown Fe_2O_3 powder
	3	nitrate	Pale Orange	
	5	nitrate	Light brown	
	10	nitrate	Orange brown	
V^{+3}	3	chloride	Pale yellow	brown/yellow
	7.5	chloride	Green	
	10	chloride	Off white	
Ce^{+3}	3	nitrate	White	pale yellow-white powder
	5	nitrate	Off white	
	10	nitrate	Pale yellow	
Mn^{+2}	3	chloride	Dark brown	Milky white powder
	5	chloride	Brown-red	
	10	chloride	Dark brown red	
Zn^{+2}	2	acetate	Light brown	White powder
	3	acetate	Pale brown	
	10	acetate	Off white	
	10	chloride	white	
Cu^{+2}	3	acac	Sky blue	Blue crystal

				powder
	5	acac	Sky blue	
	10	acac	Dark blue	
	20	acac	Dark black	
	10	chloride	Dark green	light brown

2.3.2 Structure and Thermochromism of Al-Cr-x

γ -Alumina doped with Cr^{3+} ions was obtained with different Cr:Al molar ratios. As an example for all metals. The Cr(III) precursor was well mixed with the aluminum precursor in the starting solution and no acid catalyst, which is typically employed in sol-gel synthesis, was used. These conditions would slow down the hydrolysis and condensation reactions of the aluminum alkoxide precursor allowing for more homogeneous mixing of the two precursors on the molecular level, and hence better dispersion of the Cr^{3+} ions in the aluminum hydroxide gel matrix would be obtained.

Colloidal gels were obtained upon hydrolysis which resulted in light blue powders after drying. After calcinations and cooling to room temperature, the colors were greenish yellow for Al-Cr-0.75 and Al-Cr-2, and yellowish green for Al-Cr-5 and Al-Cr-10. Al-Cr-0.75 and Al-Cr-2 showed a reversible change in color to orange-red when heated at temperatures in the range of 500-700 °C. To our knowledge, the observed thermochromism of the Cr-doped γ -phase of alumina has not been addressed before. Thermochromism behavior is known for the high-temperature stable phase of alumina (α -phase) containing $< 1\%$ Cr^{3+} ions, ruby, where its red color at room temperature becomes green upon heating at elevated temperatures. The observed thermochromism in the present study may indicate that the dispersion of the Cr^{3+} ions occurred via substituting Al^{3+} ions resulting in substitutional solid solution similar to what is known for ruby, where Cr ions substitute Al ions which are all octahedrally coordinated in the alumina corundum structure.

The change in color of an inorganic solid is usually due to a change in its crystalline phase, a change in ligand geometry, a change in coordination number, or due to lattice expansion. The thermochromism exhibited by the Al-Cr composites in the present study can be explained based on lattice expansion which was also suggested for the thermochromism exhibited by ruby [98]. Ligand Field Theory can be used to explain the possible lattice expansion and its effect on the color. The structure of $\gamma\text{-Al}_2\text{O}_3$ is cubic. It is based on an FCC structure, ABCABC, stacking of oxygen with the aluminum ions occupying both octahedral and tetrahedral positions, with $\sim 30\%$ of Al ions in tetrahedral sites and $\sim 70\%$ in octahedral sites [99]. The change in color from greenish yellow to red agrees well with the suggested lattice expansion as the red color indicates absorption of light of lower frequency than that absorbed when the color is greenish yellow reflecting a weaker crystal field at higher temperatures. This weaker field is due to weaker Cr-O

interaction and hence weaker ligand field $d-d$ splitting. Powder XRD, ^{27}Al -NMR spectroscopy, FTIR spectroscopy, and textural characterization also indicated well dispersion of the Cr ions in the alumina matrix.

^{27}Al -NMR spectrum of pure alumina, Figure 8 showed the presence of a noticeable amount of pentahedrally coordinated Al ions, Al^{V} , besides the octahedrally and tetrahedrally coordinated ions, Al^{VI} and Al^{IV} respectively, which are typically present in $\gamma\text{-Al}_2\text{O}_3$, indicating some lattice disorder. It is noticed that upon doping, the Al^{IV} and Al^{V} peaks decreased relative to that of Al^{VI} which may indicate that some Cr^{3+} ions substitute Al ions in these sites. This observation is more pronounced in the spectrum of Al-Cr-0.75 which suggests that substitution in the lower coordination sites by Cr^{3+} ions is preferred and hence at low Cr^{3+} concentration, 0.75%, substitution in tetrahedral and pentahedral positions seems to dominate. This may indicate that the substitution takes place after the formation of the alumina lattice and substituting octahedral Al sites is less favored.

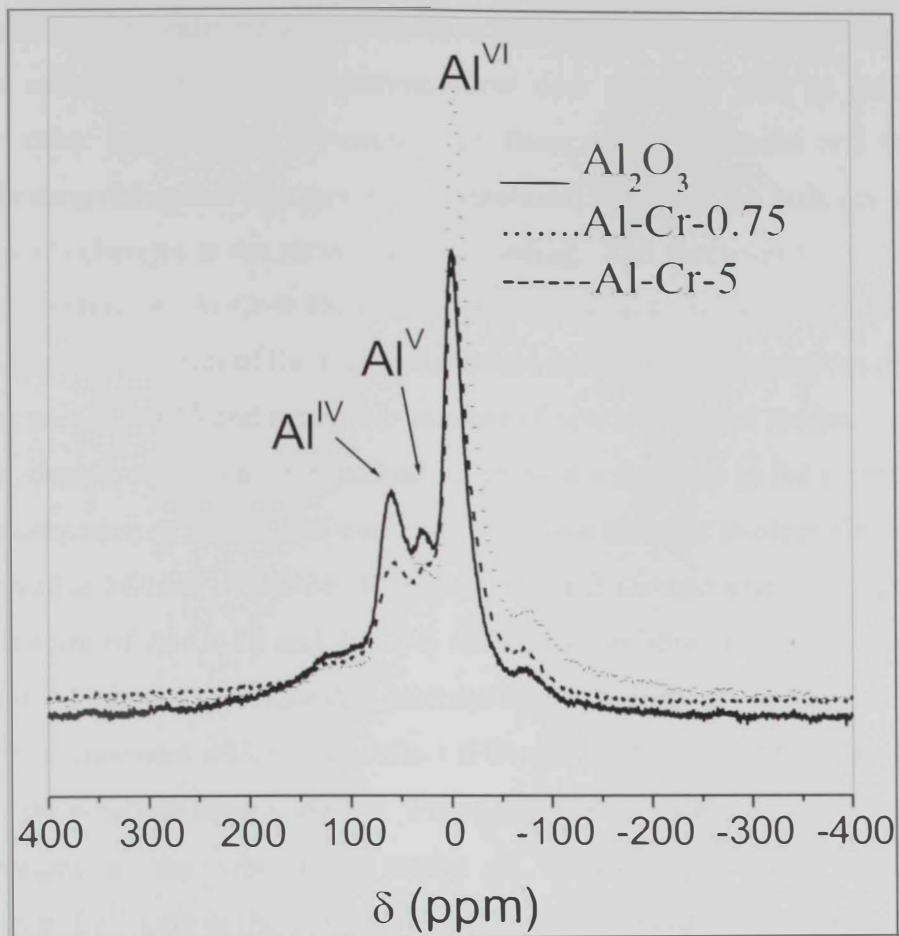


Figure 8. ^{27}Al -NMR spectrum of pure alumina compared with Al-Cr-0.75 and Al-Cr-5

2.3.3 FTIR spectroscopic characterization

Another evidence for the formation of bulk mixed oxides is obtained from the FTIR spectra of the products. DRIFT spectra of the different composites for Al-Cr-Oxide were recorded at 400 °C and the metal-oxygen bond characteristic absorptions in the spectral region of 400-900 cm^{-1} were compared, as shown in Figure 9. The characteristic absorptions of Cr_2O_3 in the physical mixture are obscured by the strong absorptions of alumina resulting in broader peaks and shoulders in the spectrum of the mixture (450-550 cm^{-1}). The spectra of the doped alumina show new peaks as well as shifting in the positions of other major peaks compared with those of pure alumina and the physical mixture indicating noticeable changes in the vibrational modes of the bulk and the surface, which represents changes in the metal-oxygen bonding. The spectrum of the composite of low Cr^{3+} concentration, Al-Cr-0.75, showed sharper peaks and less shoulder peaks as compared with the spectrum of the physical mixture indicating homogeneous dispersion of the Cr^{3+} ions in Al-Cr-0.75 and hence less number of new vibrational modes.

However, compared with alumina alone, it showed a decrease in the intensity of some absorption peaks such as that at 538 cm^{-1} , and a relative increase in other absorptions such as that observed at 544 cm^{-1} . On the other hand, Al-Cr-2 showed a new strong peak at 495 cm^{-1} . The spectra of Al-Cr-10 and Al-Cr-5 showed some broad peaks and shoulders. In addition, Al-Cr-5 showed a noticeable increase in the absorption at 483 cm^{-1} compared with all other composites which may reflect different modes of incorporation of the Cr^{3+} ions making the structure more complex. These observations and changes in the IR spectra indicate changes in the vibrational modes of metal-oxygen bonds confirming the incorporation of Cr^{3+} ions in the γ -alumina matrix which means that the modes of Cr^{3+} ion incorporation and hence the vibrational modes are strongly dependent on the Cr^{3+} concentration. These results indicate hetero-linkage formation in the prepared mixed oxides and the formation of homogeneous bulk mixed oxides in the cases of low Cr^{3+} concentrations, $\leq 2\%$.

2.3.4 Morphology characterization

The morphology of selected samples was studied by SEM. The samples studied include alumina doped with V^{3+} , Ce^{3+} , Cr^{3+} , Fe^{3+} , and Zn^{2+} with metal concentrations between 2 and 10%. All composites showed relatively homogeneous spherical aggregated particles with diameters in the range of 100-200 nm. These particles aggregate further into larger porous particles as shown in Figure 10 and Figure 11 which presents selected SEM micrographs of selected samples.

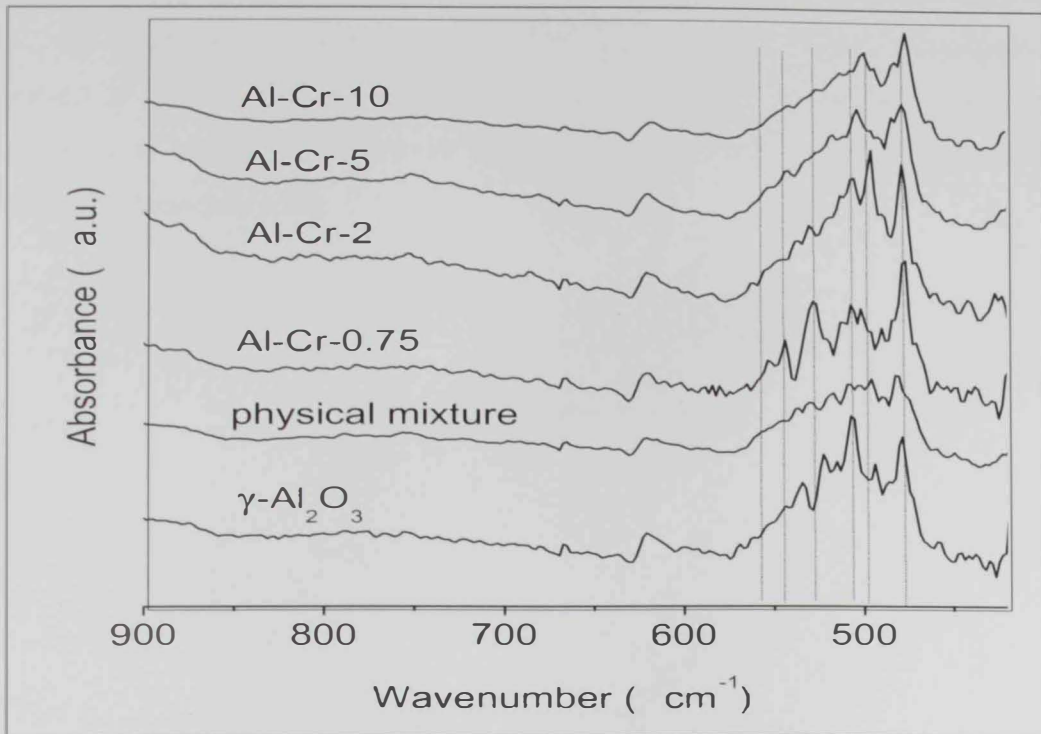
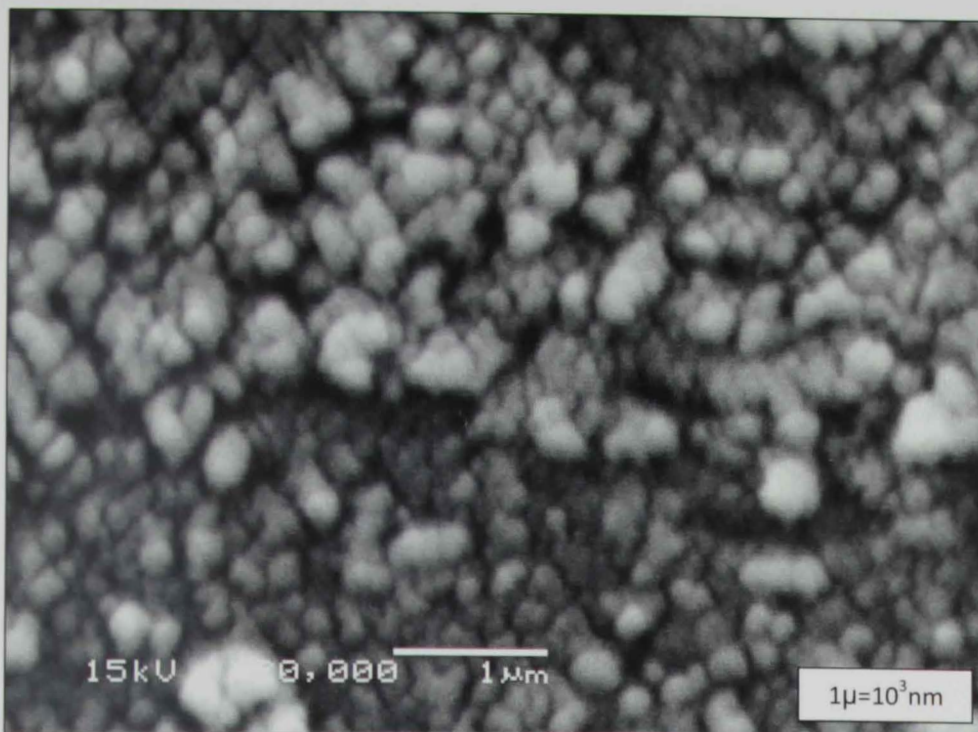
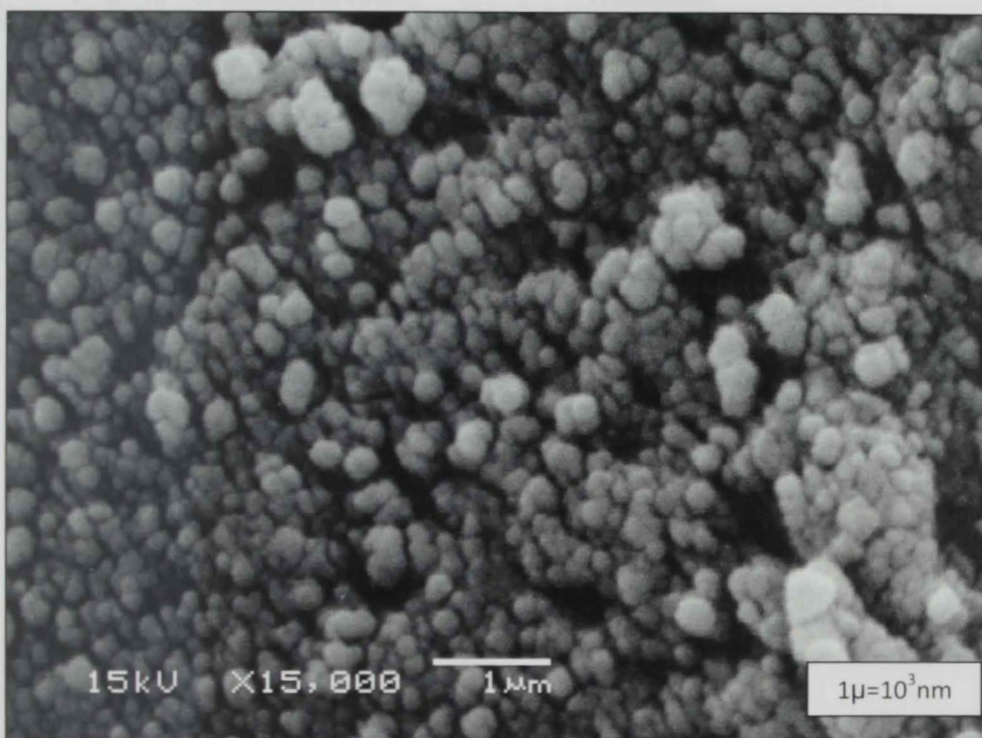


Figure 9. DRIFT spectra of different Al-Cr Oxide composites.

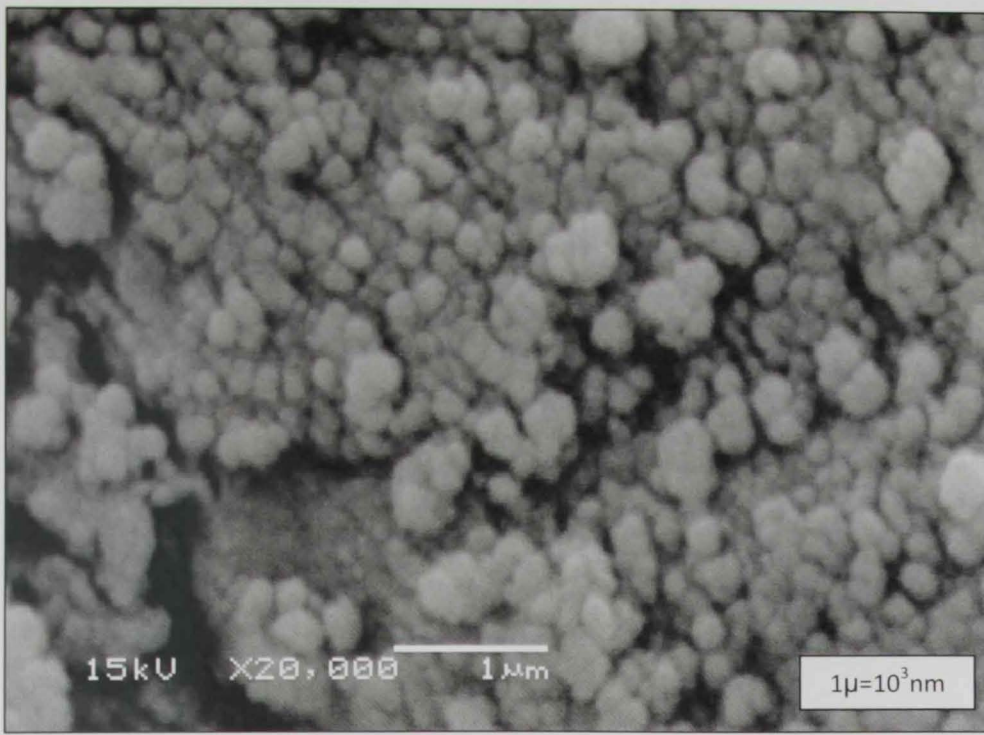


(a)

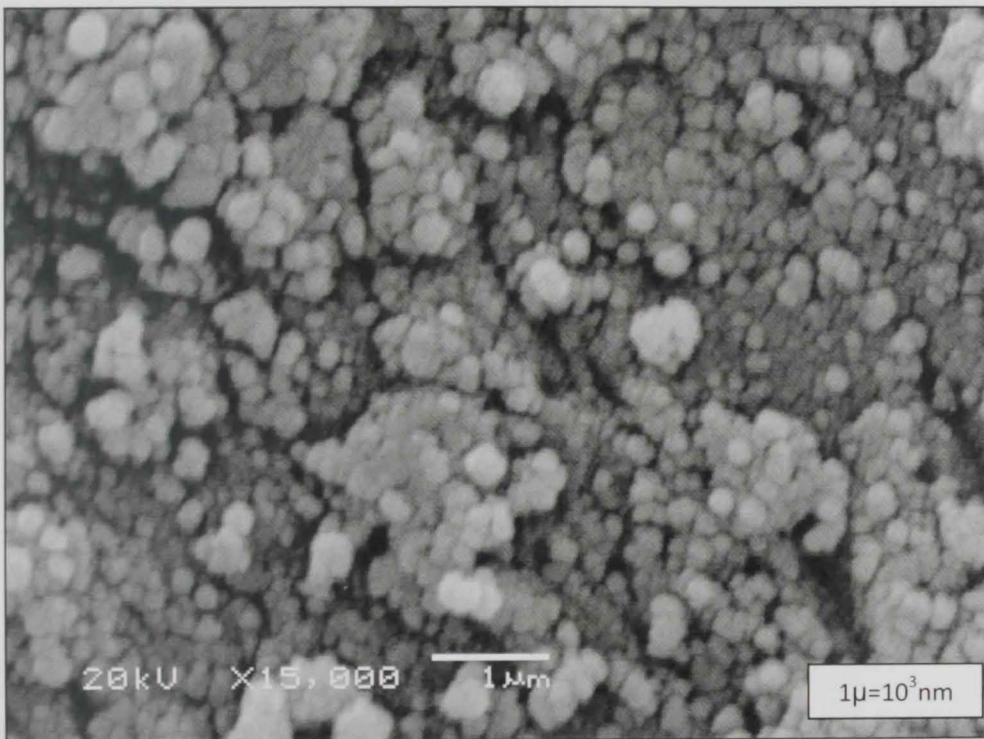


(b)

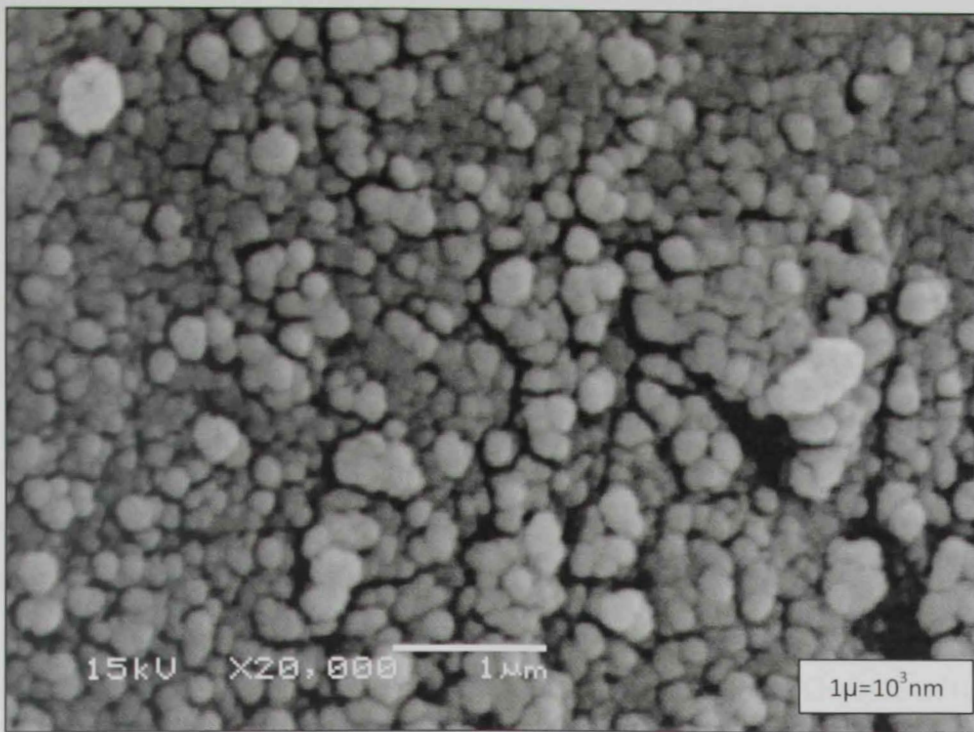
Figure 10. SEM micrographs of (a) Al-Cr-02 and (b) Al-Fe-02



(a)



(b)



(c)

Figure 11. SEM micrographs of (a) Al-Cr-05, (b) Al-Fe-05, and (c) Al-V-10

2.3.5 The Effect of the Foreign Metal ions And the Precursor on the Gel Formation

Generally, colloidal gels were obtained after hydrolysis and aging. However, the condensation reactions upon hydrolysis took place more rapidly when the acac precursors were used as compared with the nitrate or the chloride precursor. This behavior could be referred to a possible interaction between acac ligands and hydrolyzed aluminum ion intermediates by proton abstraction enhancing condensation reactions. Rapid condensation is known to be associated with the formation of a gel network of more cross-linking which usually shows better resistance to collapsing due to capillary forces during drying [85]. This explanation is well supported by the observed textural properties discussed below.

As an example, the presence of zinc acetate, dissolved in methanol, the gelation process took place within few minutes after mixing the solutions of the two precursors. This was evident by the rapid formation of a white gel just after mixing the solutions and before the addition of water which became more viscous after water addition. The role of the acetate ion was confirmed by comparing the behavior of $ZnCl_2$ salt, dissolved in 2-propanol, which gave colloidal gel after the addition of water. A clear solution was obtained upon mixing both precursor solutions and after the addition of water a colloid started to form gradually. After stirring for 4 hours and aging for 16 hours, the acetate-containing mixture resulted in turbid gel while the chloride mixture contained transparent layer and a separate colloidal gel layer. The same was observed in all cases with different Zn contents. The rapid gel formation indicates enhanced condensation reactions. As discussed above rapid gel formation results in a gel with better resistance to pore structure shrinkage [85]. This explanation is well supported by the observed higher surface areas and porosity of Al-Zn-10 composites compared with those containing 10% of other metal ions. The rapid condensation and gel formation could be explained by a rapid reaction between the acetate ion and the aluminum precursor forming CH_3COOR . This reaction enhances the condensation process and the possibility for heterolinkage formation resulting in Al-O-Zn species.

In the cases of Cu(II), where $Cu(acac)_2$ was used as the precursor, when the $Cu(acac)_2$ solution was mixed with the ASB solution, a blue viscous gel formed immediately before the addition of water. On the other hand, when $CuCl_2$, in 2-propanol, was used instead, a clear green solution was obtained upon mixing with the ASB solution and upon the addition of water, the solution turned blue and a colloid started to form. After stirring for 4 hours and aging for 16 hours, the acac-containing mixture resulted in a turbid gel while the chloride mixture gave a separate transparent layer and a colloidal gel. The color of the

acac-containing mixture was much darker blue than that of the chloride before and after the aging. After drying and calcinations, the two precursors resulted in a green powder. These observations clearly indicate a significant role of the acac ion in the condensation and gelation process. The faster condensation reactions observed in the presence of acac ions could be referred to a possible reaction of these ions with hydrolyzed aluminum precursor by proton abstraction which would enhance the condensation process.

Interestingly, particular dopant metal ions, enhanced the formation of transparent gels. In addition, the behavior of the mixture during the gelation process was dependent on the nature of the metal ion and its concentration. The strongest effect was observed in the case of Fe^{3+} ion which resulted in the formation of a transparent gel upon hydrolysis of the mixture of both precursors. The gel formed even more rapidly at high Fe^{3+} concentration, 10%, where the gel was observed before water addition, in which case the hydrolysis would take place using the water of hydration present in the structure of the iron precursor. It is noteworthy that the employed transition metal ion precursors by themselves, in the absence of the aluminum precursor, would not form a gel but may give a precipitate under these conditions [100]. This means that the dominant alumina precursor prevented such precipitation and the presence of the dopant ions enhanced the formation of the alumina intermediate gel network. These observations indicate a significant interaction between the dopant ions and the alumina network which may indicate the formation of hetero-linked intermediates, Al-O-M (M = dopant ion). The formation of a transparent gel also indicates a good homogeneity which is expected to result in homogeneous properties in the final composite.

Other metal ions showed varied behavior that was strongly dependent on the concentration. The behavior of V^{3+} was, to some extent, similar to Fe^{3+} . However, the formation of the gel was not as readily as in the case of iron. While V^{3+} in 2% and 5% concentrations resulted in turbid gels, 10% resulted in a clear gel after hydrolysis and aging. Chromium ions, on the other hand, showed almost an opposite behavior where 2% concentration resulted in a clear gel and 10% of the same ion resulted in a light precipitate. Mn^{2+} and Ce^{3+} , however, did not give a clear gel at any of the studied concentrations and resulted in a colloidal gel.

The different behavior of Fe^{3+} compared with the other metal ions could be referred to its ionic radius, 53 pm, which is very close to that of Al^{3+} ion, 54 pm. Similarity in ionic radii would enhance solid solution formation. In addition, the gel formation and

homogeneity can be referred to the d^5 configuration of Fe^{3+} which adds an electronic factor that prevents its precipitation. The d^5 configuration results in zero Ligand Field Stabilization Energy in an octahedral environment which decreases the reactivity of the iron ions and, hence, slows down the formation/segregation of iron hydroxide intermediates.

The general role of the metal ions in enhancing gelation may be referred, in part, to their tendency to coordinate to the alkoxy groups bound to Al ions enhancing condensation. However, the variations in their behavior and the dependence of their role on the concentration are not well understood and are worth further studies.

2.3.6 Powder XRD of Al-Metal oxide systems

2.3.6.1 Composites with different metal ions

γ -Alumina is identified by the peaks at 2θ angles around 38.0, 46.0, and 66.0 degrees which correspond to the (311), (400), and (440) planes respectively [101]. It is known that ions doped into the lattice of an Aluminum oxide may generate defects, by generating strain into the lattice, and/or result in the formation of new phases [102]. These effects generally result in a composite of lower degree of crystallinity as compared with parent oxides, oxides of each metal alone. The lower crystallinity can be inferred from broader diffraction peaks in the powder XRD patterns as shown in Figure 12 which displays the patterns of Al-M-10% of various metals as well as the pattern of pure γ -alumina.

As shown in the Figure, the patterns show either completely amorphous or very weakly crystalline solids. This effect on the crystallization process, which is expected to take place upon calcinations, indicates well dispersion of the dopant ions in the alumina matrix. In addition, no peaks were observed for any oxide of the dopant metal ions, which strongly supports the suggested well dispersion of the metal ions which eventually results in homogeneity in the composites. It is noticed that the patterns that show some diffraction refer to ions of oxidation state of +2. This could be an indication of less degree of incorporation in the lattice as compared with ions of +3 oxidation similar to that of aluminum ion. This makes sense as ions of the same oxidation number of Al are expected to have a better tendency to substitute Al ions more easily. However, metal ions of +2 oxidation state have a tendency to form the spinel phase of general formula MAI_2O_4 where M represent the other metal ion such as $ZnAl_2O_4$. The formation of such phase was not

evident from the XRD pattern which could be due to the amorphous nature of the products resulting in weak diffraction features.



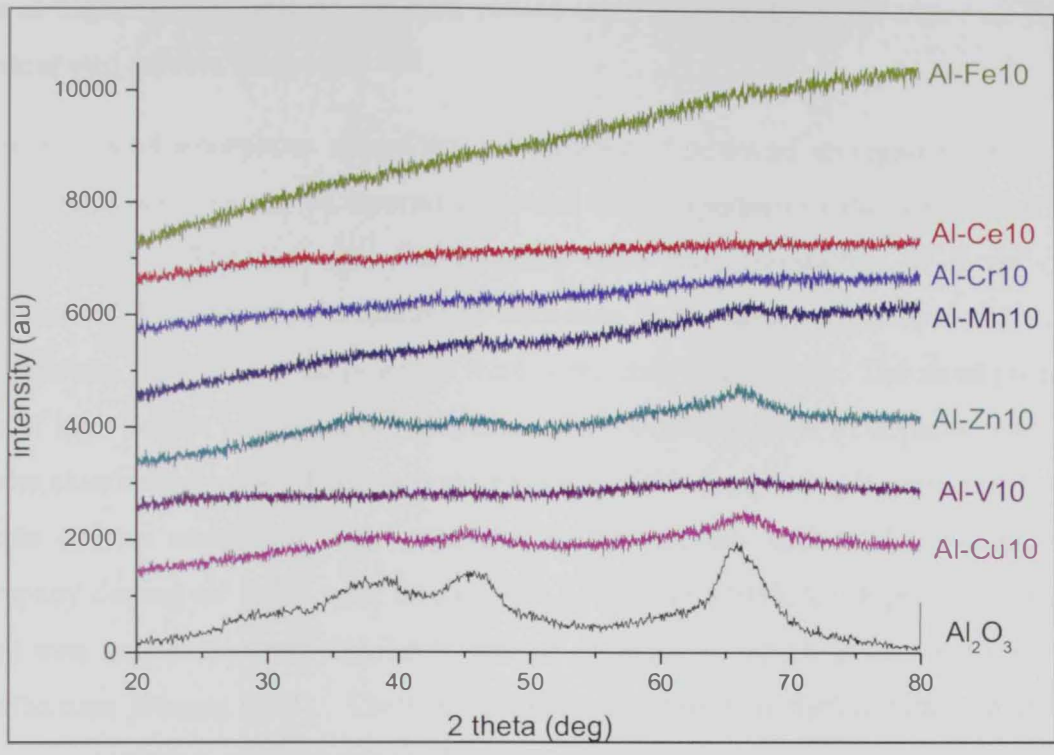


Figure 12. Powder XRD patterns of Al-M-10 of different metal ions versus γ - Al_2O_3 .

2.3.6.2 Effect of Metal ion Concentration on Crystallization

The XRD patterns of the different composites with 3% and 10% concentration of dopant metal ions as well as the pattern of undoped γ -alumina are shown in Figures 13-15. The patterns indicate that all composites are either amorphous or very weakly crystalline as compared with undoped γ -alumina which showed a higher degree of crystallinity. It was also noticed that the doped samples became more amorphous as the dopant ion concentration increased indicating an enhanced incorporation of the metal ions in the alumina lattice. Although the formation of segregated oxides of the dopant becomes more likely at higher concentrations, no such phases were detected by XRD where no features for segregated phases were observed.

The enhanced amorphous nature and the absence of peaks of segregated dopant metal oxides present an evidence of incorporation and well dispersion of the dopant ions in the alumina matrix. The fact that the powders were more crystalline at lower dopant concentration, 3%, indicates a minimum distortion in the lattice as compared with high concentration, 10%, where the powders were completely amorphous. The more pronounced effect of high dopant concentration may also reflect different ways of dopants' interaction with the alumina network. The lower crystallinity of the doped samples can be referred to possible defects associated with generated strain into the lattice which is known to accompany doping an oxide with foreign ions [102]. In addition, the presence of excess dopant ions may play a role similar to that of an impurity which is known to retard the crystallization process [103]. The fact that crystallization was further hindered at higher dopant concentration supports this explanation.

The enhanced hindering of crystallization at higher concentrations may indicate different modes of metal ions incorporation in the alumina matrix resulting in more disorder and hence lower tendency for crystallization. In addition, this behavior may indicate possible formation of segregated metal oxide species on the surface of alumina particles hindering the crystallization and growth process. Such segregated oxide particle could be too amorphous to be detected by XRD.

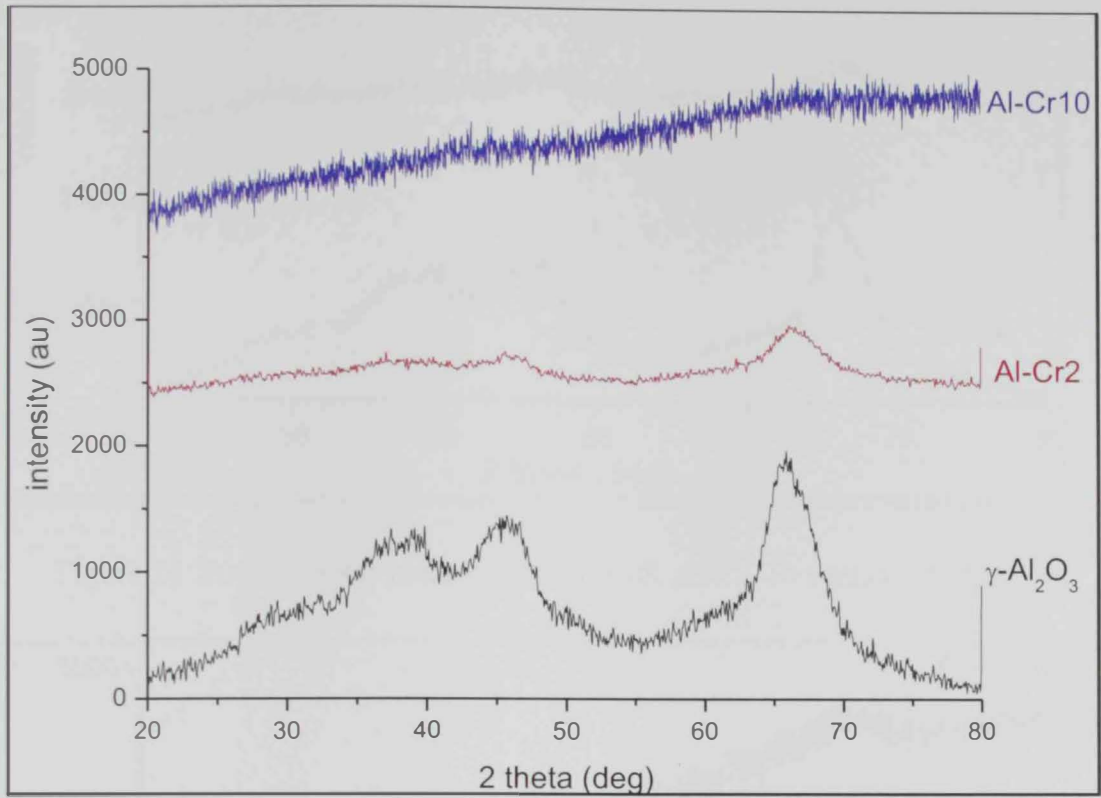


Figure 13. Powder XRD patterns of Al-Cr-3, Al-Cr-10 versus γ -Al₂O₃

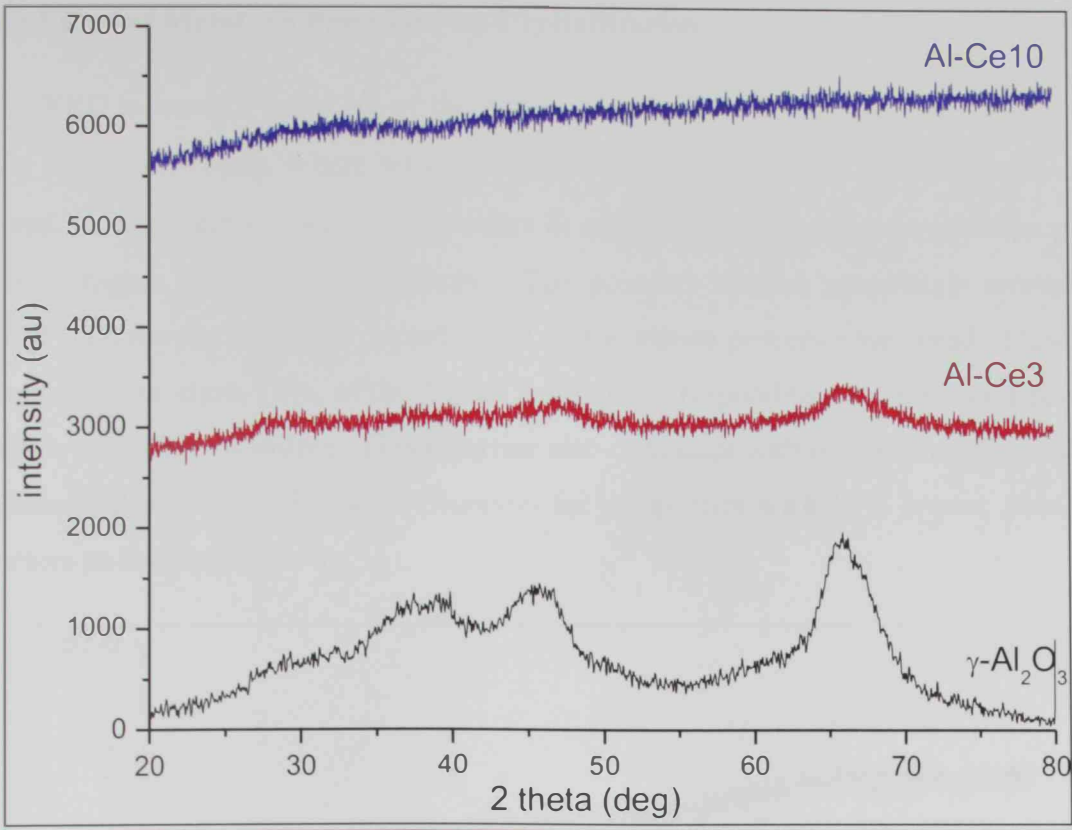


Figure 14. Powder XRD patterns of Al-Ce-03, Al-Ce-10 versus $\gamma\text{-Al}_2\text{O}_3$.

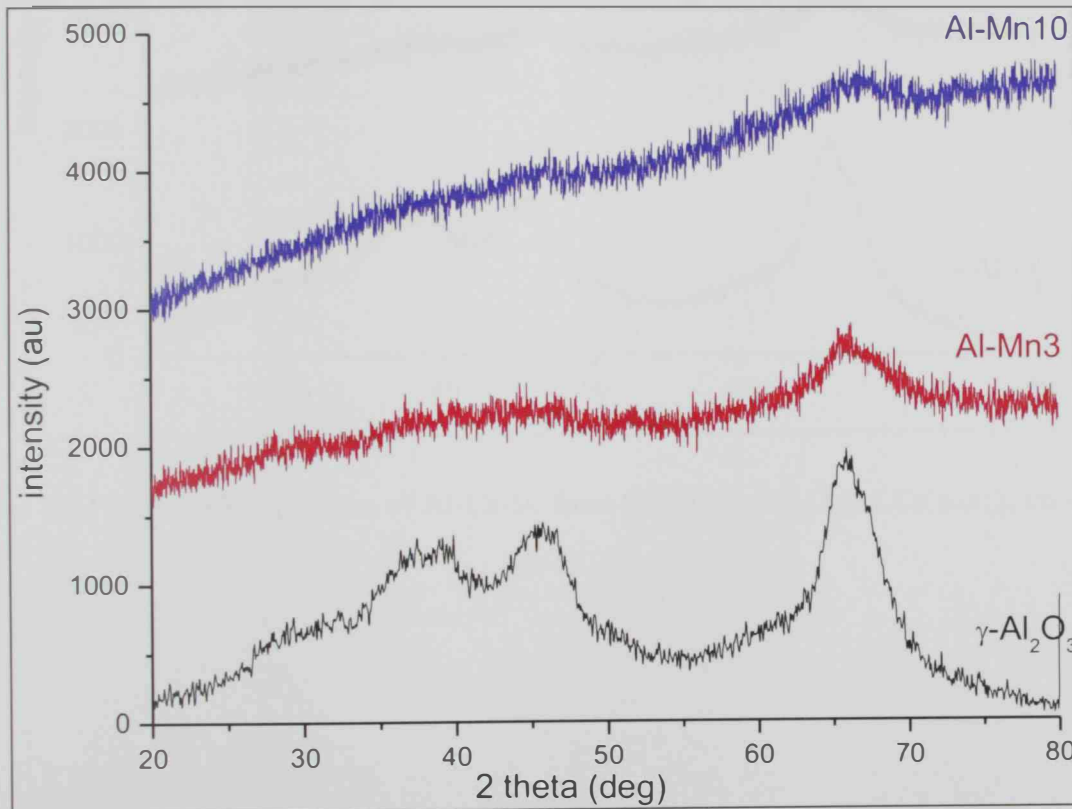


Figure 15. Powder XRD patterns of Al-Mn-03, Al-Mn-10 versus $\gamma\text{-Al}_2\text{O}_3$.

2.3.6.3 Effect of Metal ion Precursor on Crystallization

The XRD patterns, Figure 16, of the doped γ -alumina indicated the formation of very weakly crystalline solids, where weak and broad peaks that refer to γ -alumina only were observed, or completely amorphous powders as compared with undoped γ -alumina which showed a higher degree of crystallinity. The powders became completely amorphous when 10% concentration of the dopant based on the nitrate precursor was used. However, the same concentration, 10%, of the dopant from the corresponding acac precursor resulted in slightly crystalline powders. This behavior also correlates with the different textural and morphological properties that were observed for composites with 10% dopant from acac precursors as discussed below.

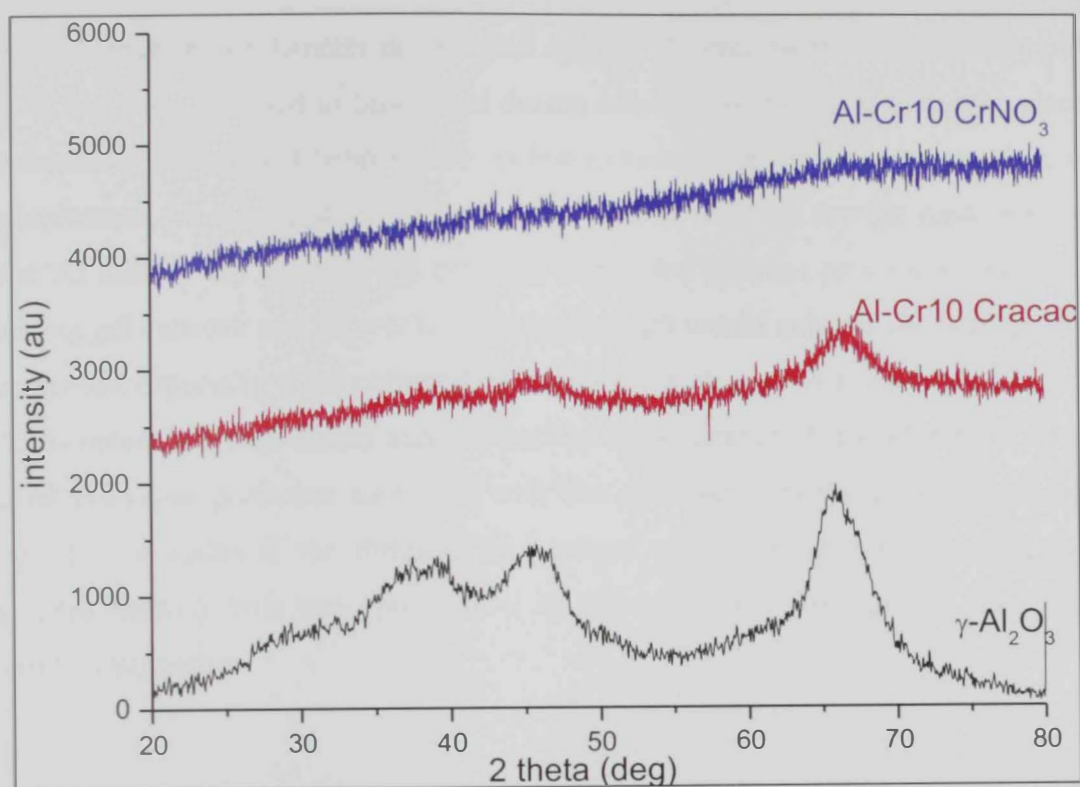


Figure 16. Powder XRD patterns of Al-Cr-10 from $\text{Cr}(\text{NO}_3)_3 \cdot 9\text{H}_2\text{O}$ and $\text{Cr}(\text{acac})_3$ versus $\gamma\text{-Al}_2\text{O}_3$.

The XRD results clearly indicate the incorporation of the metal ions in the alumina lattice and the absence of segregated oxide phase of the dopant metal. This incorporation can take place via the replacement of Al ion sites or occupying otherwise vacant interstitial sites in the alumina network. Replacing Al ions in the lattice is expected to depend largely on the ionic radius of the foreign metal ion. The closer the radius of the metal ion to that of Al³⁺ ion, the more likely the substitution to occur and a homogeneous bulk mixed oxide to form. However, some metal ions may form a different phase with aluminum ions with a different structure than γ -alumina such as Zn²⁺ which have a tendency to form the ZnAl₂O₄ of spinel structure. However the amorphous nature of the products did not help confirming the formation of such phases by XRD. Table 2 shows the ionic radii of the metals in study vs. that of Al³⁺ ion.

The substitution mechanism is expected also to depend on the precursor employed. While it has been reported to take place during calcinations [104], it may take place via transmetallation reaction at temperatures as low as room temperature in cases where metal acetylacetonate, M(acac)_n, precursor was used. In this case the foreign metal ions (Mⁿ⁺) replace Al ions in the alumina gel network during the gelation process producing Mⁿ⁺-containing gel network and Al(acac)₃. This mechanism would enhance the homogeneity of the composite especially if the radius of the metal ion is close to that of the aluminum ions. The transmetallation mechanism may explain the higher degree of crystallinity of Al-Cr-10 obtained from acac precursor compared with that obtained from the nitrate precursor, see Figure 16. In addition, the different and unique textural properties observed for the composites derived from acac precursors, as discussed in a (Section 2.3.7.4), strongly support this suggestion.

Table 2. The ionic radii (pm) of the different metal ions in study, $r(M^{n+})$, in 6- and 4- coordination.

M^{n+}	$r(M^{n+})$, 4-Coord.pm	$r(M^{n+})$, 6-Coord.pm
Al^{3+}	--	54
V^{3+}	--	64
Cr^{3+}	--	62
Mn^{2+}	--	58
Fe^{3+}	--	55
Cu^{2+}	60	--
Ce^{3+}	--	114 (8-coordinate)
Zn^{2+}	60	74

2.3.6.4 Thermal Stability of Metal doped γ -Alumina

While several studies have been reported on the enhanced thermal stability of γ -alumina by alkaline and alkaline-earth metal dopants, few studies have been reported on the stabilization of alumina structure by transition metal ions. Furthermore, the mechanism of stabilization is under debate. While some people referred the enhanced stabilization to the formation of surface layer of foreign metal aluminate [94], others referred the effect to the formation of a surface layer of the foreign oxide which decreases the surface energy [93]. The effect of foreign ions was also referred to possible occupation of interstitial holes in alumina lattice and decreasing oxygen vacancies in contact regions that are nucleation sites for the formation of γ -alumina [93]. Further work is needed to confirm the nature of the effect of the metal ions in the present work. Nevertheless, the absence of oxides of the dopant ions and the observed stability of the γ -phase of alumina indicates well dispersion of the metal ions in the alumina matrix.

One of the important properties of materials, depending on the application, is their textural and structural stability at elevated temperatures. Therefore, selected composites were calcined at elevated temperatures, as high as 900 °C, and were studied by XRD and N_2 adsorption. Al-V-7.5 was selected for an XRD study to evaluate their phase stability versus calcinations temperature as shown in Figure 17. The XRD patterns after calcination at temperatures between 500 °C and 900 °C, showed only reflection peaks that represent γ -alumina without any segregated vanadium oxide indicating a good stability of the dispersed vanadium ions in the alumina matrix as compared with pure γ -alumina which usually starts converting to θ and γ -phases at temperatures between 750 and 900°C. As the calcination temperature increased, the peaks became sharper and more intense as a consequence of enhanced crystallization associated with higher temperatures.

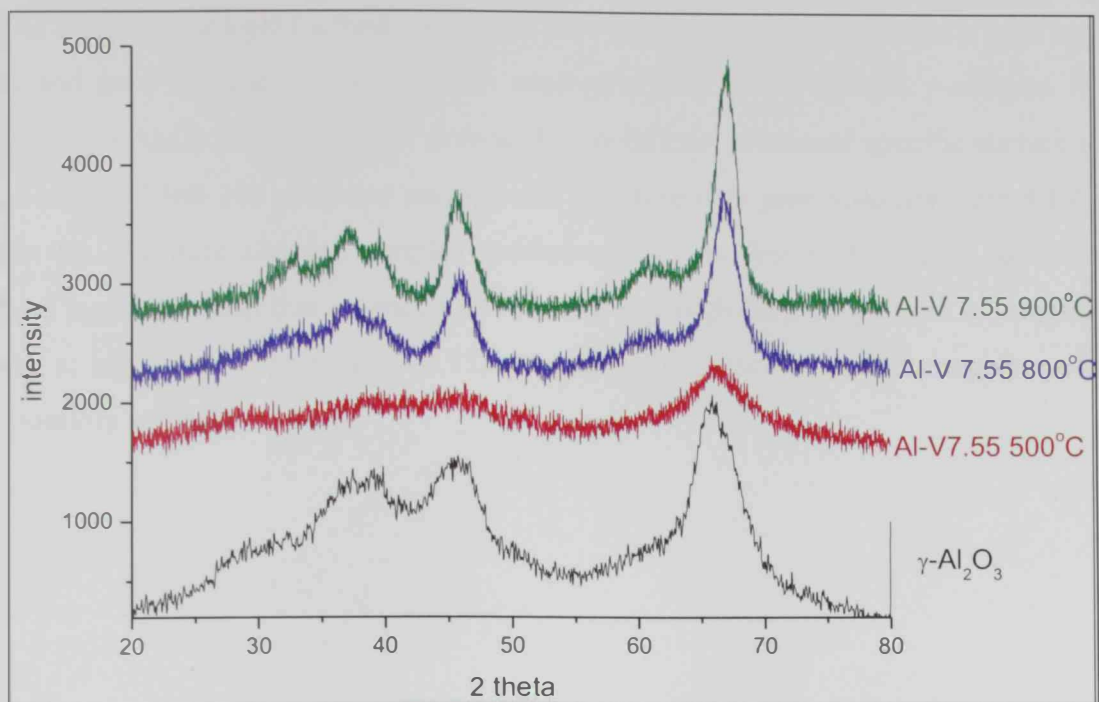


Figure 17. XRD patterns of Al-V -7.5 and calcinated at different temperatures versus the XRD pattern of pure γ -alumina.

2.3.7 Textural Properties by N₂-adsorption

2.3.7.1 Textural properties of pure γ -Al₂O₃

The employed sol-gel method resulted in pure γ -alumina with significantly high surface areas and pore volumes compared with analogous results for xerogel γ -alumina in the literature. γ -Al₂O₃ prepared under non-acidic conditions possessed specific surface areas in the range of 360-380 m²/g and mesoporous structure with pore volumes around 1.4 cc/g Figure 18. All pure alumina samples showed type-IV isotherms, Figure 19, with a well defined hysteresis loop that extended into a relatively high P/P₀ range with continuous N₂ uptake at high relative pressures >0.95, indicating the presence of high-range mesopores and possibly some macropores.

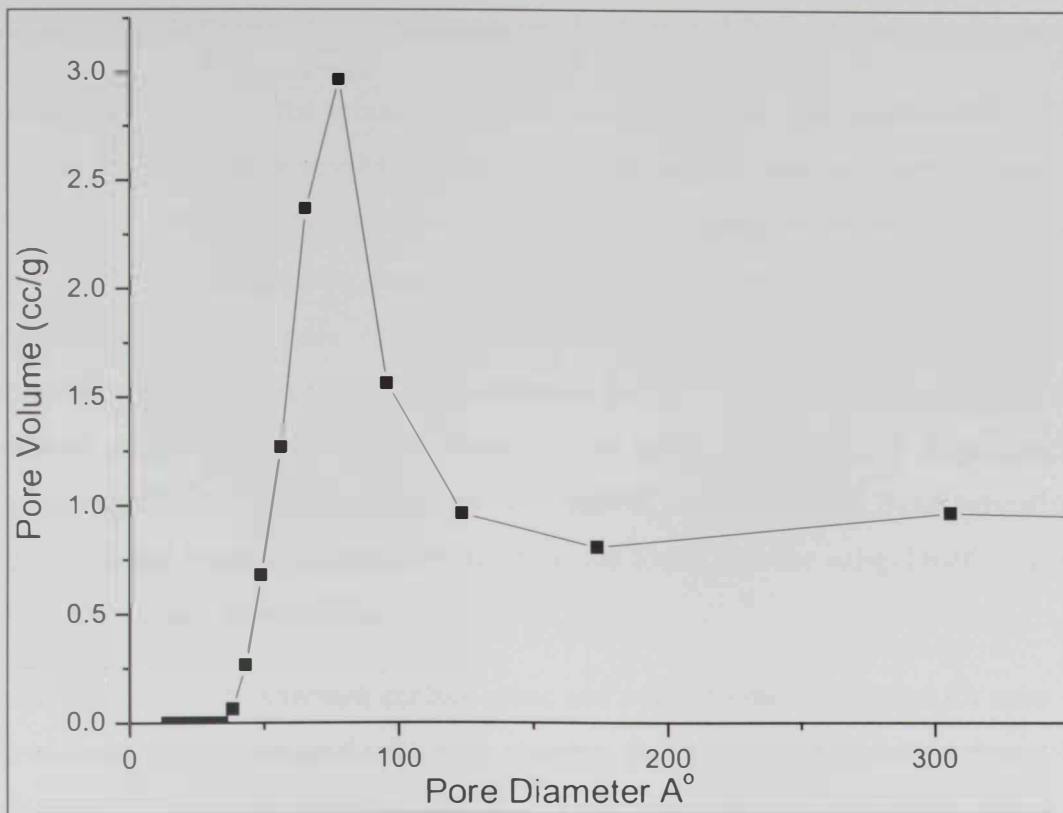


Figure 18. BJH pore size distribution of pure γ -alumina.

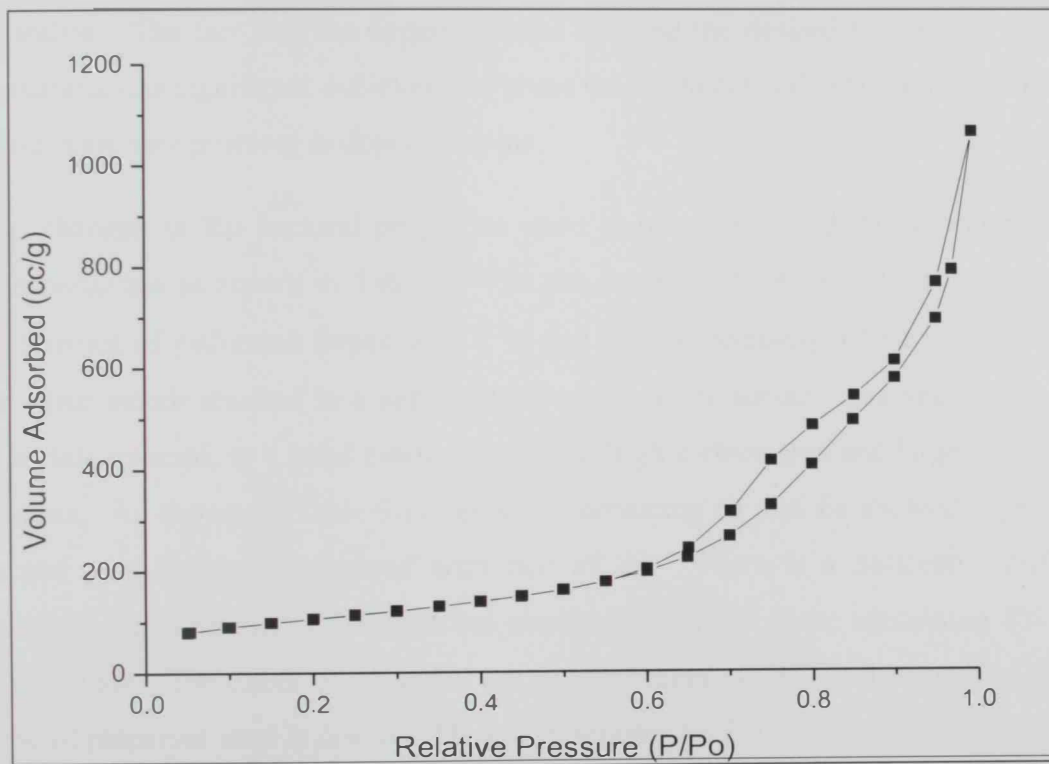


Figure 19. N_2 adsorption-desorption isotherms of pure γ -alumina.

2.3.7.2 Effect of Different Metal Dopants on the Textural Properties of γ -alumina

According to most of the literature on metal-doped alumina, the incorporation of metal ions in the alumina matrix results in a decrease in its surface area and pore volume [105]. However, the observed decrease does not necessarily result in poorer performance of doped alumina. In many cases, doped γ -alumina has shown better performance as catalyst supports compared with pure alumina [105]. In addition, the textural properties of the doped alumina depend largely on the preparative method. In a study where alumina was doped with various foreign metal ions using three preparative methods: impregnation of Al_2O_3 , impregnation of $\text{AlO}(\text{OH})$, and sol-gel method, where the other metal precursor was introduced during the sol-gel transformation, it was found that the sol-gel method gave the highest BET surface areas [106].

In the present work, although surface areas and pore volumes decreased for most of the prepared composites compared with pure alumina, they were comparable to those of pure alumina in the case of some metal ions. More importantly, they were significantly improved in most cases where $\text{Cr}(\text{acac})_3$ precursor was employed. The final textural properties were dependent on the dopant ion content, precursors, and the presence of an acid catalyst. The fact that the doped alumina retained the desired textural properties of pure alumina is a significant achievement given the chemical and structural modifications the metal ions may promote in doped alumina.

The changes in the textural properties upon doping were largely dependent on the foreign metal ion as shown in Tables 3-4 in this section. Table 3 and Table 4 show the characteristics of γ -alumina doped with 2 % and 3%, respectively, of various metal ions. While some metals resulted in a noticeable decrease in the surface area and pore volume, other metals retained, to a good extent, the typical high surface area and large pore volume of alumina. As shown in Table 3 composites containing Cr and Fe showed high surface areas and pore volumes compared with that of Zn. There is a noticeable difference between the characteristics of composites containing 2% and those containing 3% of the same metal ion. The effect of the metal ion concentration as well as the possible effect of the type of precursor used is discussed below in section 2.3.7.4.

It is noteworthy to point out that Cu(II) and Ce(III)-containing alumina retained significantly high surface areas and pore volumes at 3% concentration as compared with other metal ions such as Fe(III) which showed a considerable decrease in surface area and

porosity when the concentration increased from 2% to 3%. The observed variations clearly indicate that the metal ion plays a key role in the final textural properties, which may indicate different modes of interaction between the guest ion and the alumina network. The fact that 2% concentration showed only slight, or negligible, effect on the textural properties supports the suggestion of more homogeneous dispersion in the lattice. Based on these results, it can be suggested that doping of γ -alumina with transition metal ions should not exceed 2% if the desired textural properties are to be preserved.

Table 3. BET surface area and pore characteristics of Al-M-2% after calcinations at 500 °C.

M ⁿ⁺	M ⁿ⁺ precursor	Surface area (m ² /g)	Pore volume (cc/g)	Pore size (Å°)
γ-alumina	-	377	1.65	174.6
Cr	nitrate	325	0.92	113.5
Fe	nitrate	302	0.87	115.4
Zn	acetate	226	0.60	105.9

Table 4. BET surface area and pore characteristics of Al-M-3% after calcinations at 500 °C.

M ⁿ⁺	M ⁿ⁺ Precursor	Surface area (m ² /g)	Pore volume (cc/g)	Pore size (Å°)
γ-alumina	-	377	1.65	174.6
Fe	nitrate	218	0.47	86.0
Ce	nitrate	280	0.84	120.7
Mn	chloride	258	0.56	87.2
V	chloride	199	0.53	107.2
Zn	acetate	246	0.58	94.4
Cu	acac	279	0.77	110.1
Cr	nitrate	261	0.46	70.3

All composites containing 2% and 3% metal ions showed type-IV N_2 -adsorption-desorption isotherms as shown in Figure 20. All isotherms exhibit a well defined hysteresis loop in the P/P_0 range of 0.65-0.85 and a plateau at higher relative pressures indicating the presence of relatively homogenous mesopores only.

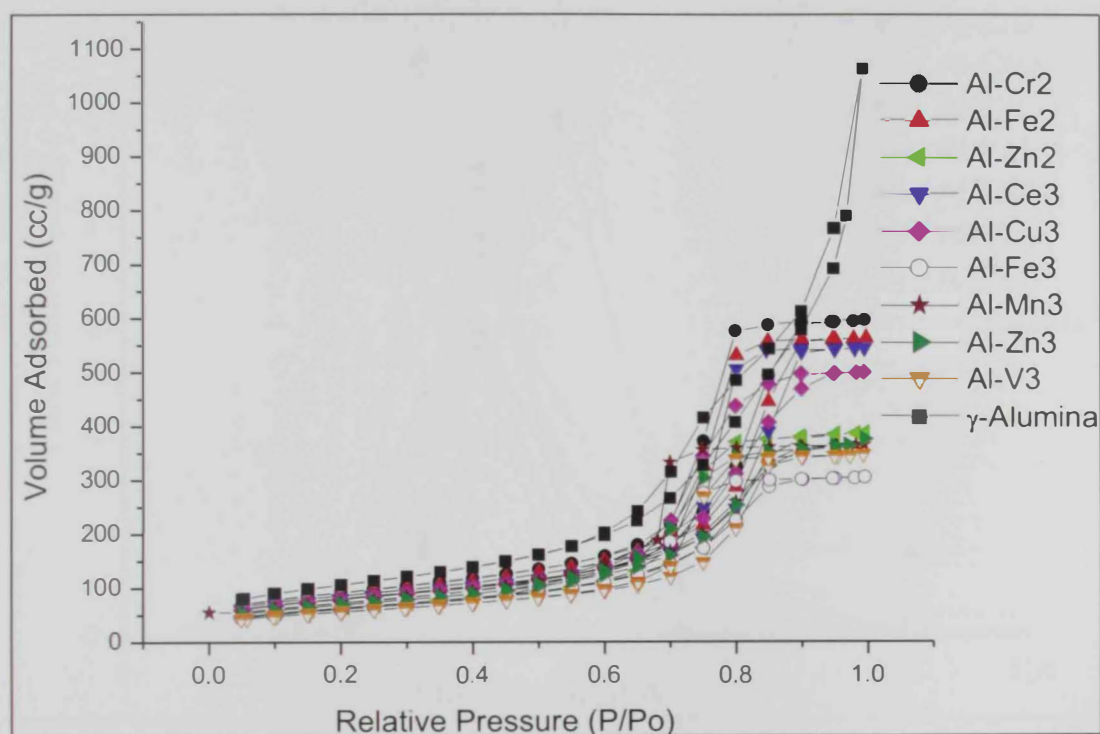


Figure 20. N_2 adsorption-desorption isotherms of composites containing 2% and 3% of various metal ions.

The BJH pore size distribution of all composites containing 2% and 3% metal ions are shown in Figure 21. They all exhibited sharper pore size distribution compared with pure alumina indicating more homogeneous pore structures of the composites. While the pore average diameter varied slightly, the pore size distributions are generally similar to that of pure alumina shown in Figure 18.

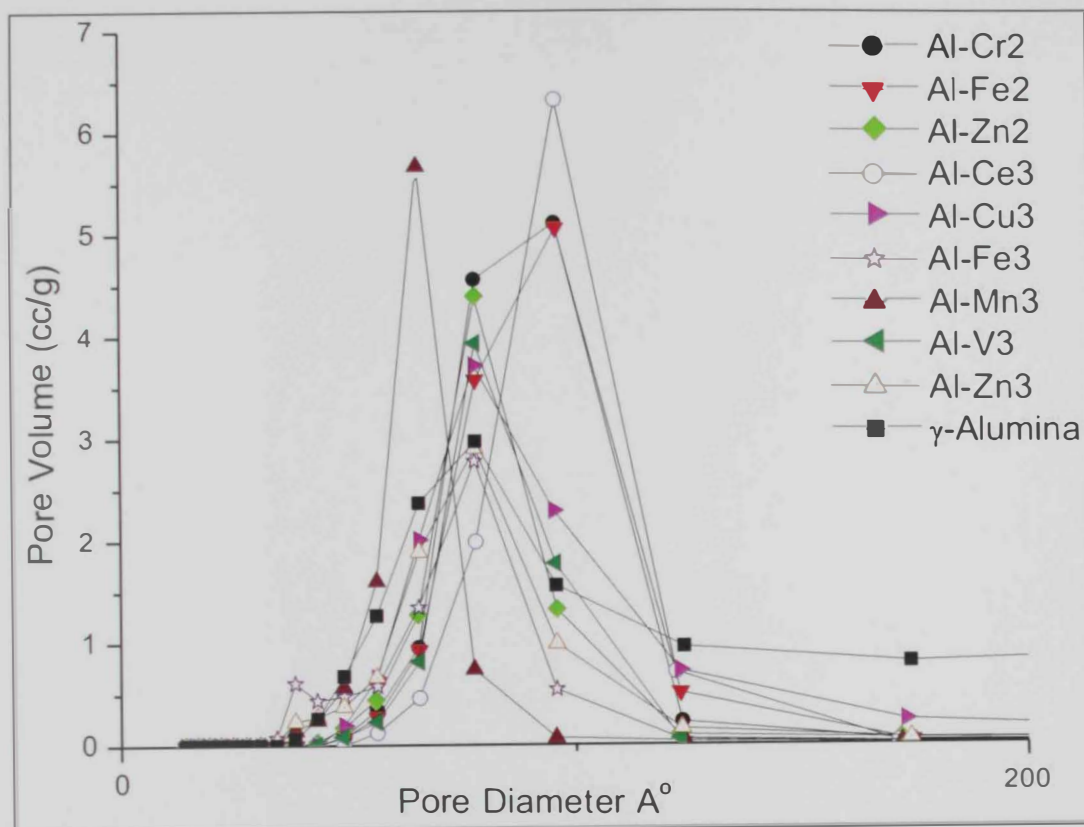


Figure 21. BJH pore size distribution of all composites containing 2% and 3% of various metal ions versus γ -alumina.

While all composites showed the same trend of surface area decrease as the concentration increased, some dopants retained noticeably higher surface areas than others as the concentration was increased to 5% as shown in Table 5. In particular, Mn^{2+} and Ce^{3+} showed the highest surface area and the slowest rate of decrease. It is noteworthy to remind here that Mn^{2+} and Ce^{3+} are the two ions that resulted in colloidal gels during the preparation as compared with clear gels in the case of other metal ions. These variations, although not well understood, indicate that the nature of the metal ion plays a key role in the gel formation process which eventually affects the final textural properties, which may indicate different modes of interaction between the guest ion and the alumina network.

Table 5. BET surface area and pore characteristics of Al-M-5% after calcinations at 500 °C.

M ⁿ⁺	M ⁿ⁺ precursor	Surface area (m ² /g)	Pore volume (cc/g)	Pore size (Å)
Fe	nitrate	175	0.44	99.6
Ce	nitrate	326	0.78	95.8
Cr	nitrate	261	0.46	70.3
Mn	chloride	326	0.82	101.0
Cu	acac	217	0.42	77.8
Zn	acetate	290	0.79	109.9

Table 5. BET surface area and pore characteristics of Al-M-5% after calcinations at 500 °C.

M ⁿ⁺	M ⁿ⁺ precursor	Surface area (m ² /g)	Pore volume (cc/g)	Pore size (Å)
Fe	nitrate	175	0.44	99.6
Ce	nitrate	326	0.78	95.8
Cr	nitrate	261	0.46	70.3
Mn	chloride	326	0.82	101.0
Cu	acac	217	0.42	77.8
Zn	acetate	290	0.79	109.9

Again all powders are mesoporous as indicated by their type-IV isotherms, Figure 22, with relatively homogeneous pore sizes in the range between 50-150 Å, Figure 23. However, Cu(II)-containing powder shows a very sharp pore size distribution compared with all other composites. While the effect of concentration will be discussed for each metal separately, it is noteworthy to point out that some ions retained higher surface areas and pore volumes than others at 5% concentration and the metal ion that showed the largest decrease is Fe³⁺.

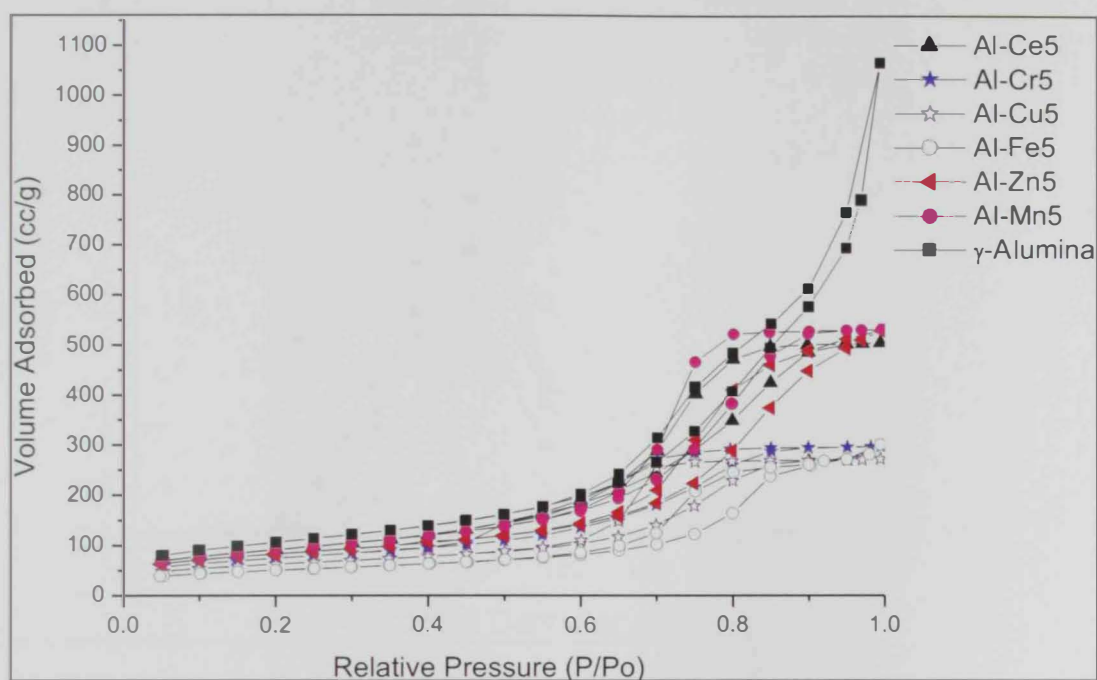


Figure 22 . N₂ adsorption-desorption isotherms of composites containing 5% of various metal ions.

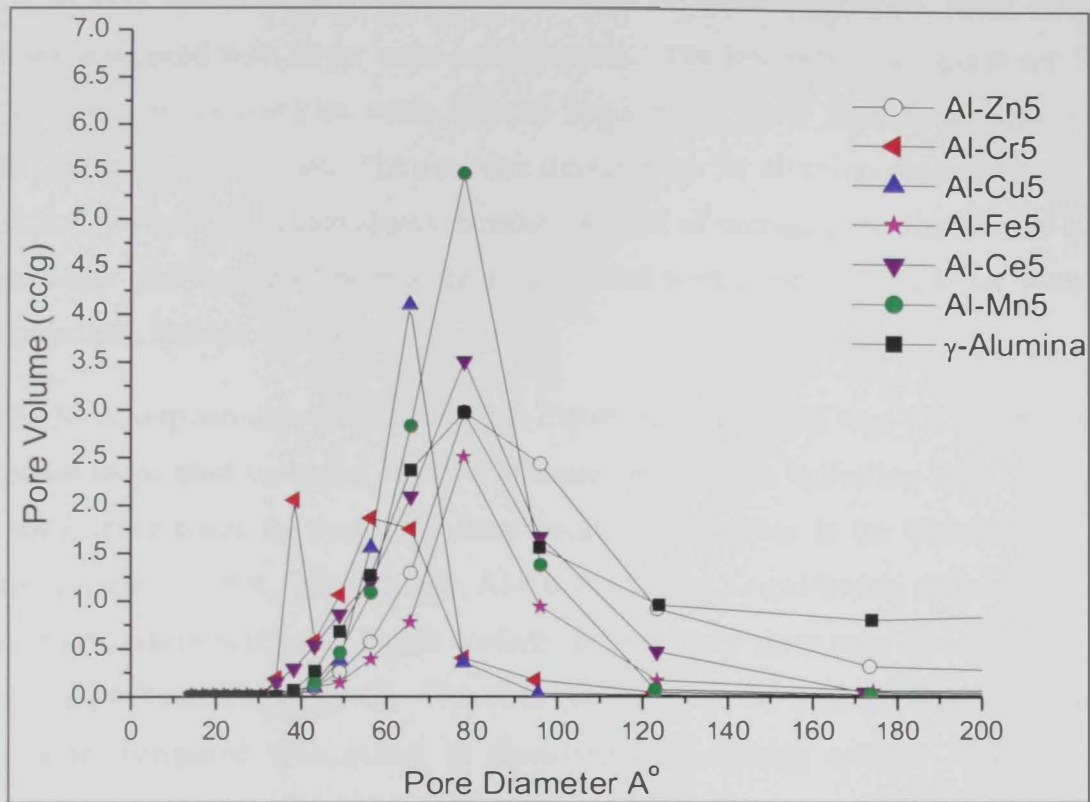


Figure 23. BJH pore size distribution of all composites containing 5% of various metal ions versus alumina.

While concentration of 2% showed no significant changes in the desired textural properties of γ -alumina, 10% concentration was accompanied by a considerable decrease in the surface area and the pore volume indicating a noticeable sintering, as shown in Table 6. The highest specific surface areas at 10% concentration were observed for the Al-Cu, and Al-Zn composites. While only copper showed small average pore diameter comparable with previous composites, all others showed a noticeable shift in the average pore diameter to a larger range of size. The observed smaller surface areas and larger pore diameters may indicate that higher concentrations of metal ion dopant result in larger particles associated with larger inter-particle pores. The low range mesopores are likely due to inter-primary particles voids and the larger pores result from voids between the larger aggregates of particles. The pore size distributions for all composites of 10% dopant are shown in Figure 24 which shows, besides the shift of average pore diameters to higher range, wider distribution of pore sizes as compared with composites of lower metal ion concentrations discussed before.

The N_2 adsorption-desorption isotherms Figure 25 are still of type-IV except that the hysteresis loops shift to higher relative pressure, P/P_0 range indicating large mesopores and some macropores for those that show continuous increase in the adsorption at high relative pressures, > 0.9 . Interestingly, Al-Cu-10 showed a significantly different behavior from others, where noticeably higher surface area and very sharp pore size distribution of mesopores, 4-7 nm, was observed. This could be related to the different precursor that was used, acac, compared with others as discussed in a coming section. The observed characteristics encourage for further work on additional structural and morphological characterization of this composite. Another composite that is worth further studies is Al-Zn-10 which showed relatively high surface area and large total pore volume in the mesopore range only.

Table 6. BET surface area and pore characteristics of Al-M-10% after calcinations at 500 °C.

M ⁿ⁺	M ⁿ⁺ precursor	Surface area (m ² /g)	Pore volume (cc/g)	Pore size (Å)
γ-Alumina	ASB	377	1.65	174.6
Cr	nitrate	188	0.70	148.7
Fe	nitrate	168	0.58	138.4
Ce	nitrate	126	0.59	188.1
Mn	chloride	173	0.71	165.6
V	chloride	143	0.60	167.3
Cu	acac	300	0.45	64.8
Zn	acetate	265	0.76	116.5

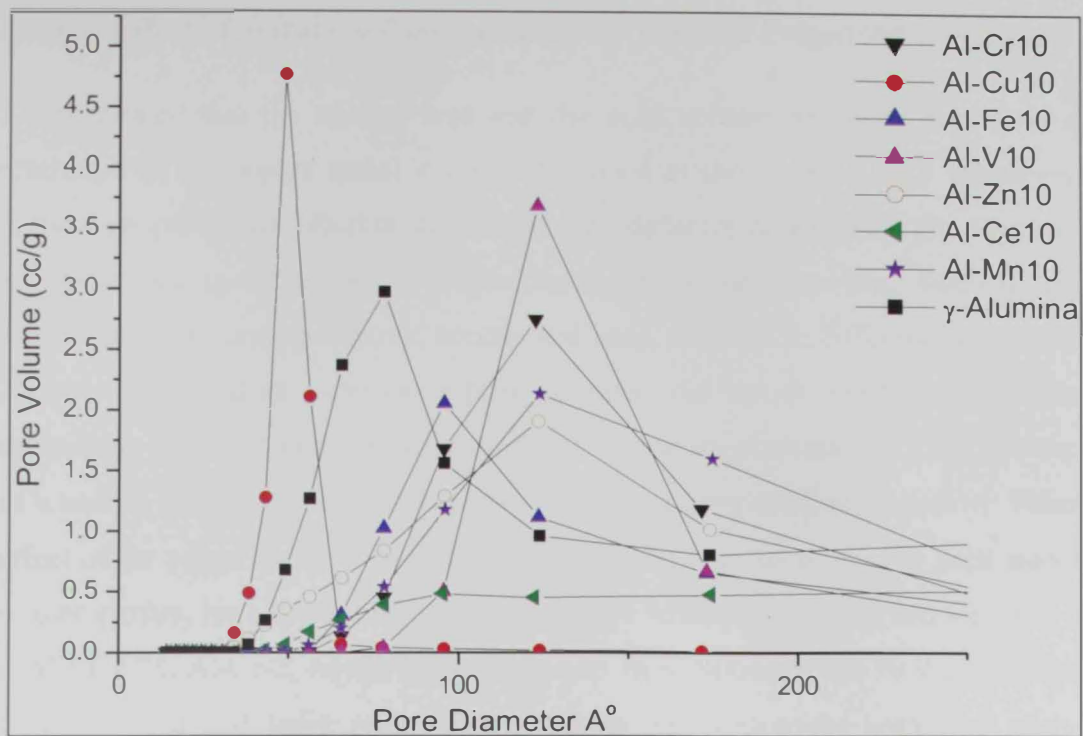


Figure 24. BJH pore size distribution of all composites containing 10% of various metal ions versus pure alumina.

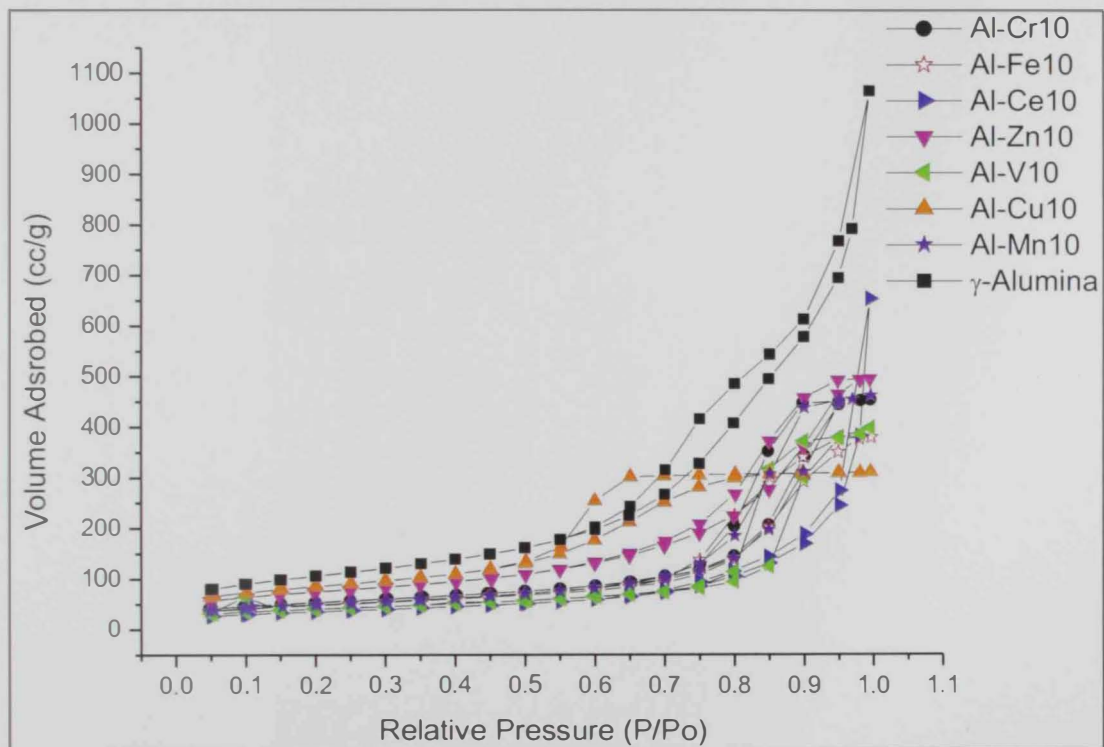


Figure 25. N_2 adsorption-desorption isotherms of composites containing 10% of various metal ions versus pure alumina.

2.3.7.3 The Effect of Metal ion Concentration on Textural Properties of γ -Alumina

It was noticed that the surface area and the pore volume generally decreased as the concentration of the dopant metal ion was increased as shown in Table 7 which presents the textural properties of different metal ions with different concentrations. However, the extent of decrease in the surface area was dependent on the metal ion. Interestingly, the precursors based on organic anions, acetate and acac, resulted in different behavior where the surface areas, and in some cases pore volumes, did not decrease at high metal ion concentrations and were comparable with those of low concentrations. This was the case with Cu and Zn ions where acac and acetate precursors were used, respectively. Therefore, the effect of the precursor is discussed separately in the next section. The most interesting textural properties, high surface areas and large pore volumes, are observed for Al-V-3, Al-Fe-2, Al-Cr-0.75, Al-Cr-2, Al-Ce-5 and Al-Mn-5. In addition, Al-Zn-10 showed relatively high surface area and large pore volume among the composites with high metal ion concentrations.

Table 7. BET surface area and pore characteristics of composites with different metal ions concentrations after calcinations at 500 °C.

M ⁿ⁺	M ⁿ⁺ (%)	M ⁿ⁺ Precursor	Surface area (m ² /g)	Pore volume (cc/g)	Pore size (Å ^o)
Cr	0.75	nitrate	292	0.96	130.1
	2	nitrate	325	0.92	113.5
	3	nitrate	261	0.46	70.3
	10	nitrate	166	0.65	155.7
Fe	2	nitrate	302	0.875	115.4
	3	nitrate	218	0.47	86.0
	5	nitrate	175	0.44	99.6
	10	nitrate	168	0.58	138.4
V	3	chloride	328	1.23	150.2
	7.5	chloride	220	0.57	104.5
	10	chloride	143	0.60	167.3
Ce	3	nitrate	280	0.84	120.7
	5	nitrate	326	0.78	95.8
	10	nitrate	126	0.59	188.1
Mn	3	chloride	258	0.56	87.2
	5	chloride	326	0.82	101.0
	10	chloride	173	0.71	165.6
Zn	2	acetate	226	0.60	105.9
	3	acetate	246	0.58	94.4
	10	acetate	254	0.73	115.5
Cu	3	acac	279	0.77	11.1
	5	acac	217	0.42	77.8
	10	acac	277	0.45	64.8
	20	acac	125	0.13	41.5

The N₂ adsorption-desorption isotherms and pore size distributions of selected systems for different metal ion concentrations from different precursors are shown in Figure 26 - Figure 39. It is noticed that generally a concentration of 10% of metal ion shifted the hysteresis loop to higher mesopore range and the pore size distribution became less homogeneous. The only exception was for Al-Cu-10 which showed narrow pore size distribution in the low range mesopore. This behavior could be referred to the acac ligand which was used in the copper-containing composites as discussed below. In addition, a high concentration of 20% was studied for Cu (II) ions and it was found that the surface area and the pore volume decreased considerably while the average pore diameter shifted to low range mesopores and the pore size distribution became very narrow.

These changes at 20% concentration reflect a noticeably less porous powder. Interestingly, the surface areas and the pore volumes exhibited by most of the prepared metal-doped alumina samples are higher than those reported in analogous studies in the literature. As an example, in a study on Cr(III)-doped γ -alumina, composites with Cr ion concentrations between 0.05 and 1% possessed surface areas below 200 m²/g [99]. In the present study Cr(III) concentration of 0.75% resulted in surface areas between 292 and 455 m²/g depending on the precursor employed. In another study, La-doped alumina prepared by sol-gel method showed a surface area around 100 m²/g and pore volume of 0.324 cc/g after calcinations at 600 °C which are considerably lower than analogous results in the present work [107].

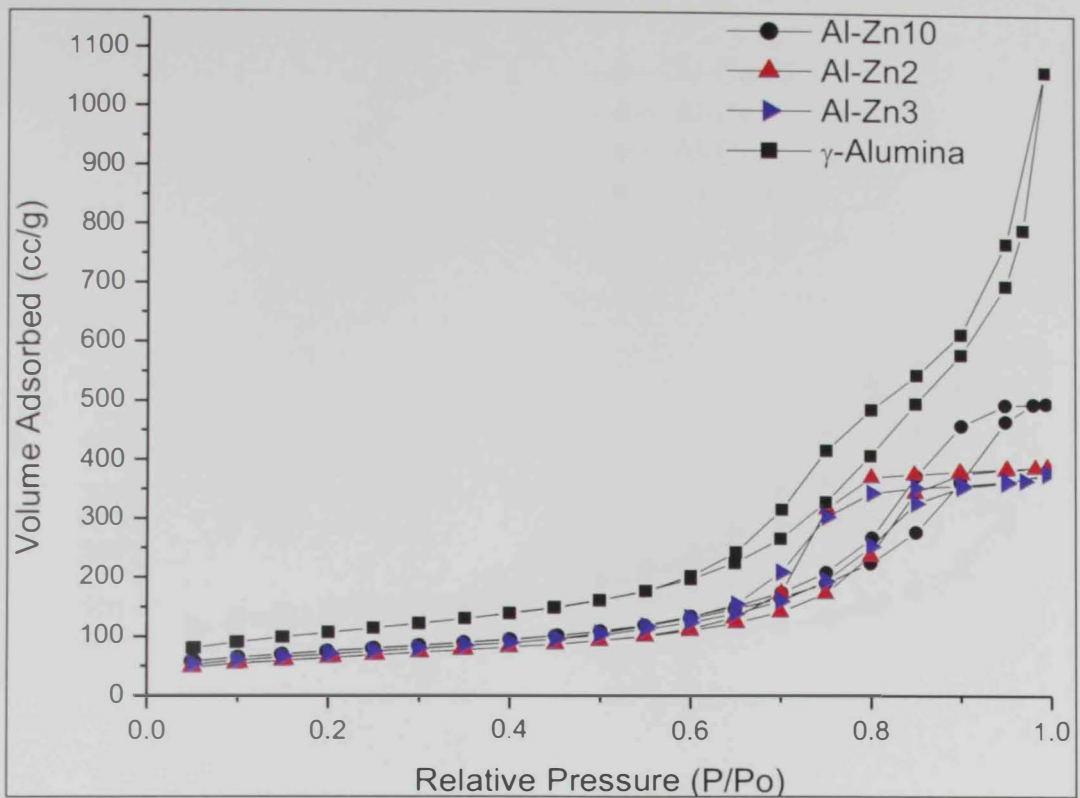


Figure 26. N₂ adsorption-desorption isotherms of Al-Zn-2, Al-Zn-3 and Al-Zn-10 versus alumina.

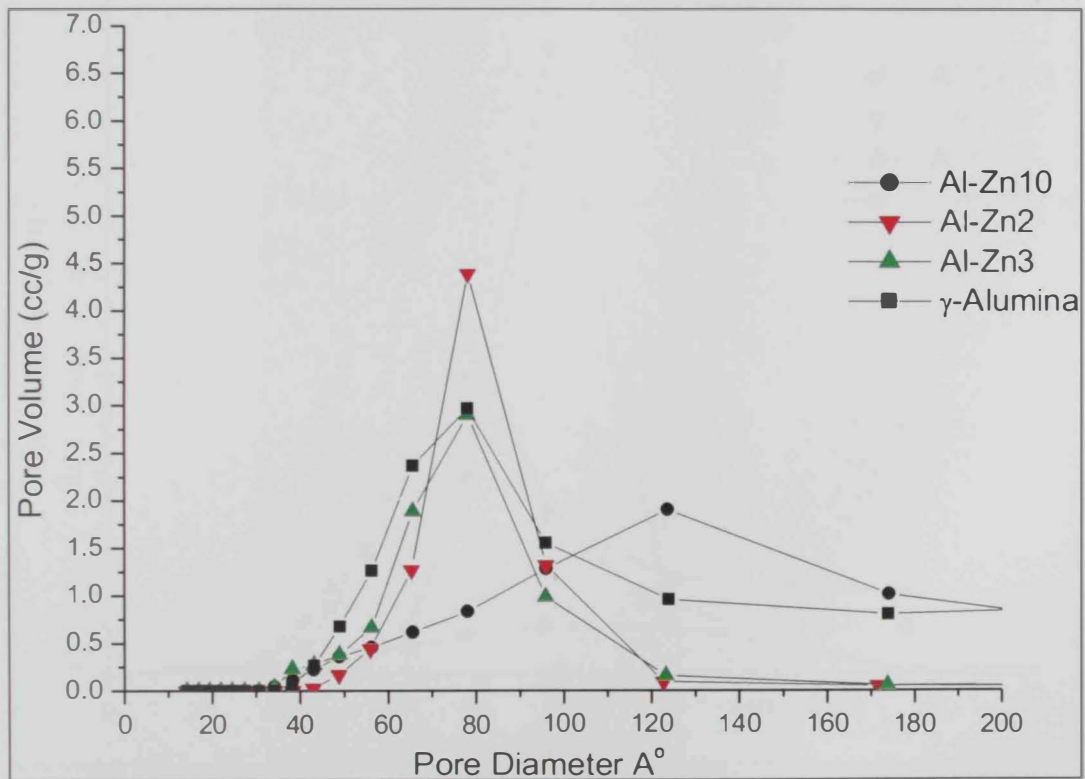


Figure 27. BJH pore size distribution of Al-Zn-2, Al-Zn-3 and Al-Zn-10 versus alumina.

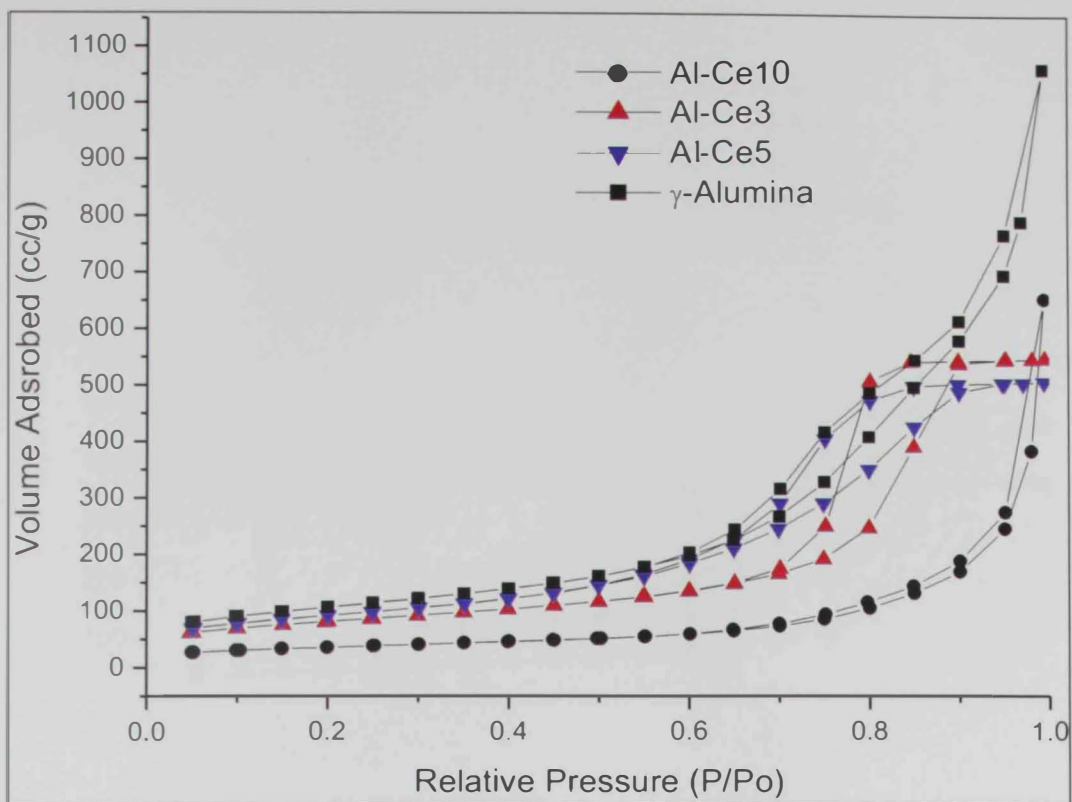


Figure 28. N₂ adsorption-desorption isotherms of Al-Ce-3, Al-Ce-5 and Al-Ce-10.

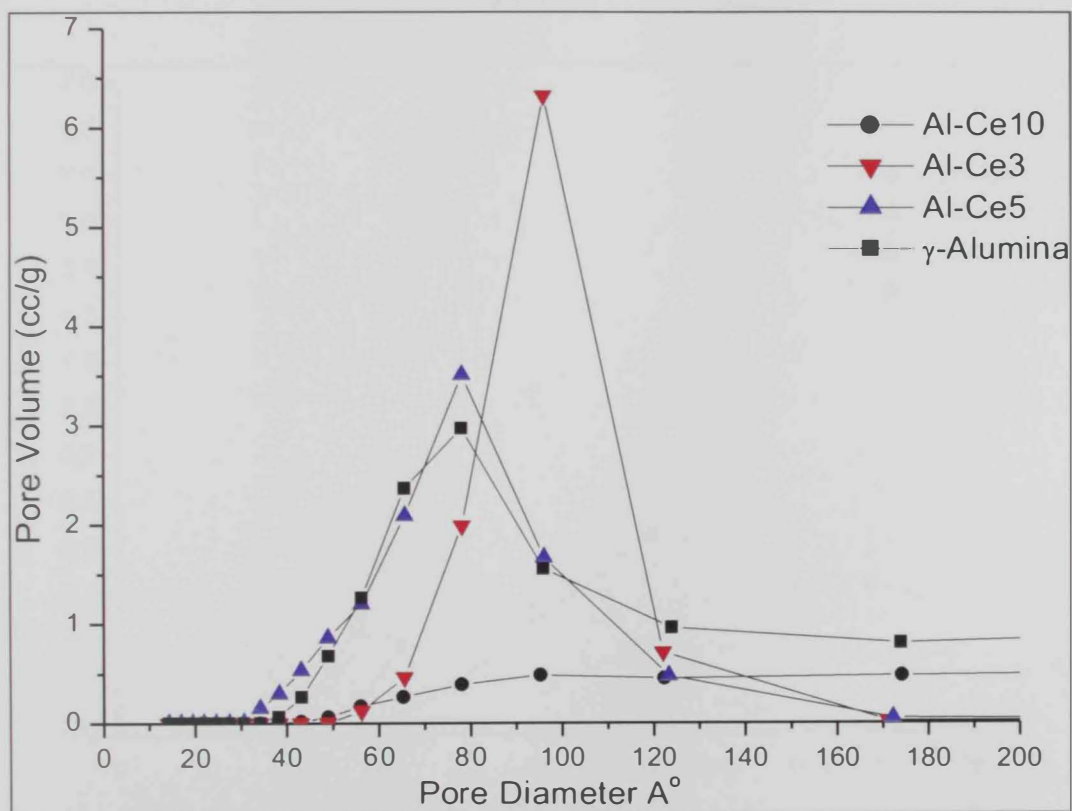


Figure 29. BJH pore size distribution of Al-Ce-3, Al-Ce-5 and Al-Ce-10 versus alumina.

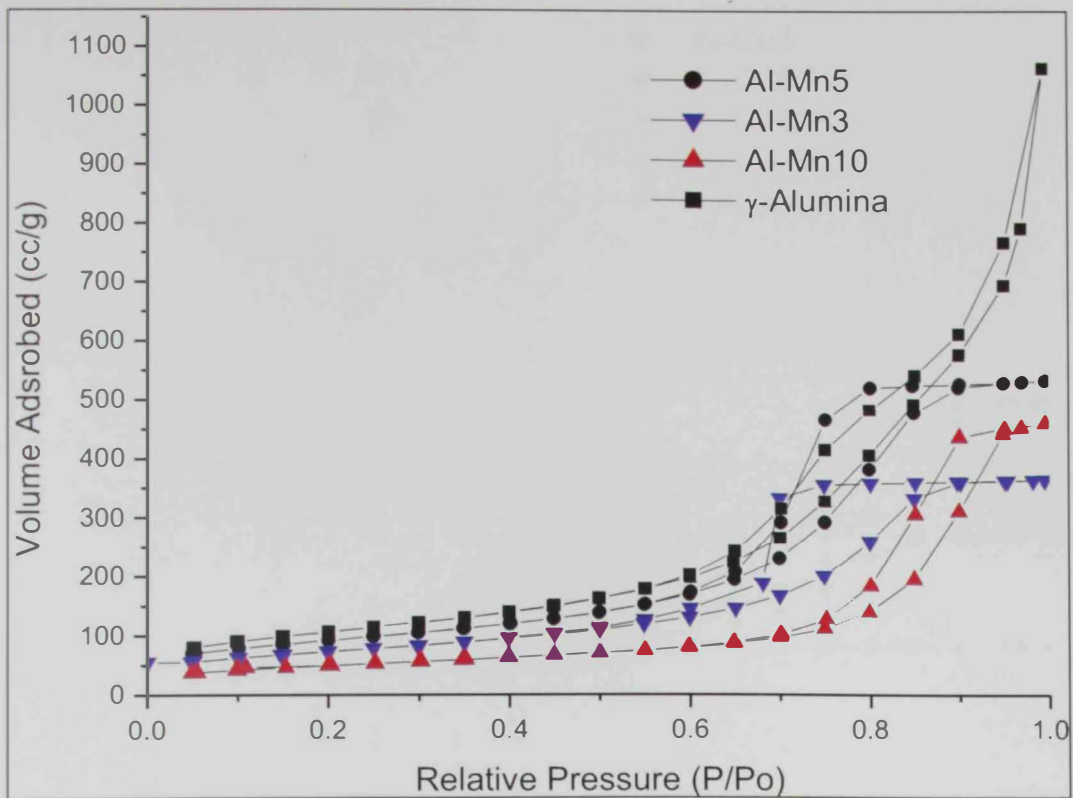


Figure 30. N₂ adsorption-desorption isotherms of Al-Mn-3, Al-Mn-5 and Al-Mn-10 versus alumina

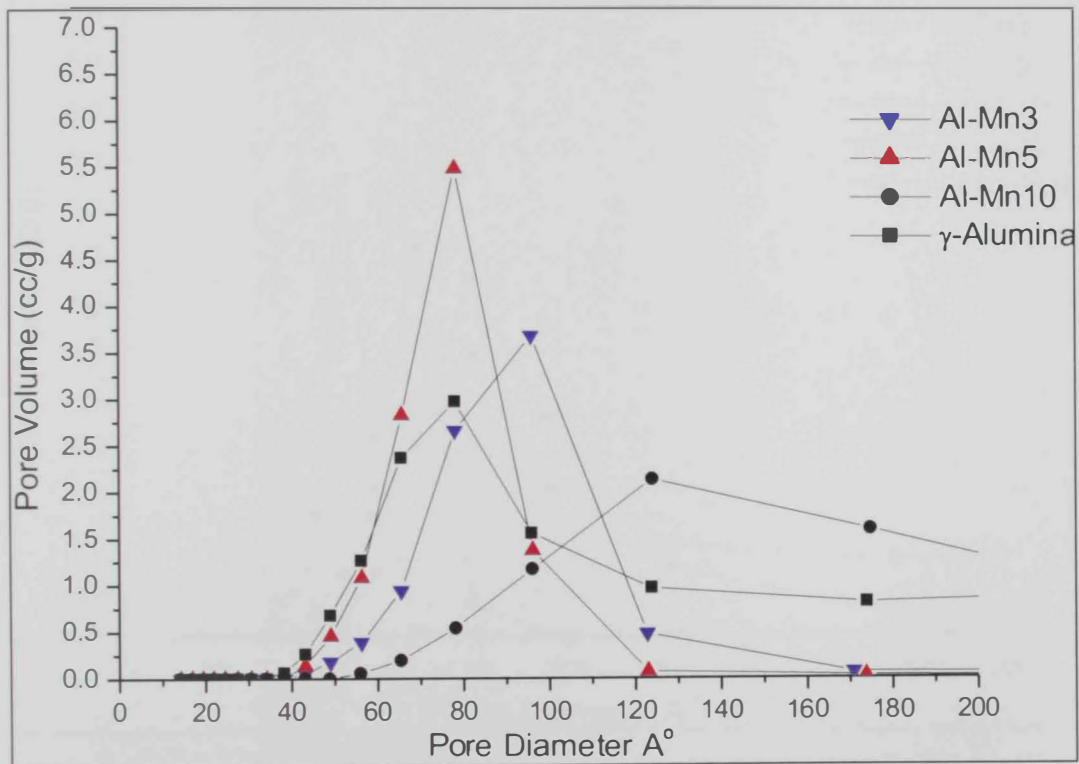


Figure 31. BJH pore size distribution of Al-Mn-3, Al-Mn-5 and Al-Mn-10 versus alumina.

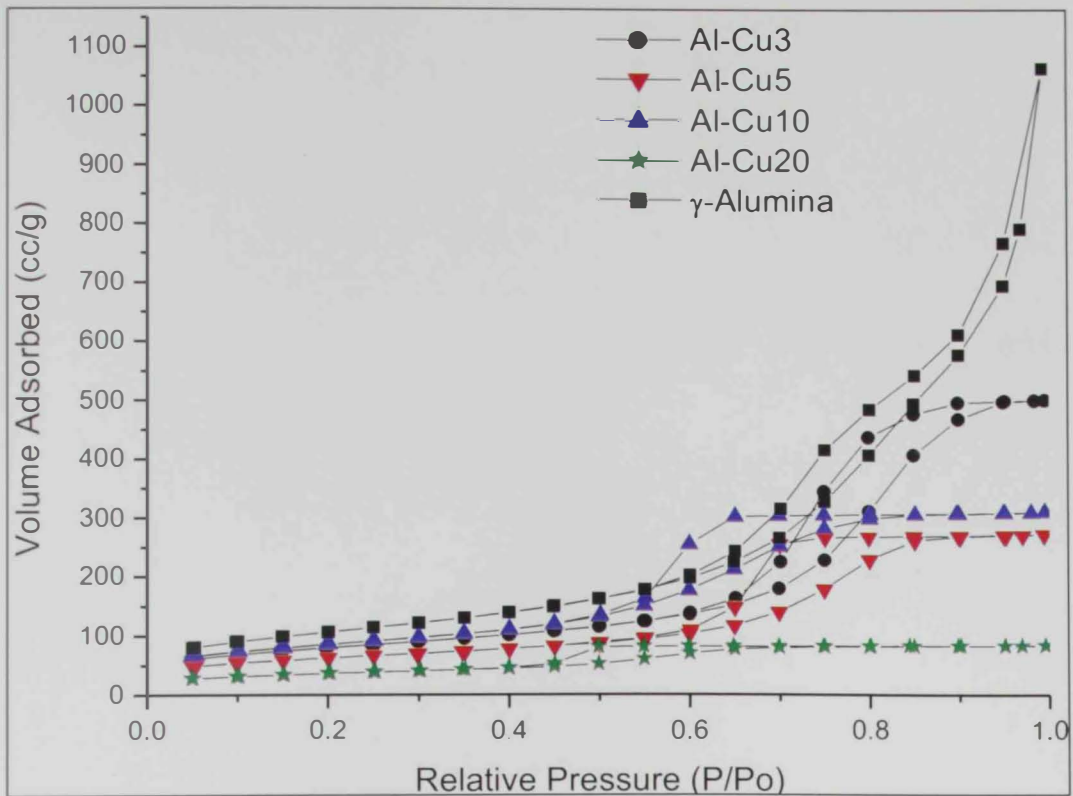


Figure 32. N₂ adsorption-desorption isotherms of Al-Cu-3, Al-Cu-5, Al-Cu-10 and Al-Cu-20

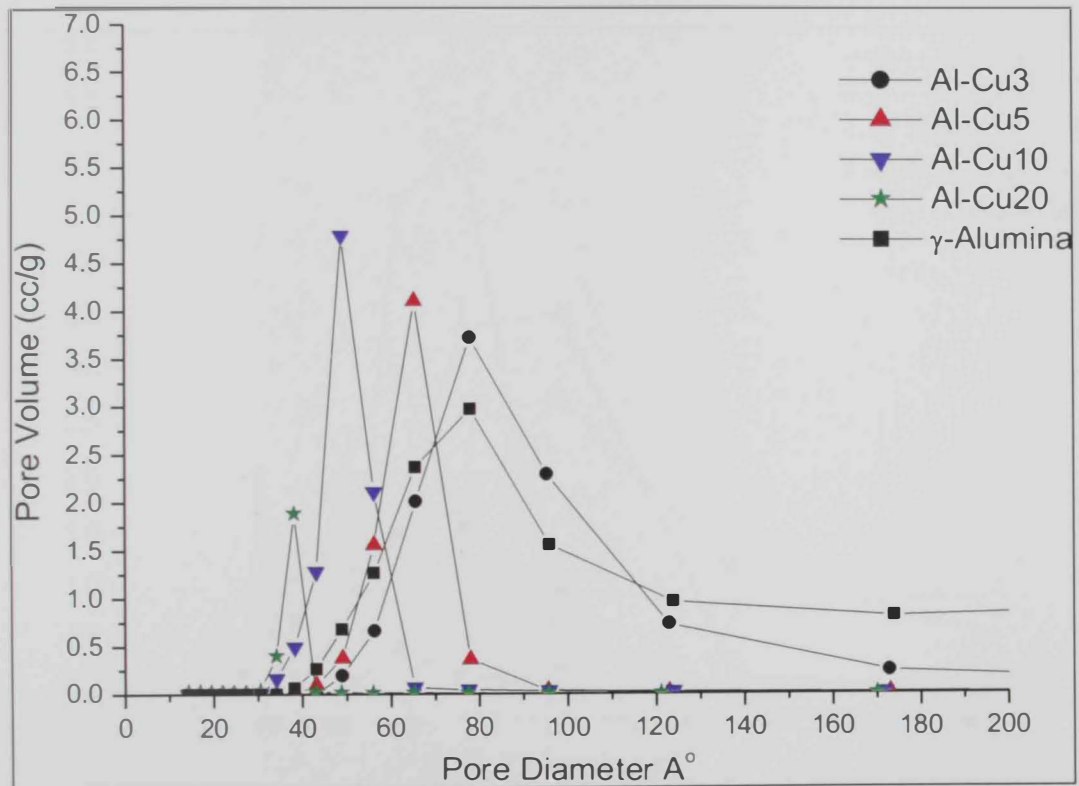


Figure 33. BJH pore size distribution of Al-Cu-3, Al-Cu-5, Al-Cu-10 and Al-Cu-20 versus alumina.

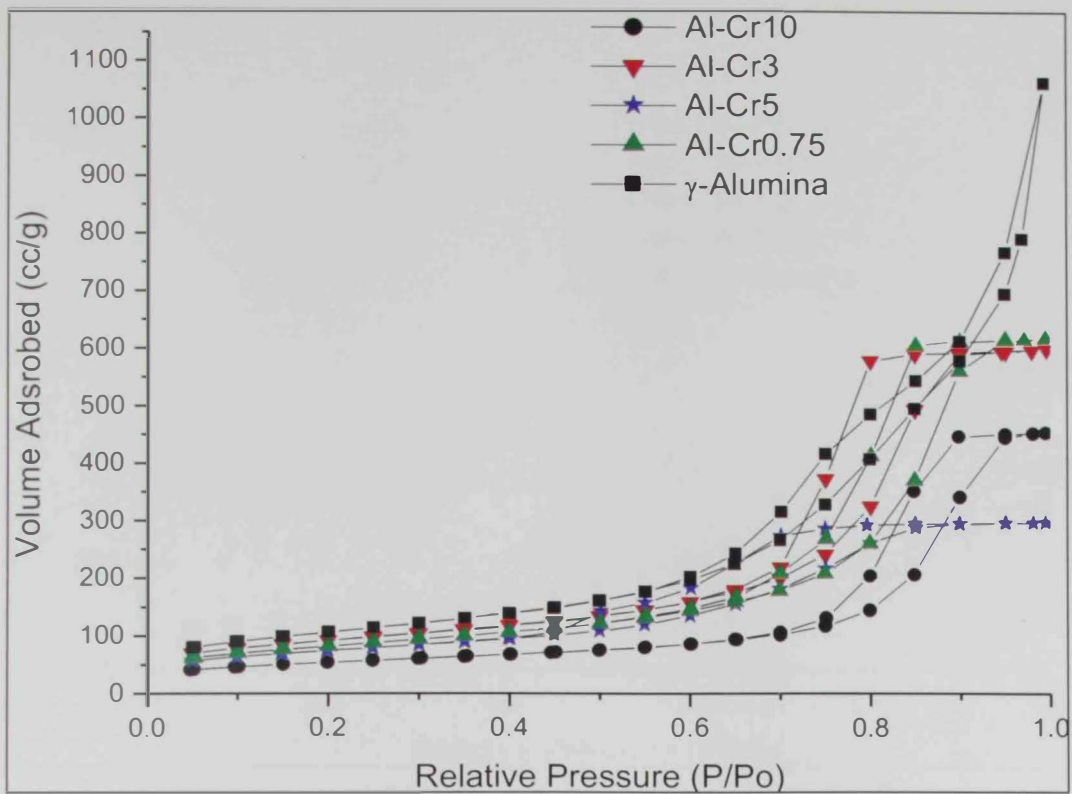


Figure 34. N₂ adsorption-desorption isotherms of Al-Cr-0.75, Al-Cr-3, Al-Cr-5 and Al-Cr-10.

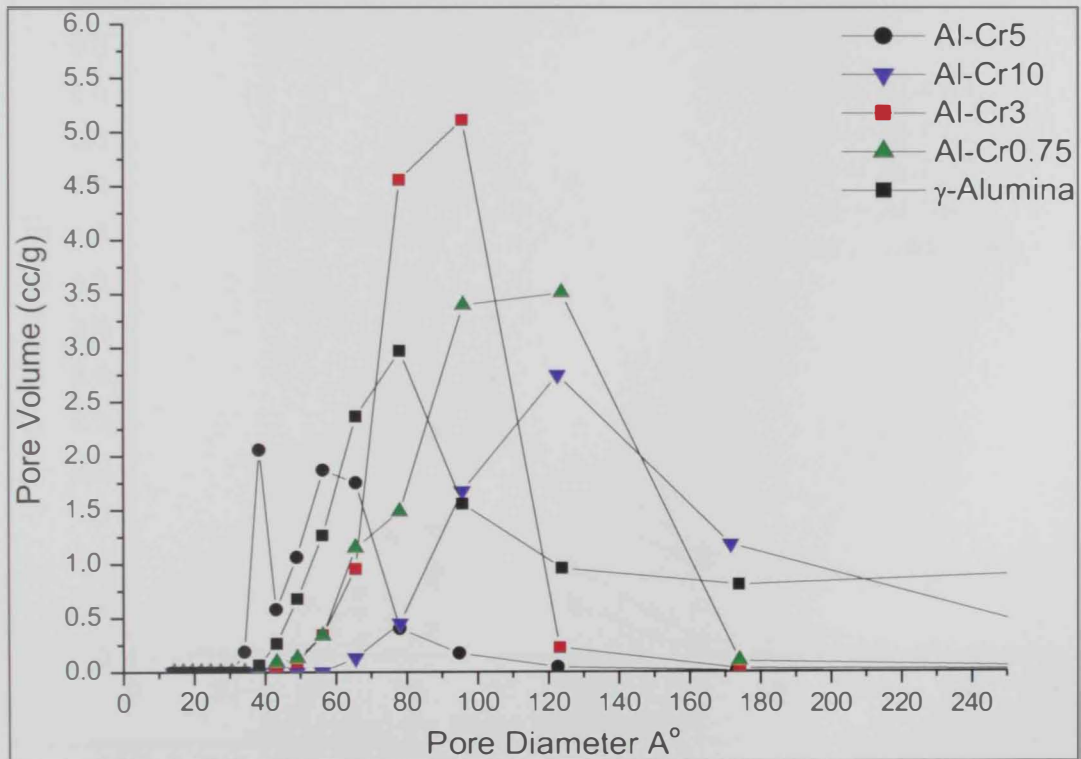


Figure 35. BJH pore size distribution of Al-Cr-0.75, Al-Cr-3, Al-Cr-5 and Al-Cr-10 versus alumina.

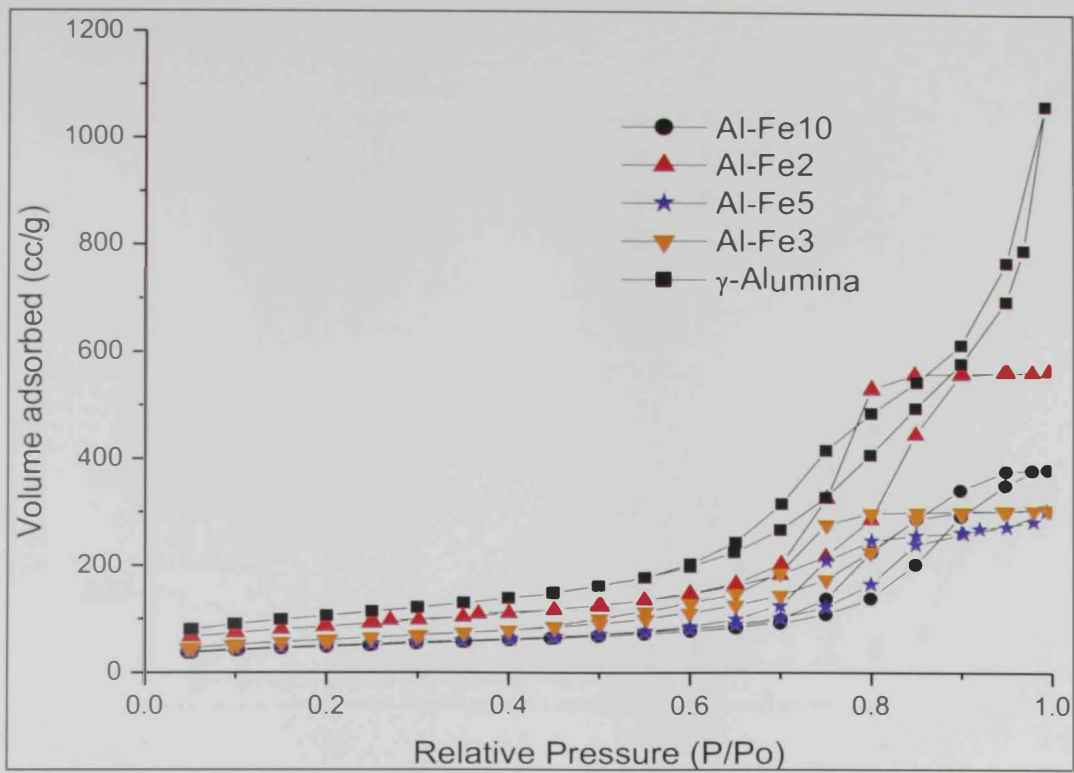


Figure 36. N_2 adsorption-desorption isotherms of Al-Fe-2, Al-Fe-3, Al-Fe-5 and Al-Fe-10.

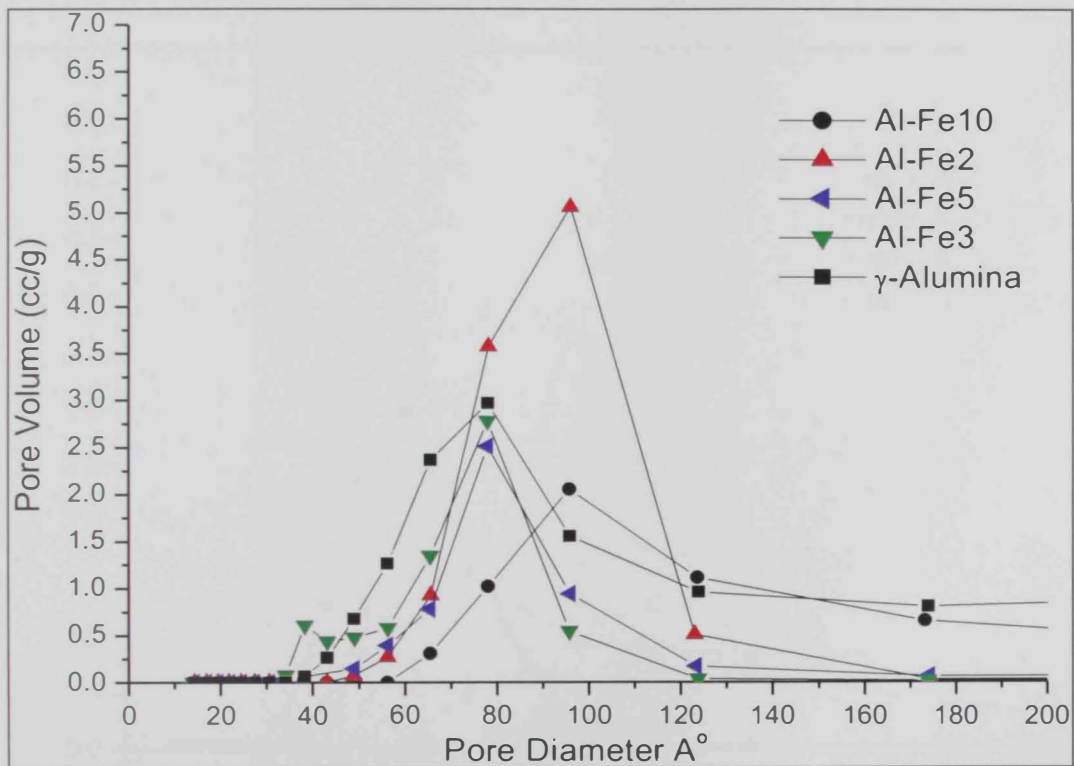


Figure 37. BJH pore size distribution of Al-Fe-2, Al-Fe-3, Al-Fe-5 and Al-Fe-10 versus alumina.

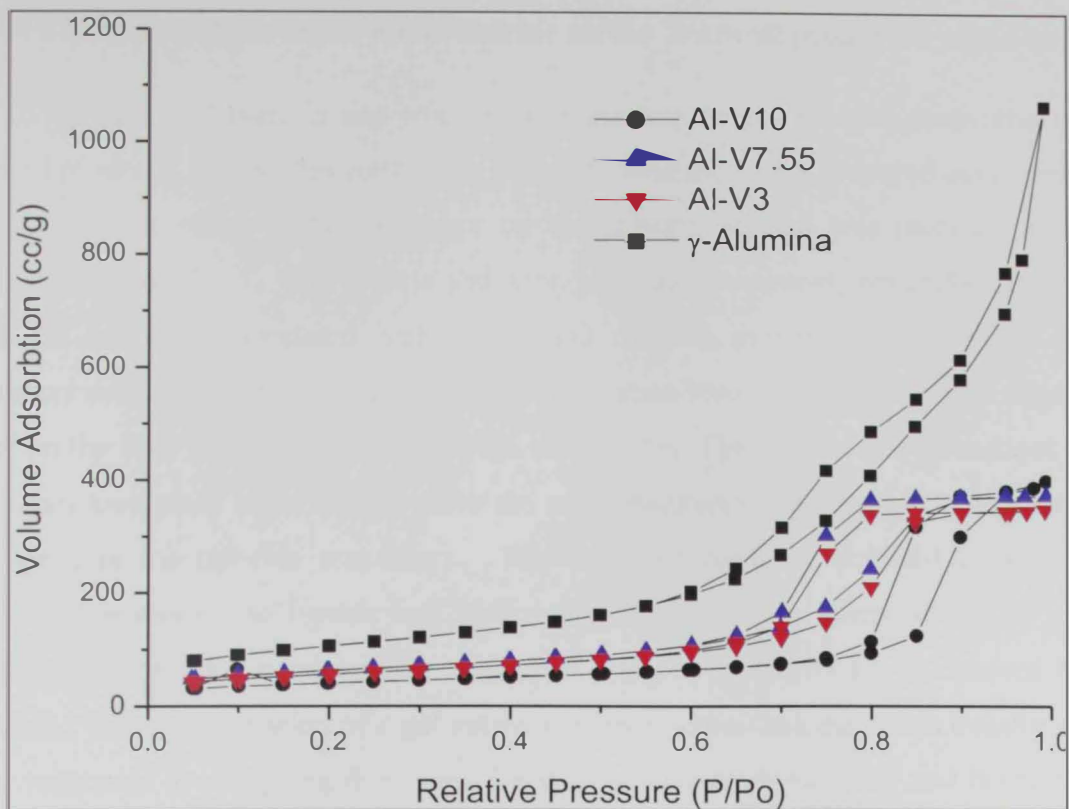


Figure 38. N₂ adsorption-desorption isotherms of Al- V-3, Al- V-7.55 and Al-V-10

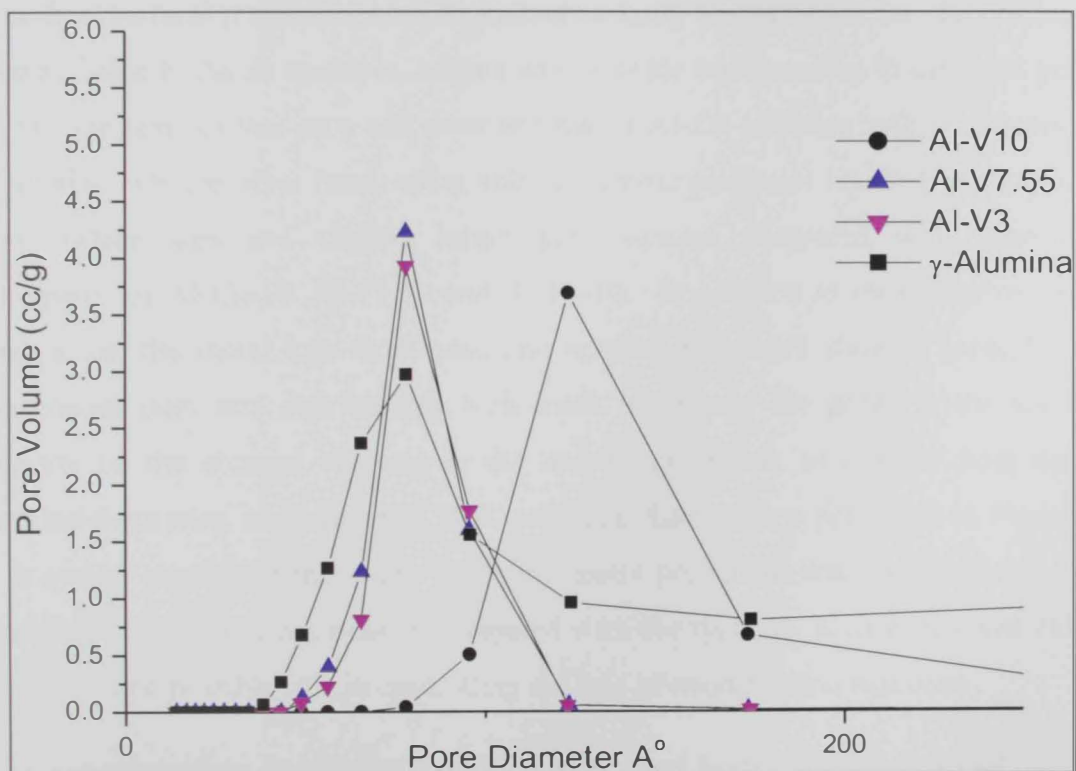


Figure 39. BJH pore size distribution of Al- V-3, Al- V-7.55 and Al-V-10 versus alumina.

2.3.7.4 The Effect of the Metal ion precursor on the Textural properties of γ -Alumina

To determine if there is any role of the precursor on the textural properties of the calcined products, composites containing selected metal ions were prepared using different precursors. The effect of the precursor on the gelation process was recorded and was discussed Section 2.3.5. The acetate and acetylacetonate precursors, generally, resulted in faster gel formation compared with nitrate and chloride precursor. The effect of the precursors on the condensation reactions during gelation resulted eventually in a noticeable effect on the final textural properties of the composites. The condensation reactions upon hydrolysis took place more rapidly when the acac precursors were used as compared with the nitrate or the chloride precursors. This behavior could be referred to a possible interaction between acac ligands and hydrolyzed aluminum ion intermediates by proton abstraction enhancing condensation reactions. Rapid condensation is known to be associated with the formation of a gel network of more cross-linking which usually shows better resistance to collapsing due to capillary forces during drying [86] and hence higher surface area and porosity. This explanation is well supported by the observed textural properties of the composites.

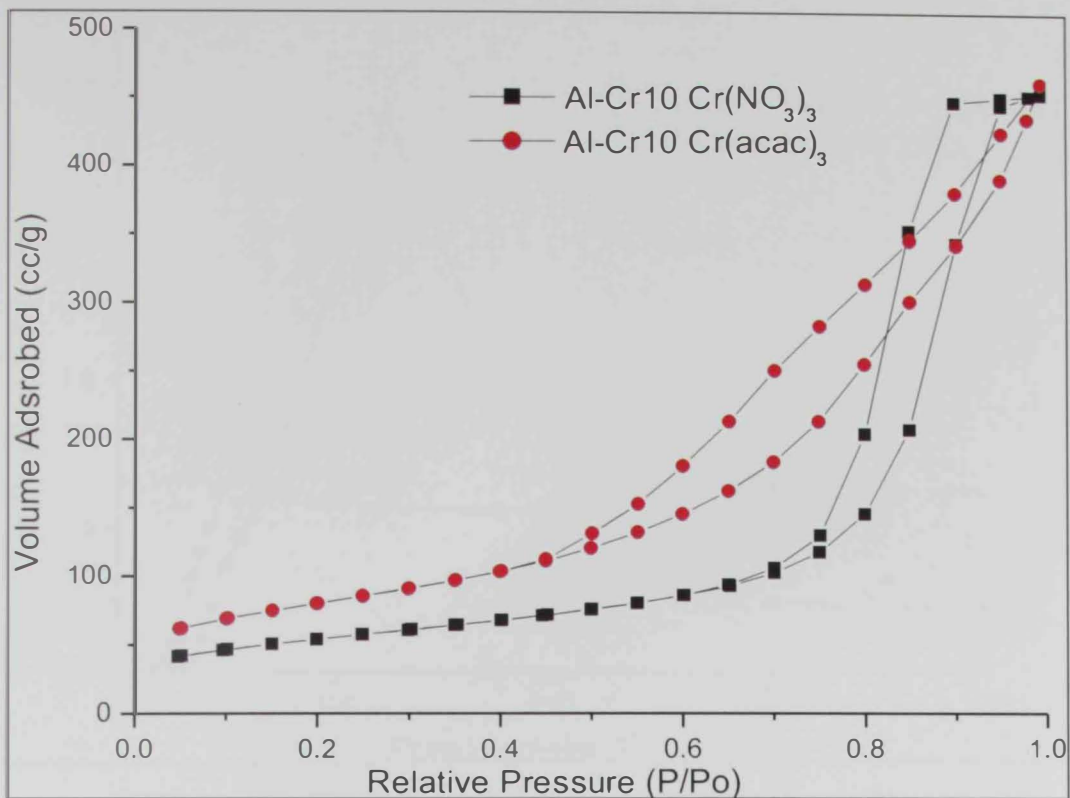
The final textural properties were dependent on both, the metal ion and the precursor as shown in Table 8. As an example, acetate and chloride ions resulted in different gelation rates but the final surface area and pore volume of Al-Zn-10 from both precursors were very similar. On the other hand, using acetylacetonate precursor resulted in significantly higher surface area and slightly larger pore volume compared with their nitrate counterparts for Al-Cu-10, Al-Cr-10 and Al-Fe-10. In addition to their relatively higher surface areas, the metal ions from acac and acetate precursors showed generally more homogeneous pore size distributions with more portion of the pores in the low-range mesopores on the account of those in the macropores region, as evident from their N_2 adsorption-desorption isotherms and BJH pore size distributions presented in Figures 40-47. It can be concluded that metal acetylacetonate precursors may be preferred for the preparation of particular composites compared with the typically used nitrate and chloride salts due to their possible role in controlling the rate of condensation reactions.

The lower tendency to aggregate and the associated higher surface areas of the solids prepared from acac precursors may indicate an enhanced dispersion and incorporation of the dopant ions into the alumina matrix. This effect of the acac precursor can be explained based on a possible role of the acac ligand in the gelation process and in hetero-linkage

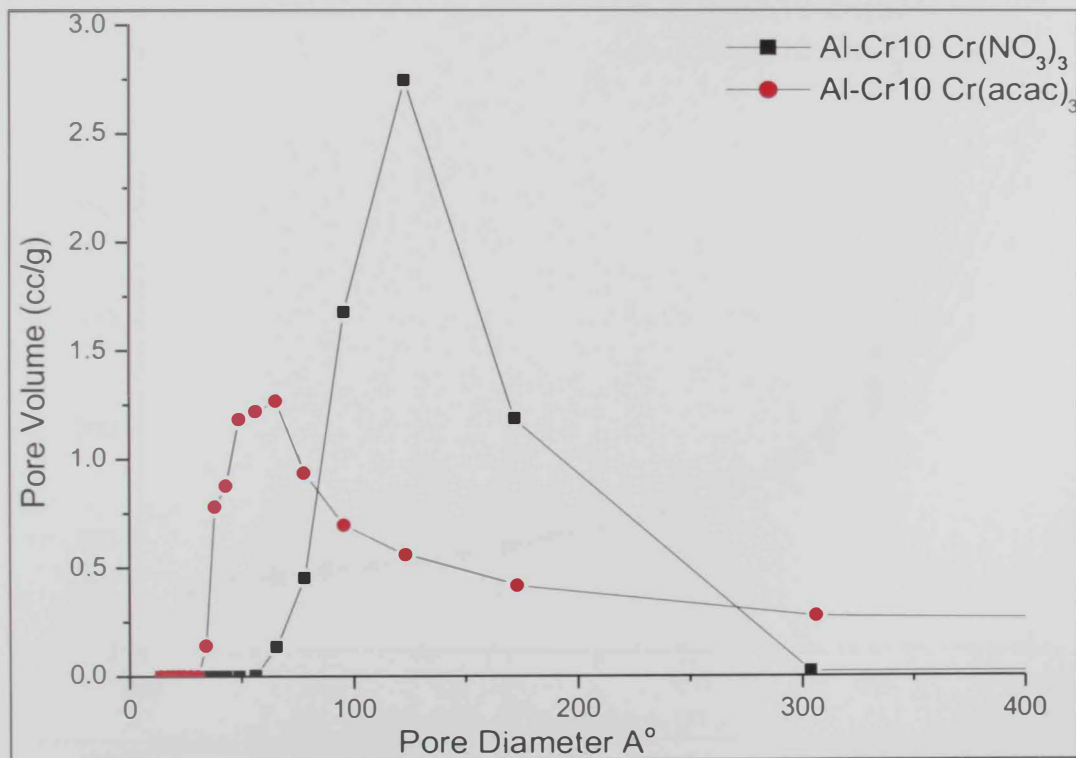
formation. While the incorporation of a hetero-ion in the matrix of alumina, by Al^{3+} substitution or by occupation of a vacant interstitial hole, can take place during calcination, it may take place during the hydrolysis and condensation process via a transmetallation reaction in the presence of the acac precursor. In this case some acac ligands may coordinate to Al ions and, consequently, the dopant metal ions bind to the gel producing M^{n+} -containing gel network. The reaction can also take place via the abstraction of an H^+ from an OH group in the gel network by an acac ligand producing an acac molecule and M-O-Al intermediate. This enhanced homogeneous incorporation of the dopant ions might be correlated with the slightly higher degree of crystallinity of the acac-based composites observed by XRD.

Table 8. BET surface area and pore characteristics of Al-M-10% compositions after calcinations at 500 °C.

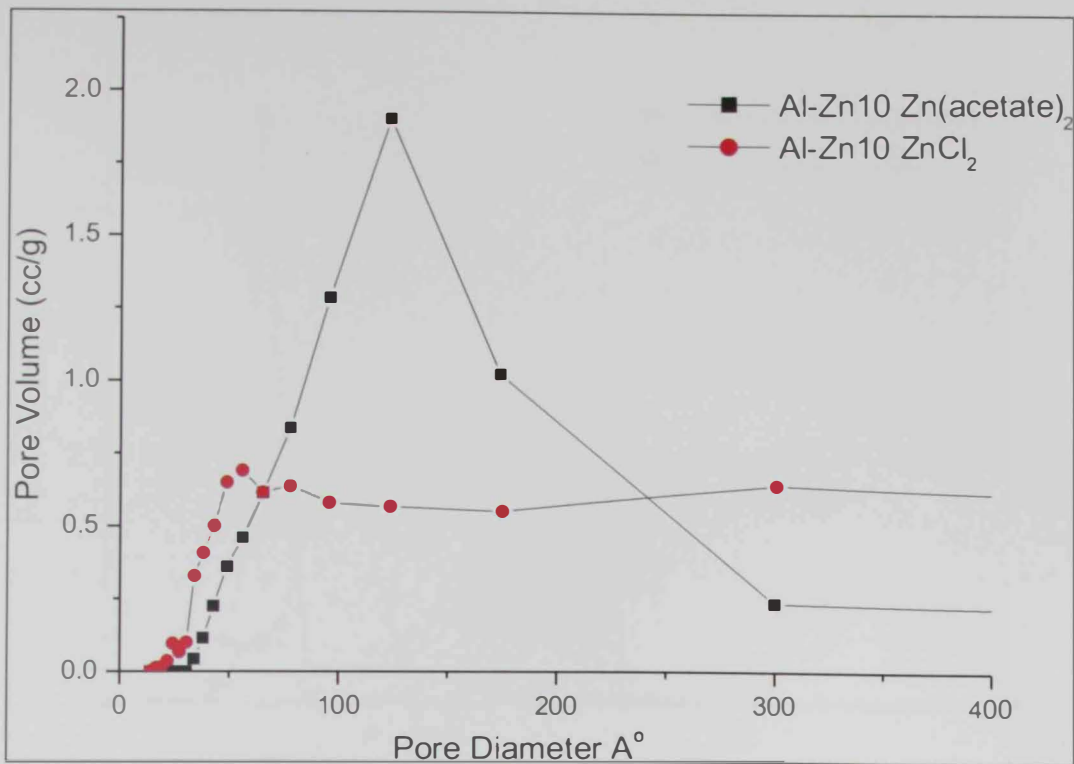
M ⁿ⁺ (10%)	M ⁿ⁺ precursor	Surface area (m ² /g)	Pore volume (cc/g)	Pore size (Å)
Cr	nitrate	166	0.65	155.7
Cr	acac	281	0.67	95.8
Fe	nitrate	168	0.58	138.4
Fe	acac	279	0.30	42.7
Zn	chloride	261	0.72	110.7
Zn	acetate	253	0.73	115.5
Cu	chloride	174	0.38	87.5
Cu	acac	277	0.45	64.8



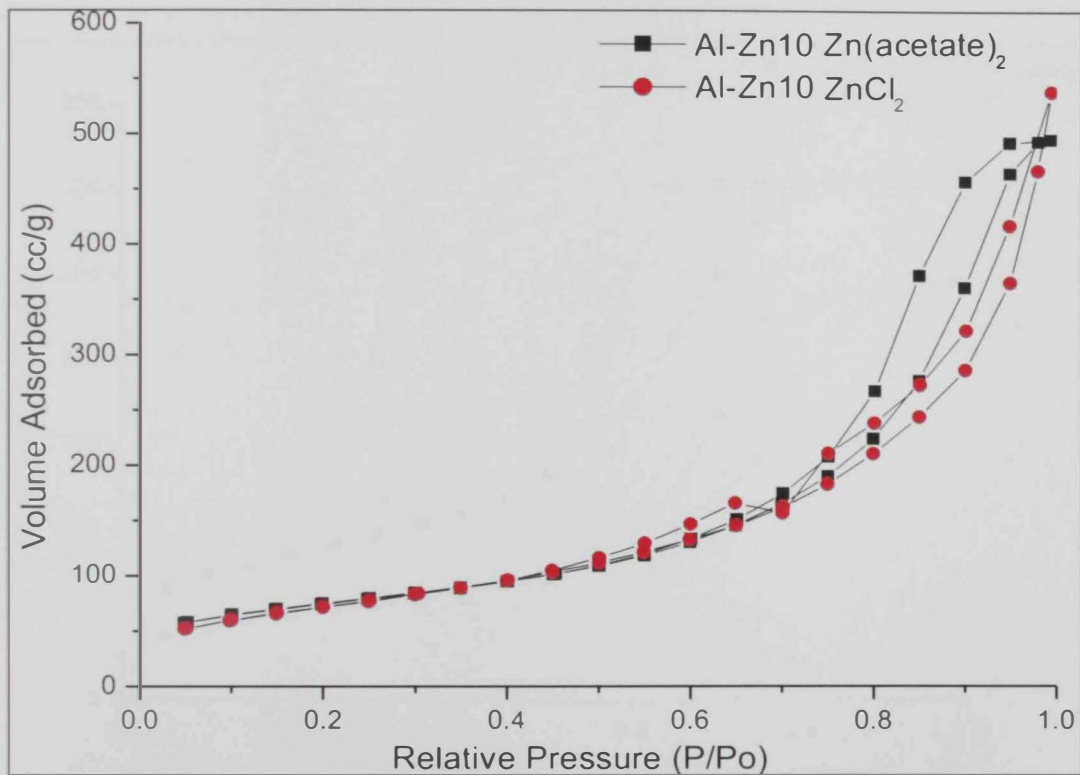
Figures 40. N₂ adsorption-desorption isotherms of Al-Cr-10 prepared from Cr(NO₃)₃ and from Cr(acac)₃.



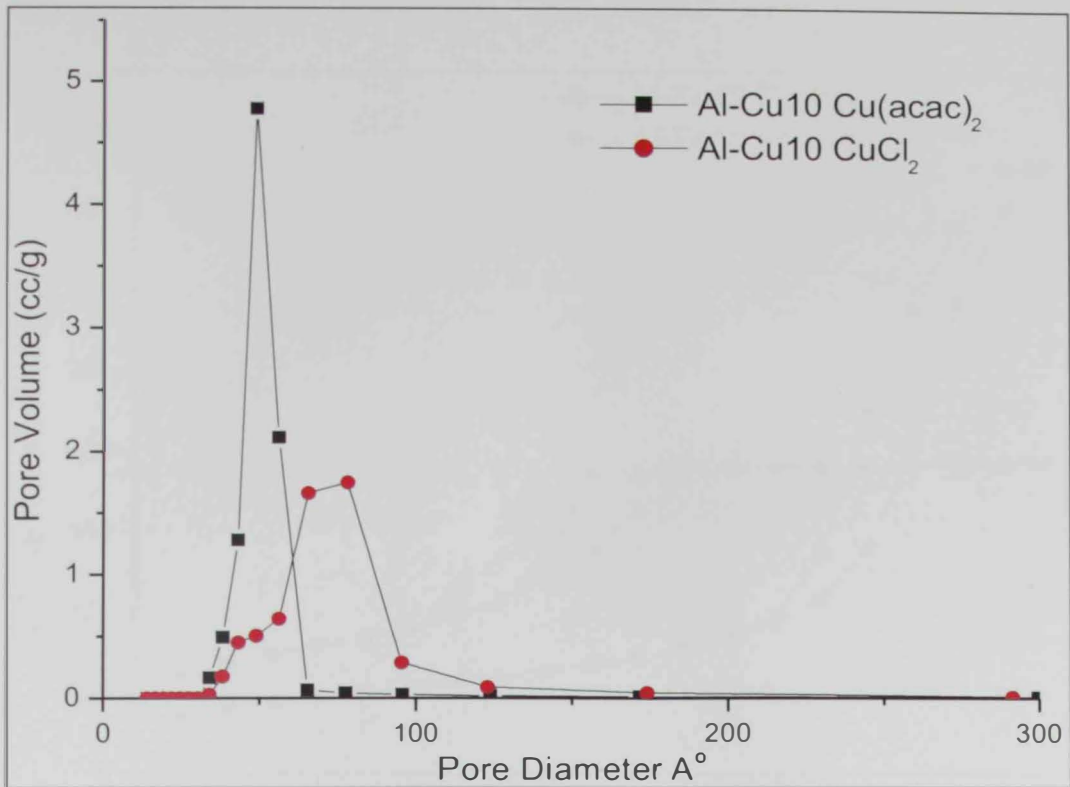
Figures 41. BJH pore size distribution of Al-Cr-10 Al-Cr-10 prepared from Cr(NO₃)₃ and from Cr(acac)₃.



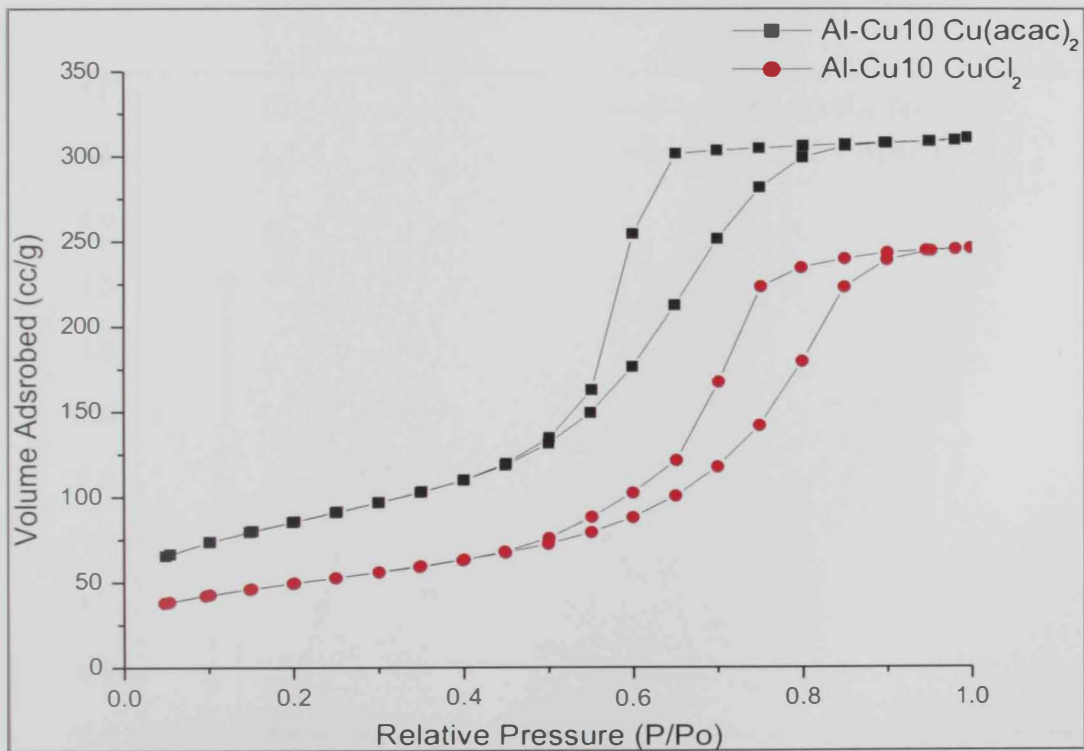
Figures 42. BJH pore size distribution of Al-Zn-10 prepared from ZnCl₂ and from Zn(acetate)₂



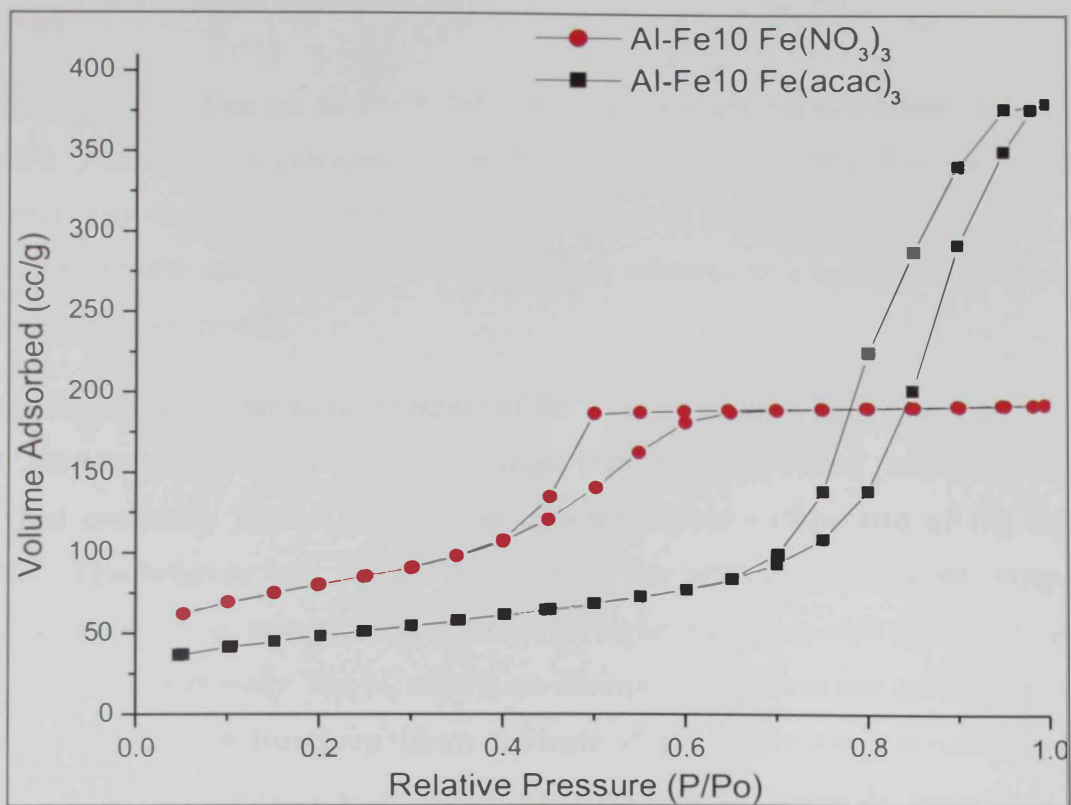
Figures 43. N₂ adsorption-desorption isotherms of Al-Zn-10 prepared from ZnCl₂ and from Zn(acetate)₂



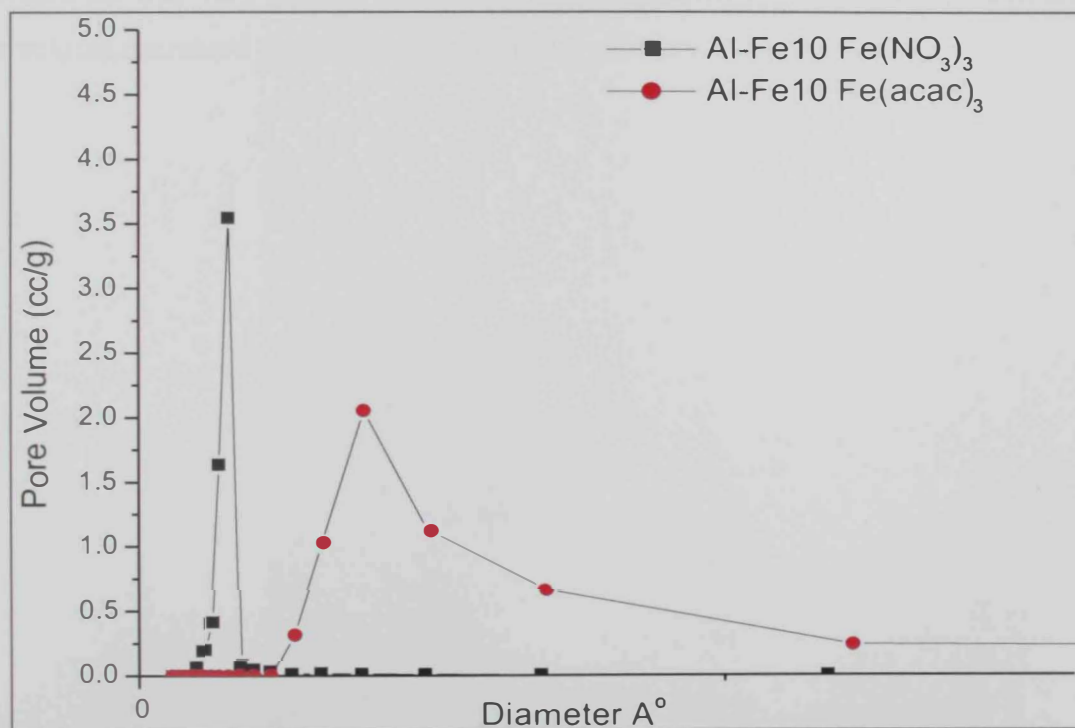
Figures 44. BJH pore size distribution of Al-Cu-10 prepared from CuCl_2 and from $\text{Cu}(\text{acac})_2$.



Figures 45. N_2 adsorption-desorption isotherms of Al-Cu-10 prepared from CuCl_2 and from $\text{Cu}(\text{acac})_2$.



Figures 46. N₂ adsorption-desorption isotherms of Al-Fe-10 prepared from Fe(NO₃)₃ and from Fe(acac)₃.



Figures 47. BJH pore size distribution of Al-Fe-10 prepared from Fe(NO₃)₃ and from Fe(acac)₃.

2.3.7.5 The Effect of Different Solvents on the Textural properties of doped γ -Alumina

This study was done on Al-Fe-10 following the same general procedure using various solvents. While the Fe precursor $\text{Fe}(\text{NO}_3)_3 \cdot 9\text{H}_2\text{O}$ was dissolved in 2-propanol, the Al precursor was dissolved in other solvents as shown in Table 9. In addition, 0.1 ml of concentrated nitric acid was added to the starting solution, as a hydrolysis acid catalyst, before the hydrolysis step.

It is known that higher surface tension of the solvent results in higher capillary pressure inside the pores of the gel which leads to more pore shrinkage during the solvent removal step, and eventually results in lower porosity and lower surface area of the calcined product. This behavior may explain the lower surface areas obtained for the composites prepared in solvents containing toluene due to its higher surface tension compared with the alcoholic solvents in study. The N_2 adsorption-desorption isotherms and pore size Al-Fe-10 prepared in different solvents are shown in Figure 48 and Figure 49. It is noticed that Al-Fe-10 in 1-butanol produced well defined hysteresis loop indicating the presence of some mesoporous structures while composites prepared in other solvents showed hysteresis loop in lower relative pressure region indicating low mesopores range. In addition, Al-Fe-10 in 1-butanol showed very narrow pore size distribution. However, the surface area and the pore volume decreased considerably using other solvents.

Table 9: BET surface area and pore characteristics Al-Fe-10% prepared from nitrate precursor in different solvents after calcinations at 500°C.

Solvent	Surface tension (mN/m)	Surface area (m ² /g)	Pore volume (cc/g)	Pore size (Å ^o)
2-propanol	22.3	168	0.58	138.4
1-butanol	25.00	100	0.14	54.1
Toluene	28.53	52	0.09	68.7
2-propanol+toluene	--	37	0.30	322.7

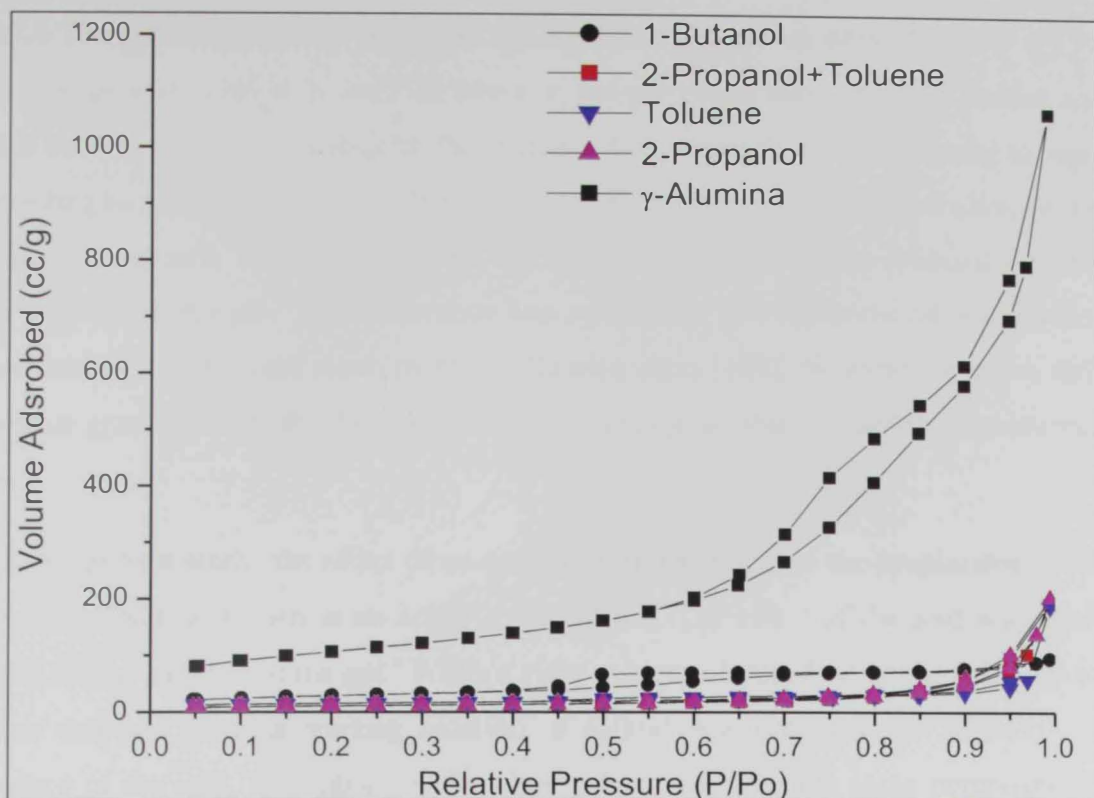


Figure 48. The N_2 adsorption-desorption isotherm of Al-Fe-10 prepared in different solvents.

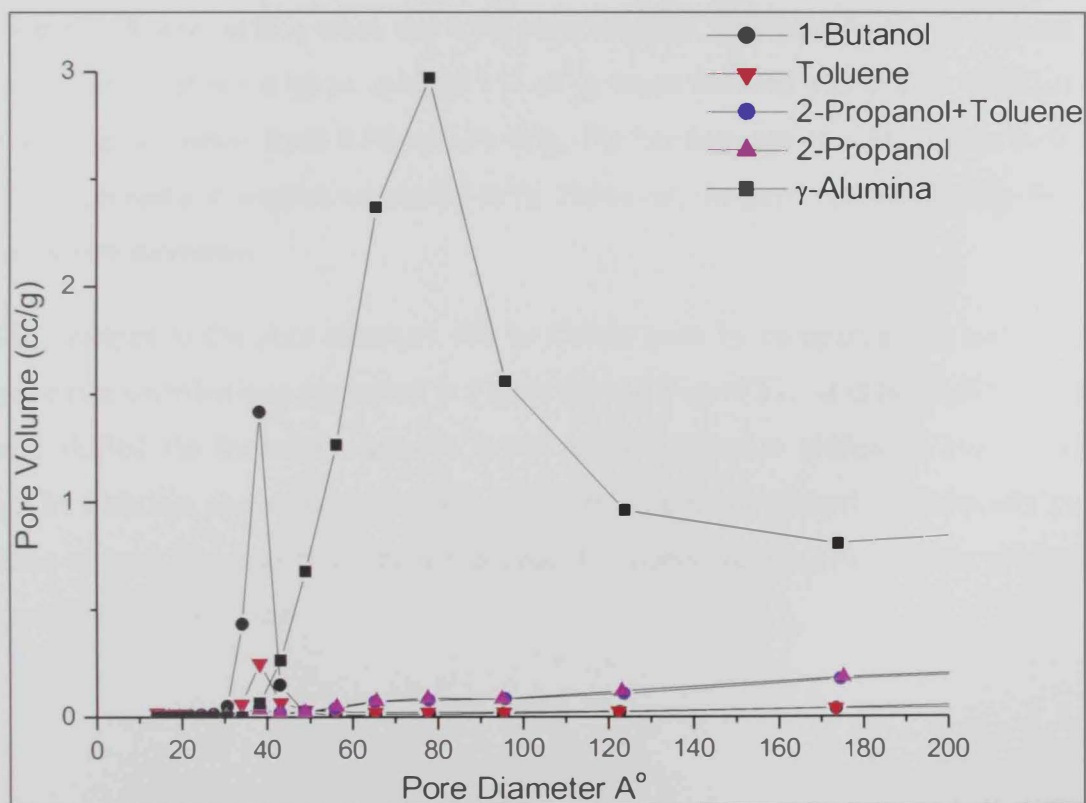


Figure 49. BJH pore size distribution of Al-Fe-10 prepared in different solvents

3.7.6 The Effect of Acid catalysts on the Textural properties of γ -Alumina

Using an acid catalyst is very common in sol-gel preparation of metal oxides and its effect on the textural properties of the final product varies from one material to another. According to Balakrishnan et al. [108], the surface area of sol-gel prepared silica decreased as the pH increased. On the other hand, the surface area was roughly constant for alumina as a function of the pH. This difference was referred to their different rates of hydrolysis where alumina hydrolyzes much more rapidly than silica [108]. However, it seems difficult to derive general trends for the role of the acid catalyst as other variables may override its effect.

In the present study, the effect of an acid catalyst was tested in the preparation of Al-Fe-10 where HNO_3 was used in an acid/Al ratio of 0.1. The effect of the acid was observed during the preparation of the gel. While a clear gel was obtained when the acid was added to the undoped alumina starting solution, a colloid was obtained for Al-Fe-10 in the presence of the acid, in contrast to the clear gel obtained for the same composite in the absence of the acid. These observations clearly indicate a role played by the acid during the progress of the condensation reactions that eventually had a negative impact on the textural properties as shown in Table 10. In general, the presence of an acid resulted in considerably lower surface areas and total pore volumes. The surface area decreased from $168 \text{ m}^2/\text{g}$, in the absence of an acid, to $111 \text{ m}^2/\text{g}$ when the acid was added. Similarly, the pore volume decreased from 0.58 to 0.36 cc/g. Further increase of acid/Al ratio to 0.3, led to further decrease in surface area to $69 \text{ m}^2/\text{g}$. However, the pore volume slightly increased and pore size increased.

The changes in the pore structure can be clearly seen by comparing the isotherms and the pore size distributions presented in Figure 50 and Figure 51. It is noticed that addition of acid shifted the hysteresis loop to lower relative pressure indicating low mesopores range. In addition, the surface area and the pore volume decreased considerably by the addition of acid. More work is needed in order to understand the effect of the acid catalyst under different conditions.

2.3.7.6 The Effect of Acid catalysts on the Textural properties of γ -Alumina

Using an acid catalyst is very common in sol-gel preparation of metal oxides and its effect on the textural properties of the final product varies from one material to another. According to Balakrishnan et al. [108], the surface area of sol-gel prepared silica decreased as the pH increased. On the other hand, the surface area was roughly constant for alumina as a function of the pH. This difference was referred to their different rates of hydrolysis where alumina hydrolyzes much more rapidly than silica [108]. However, it seems difficult to derive general trends for the role of the acid catalyst as other variables may override its effect.

In the present study, the effect of an acid catalyst was tested in the preparation of Al-Fe-10 where HNO_3 was used in an acid/Al ratio of 0.1. The effect of the acid was observed during the preparation of the gel. While a clear gel was obtained when the acid was added to the undoped alumina starting solution, a colloid was obtained for Al-Fe-10 in the presence of the acid, in contrast to the clear gel obtained for the same composite in the absence of the acid. These observations clearly indicate a role played by the acid during the progress of the condensation reactions that eventually had a negative impact on the textural properties as shown in Table 10. In general, the presence of an acid resulted in considerably lower surface areas and total pore volumes. The surface area decreased from $168 \text{ m}^2/\text{g}$, in the absence of an acid, to $111 \text{ m}^2/\text{g}$ when the acid was added. Similarly, the pore volume decreased from 0.58 to 0.36 cc/g. Further increase of acid/Al ratio to 0.3, led to further decrease in surface area to $69 \text{ m}^2/\text{g}$. However, the pore volume slightly increased and pore size increased.

The changes in the pore structure can be clearly seen by comparing the isotherms and the pore size distributions presented in Figure 50 and Figure 51. It is noticed that addition of acid shifted the hysteresis loop to lower relative pressure indicating low mesopores range. In addition, the surface area and the pore volume decreased considerably by the addition of acid. More work is needed in order to understand the effect of the acid catalyst under different conditions.

Table 10. BET surface area and pore characteristics of Al-Fe-10% prepared from nitrate precursor in the presence and in the absence of an acid catalyst

Acid/Al ratio	Surface area (m ² /g)	Pore volume (cc/g)	Pore size (Å)
0	168	0.58	138.4
0.1	111	0.36	131.3
0.3	69	0.40	233.9

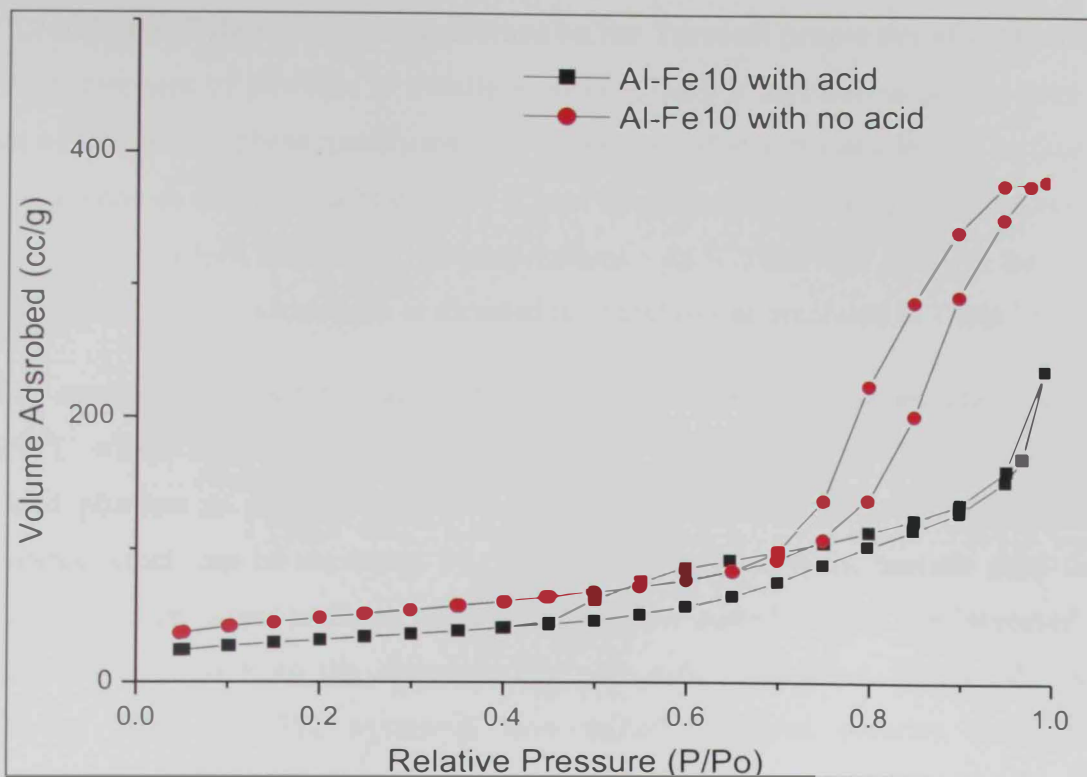


Figure 50. The N₂ adsorption-desorption isotherm of Al-Fe-10 prepared in the presence and in the absence of an acid.

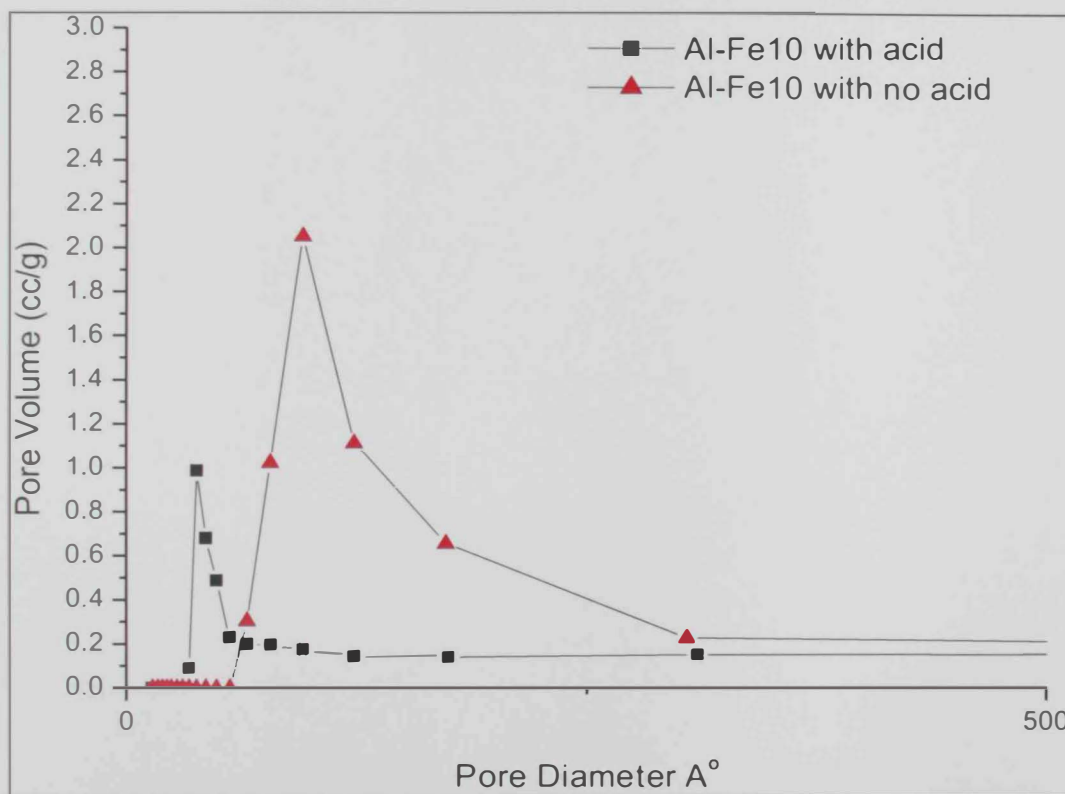


Figure 51 . BJH pore size distribution of Al-Fe-10 prepared in presence and in the absence of an acid.

2.3.7.7 Effect of Calcinations Temperature on the Textural properties of γ -Alumina

Heat treatment of powders is usually associated with a decrease in surface area as a result of sintering or phase transformation. In the case of alumina any loss of surface area that accompanies calcinations below 700 °C can be referred to sintering of γ -alumina since phase transformations require higher temperatures. Al-V-7.5% was selected for textural characterization after calcinations at elevated temperatures as presented in Table 15.

The composite retained a relatively high surface area and pore volume after calcination at 900°C where no phase changes took place as evident from the XRD study of the calcined powders as discussed earlier. However, the average pore diameter increased noticeably which can be explained by the expected increase in the particle sizes due to sintering. Hence, larger particles result in larger inter-particle voids. The increased pore diameter is inferred from the corresponding pore size distribution, Figure 52, and N_2 isotherms, Figure 53. The hysteresis loop shifted to higher pressure range as the temperature increased indicating larger mesopores which fill up at higher pressures.

Table 15. BET surface area and pore characteristics of Al-V-7.5% after calcinations at different temperatures.

Calcinations temperature (C°)	Surface area (m ² /g)	Pore volume (cc/g)	Pore size (A°)
500	328	1.23	150.0
800	188	0.95	202.0
900	132	0.73	222.0

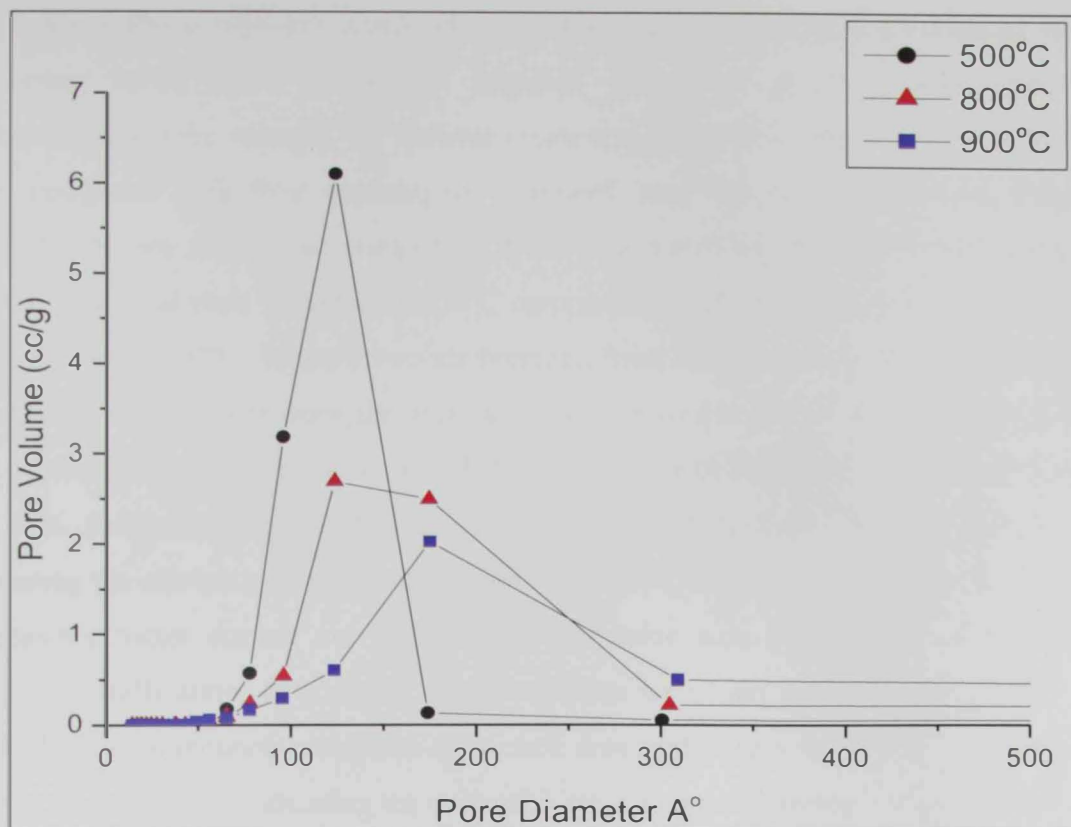


Figure 52 . BJH pore size distribution of Al-V-7.5 at different calcinations temperatures.

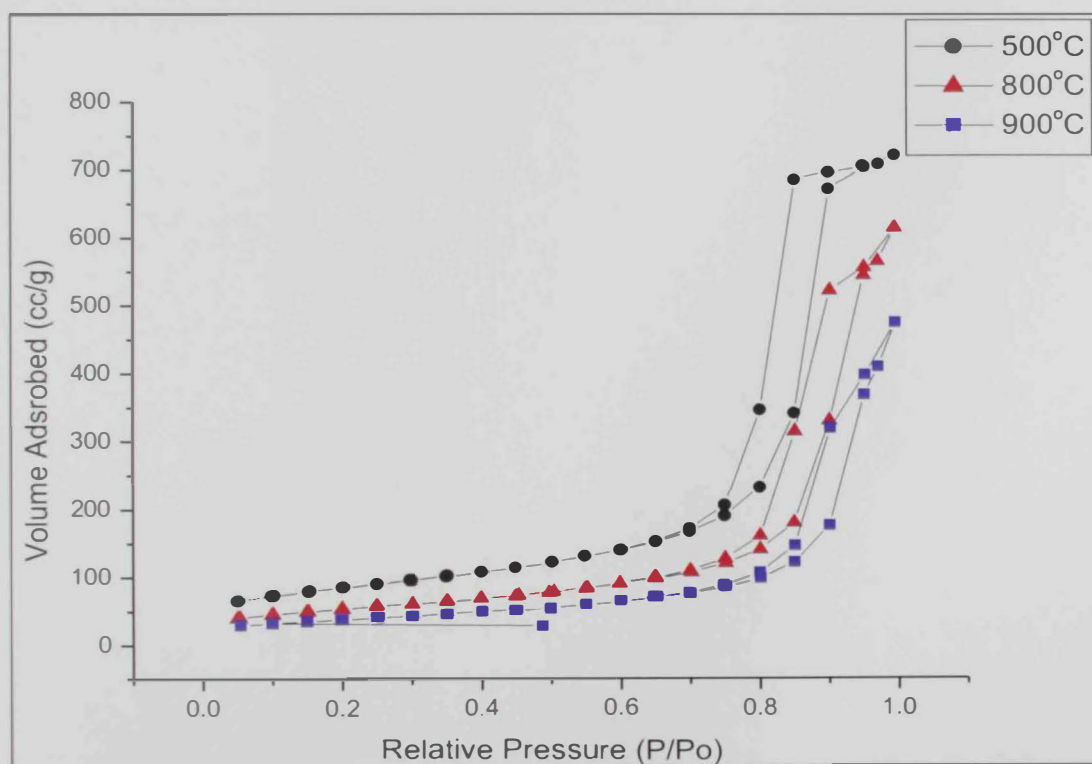


Figure 53. The N₂ adsorption-desorption isotherm of Al-V-7.5 at different calcination temperatures.

Since the composites prepared from acac precursors exhibited enhanced textural properties, Al-Cr oxide composites prepared from acac precursor with various Cr concentrations were selected for textural characterization after calcinations at 800°C and were compared with their counterparts prepared from the nitrate precursor, Table 12. Interestingly, we found that composites from acac precursor retained significantly high surface areas and pore volumes at 800°C comparable with those obtained for composites from nitrates at 500°C. While the solids prepared from nitrates lost 25-30% of their surface areas, their counterparts from the acac precursor showed a loss in the range of 14-19% . The other significant observation was that composites with high Cr ion concentrations, 5% and 10%, suffered noticeably less decrease in their surface areas and pore volumes upon increasing the calcination temperature from 500 to 800°C. This behavior could be referred to possibly better dopant ion dispersion when using acac precursor which eventually hinders crystallization. In addition, the composites with high dopant concentration, 10%, showed more pronounced resistance to surface area and pore volume loss when prepared from acac precursors indicating an enhanced resistance to sintering. These observations support the suggested enhancement of the incorporation of the dopant ions in the alumina matrix in the presence of acac ligands as discussed above.

Table 12: BET surface area and pore characteristics of Al-Cr-x after calcinations at different temperatures.

M ⁿ⁺ (%)	M ⁿ⁺ precursor	Calcinations temperature C ^o	Surface area (m ² /g)	Pore volume (cc/g)	Pore size (A ^o)
Cr0.75	nitrate	500	292	0.96	130.1
Cr0.75	nitrate	800	217	0.82	150.9
Cr0.75	acac	500	455	0.98	86.1
Cr0.75	acac	800	306	0.72	94.0
Cr2	acac	500	291	0.71	98.0
Cr2	acac	800	234	0.69	118.0
Cr5	acac	500	285	0.75	105.2
Cr5	acac	800	239	0.73	123.0
Cr10	acac	500	259	0.71	109.0
Cr10	acac	800	221	0.73	132.0

Interestingly, the acac precursor showed a positive effect on the behavior at elevated temperatures. In contrast to what was observed for Al-V composites from chloride precursor, the typical decrease in surface area and pore volume as well as the increase in the pore diameter associated with elevated temperatures were generally minimized when an acac precursor was used. Figure 54 - Figure 57 display the N₂ isotherms and the corresponding pore size distributions of Al-Cr-0.75 and Al-Cr-5, as examples, from acac precursor after calcinations at 500 and 800°C. The characteristics of the composite at 800° C are very similar to those at 500 C. This behavior may be referred, to a possible carbonaceous layer on the surface of the particles that hindered particle growth or to role of the acac species in the gel formation process and dopant dispersion as discussed earlier.

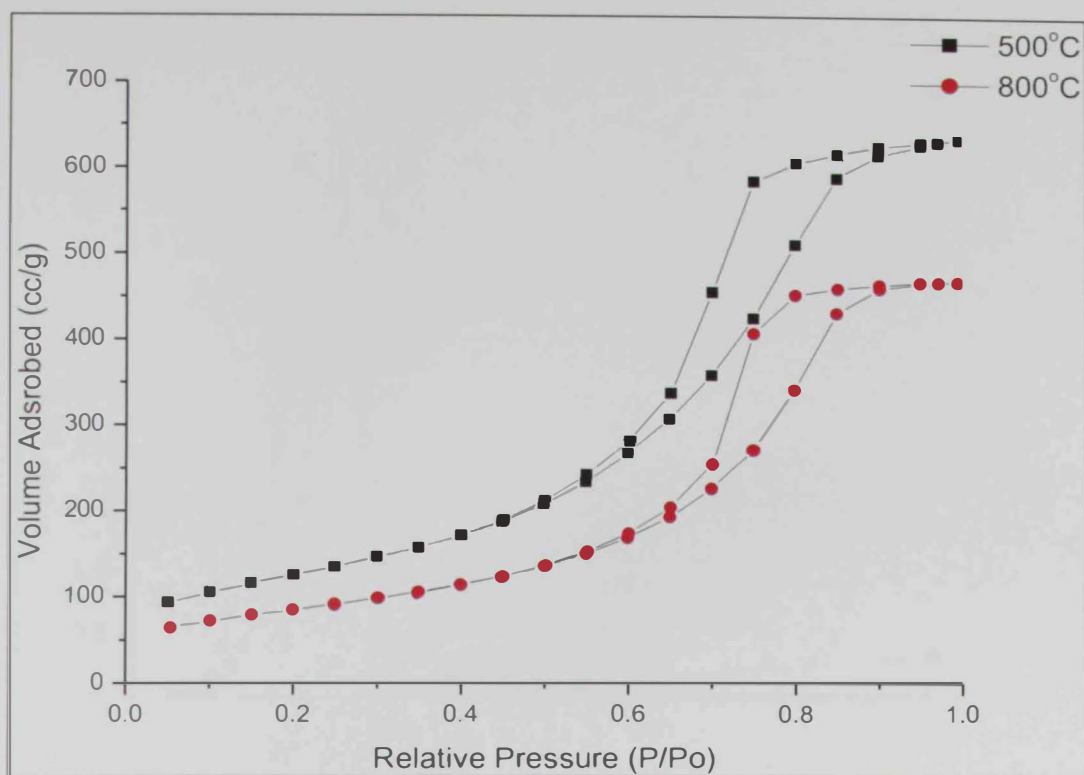


Figure 54. The N_2 adsorption-desorption isotherm of Al-Cr-0.75 prepared from $Cr(acac)_3$ and calcinated at different temperatures.

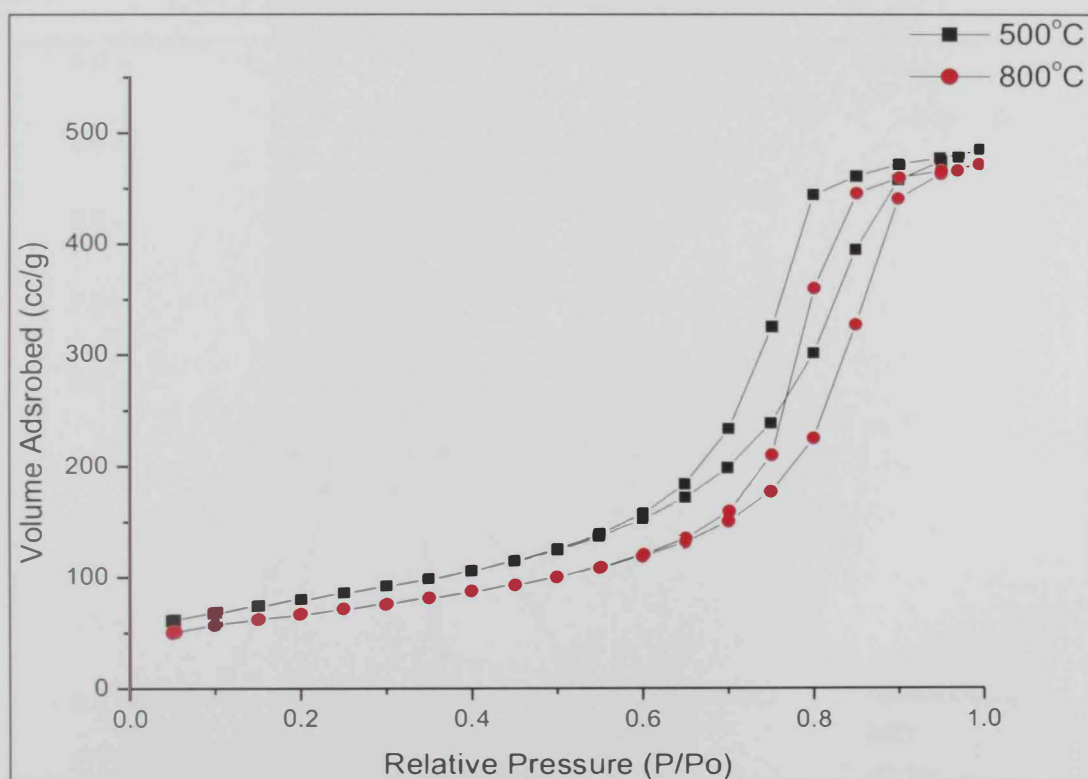


Figure 55. The N_2 adsorption-desorption isotherm of Al-Cr-5 prepared from $Cr(acac)_3$ and calcinated at different temperatures.

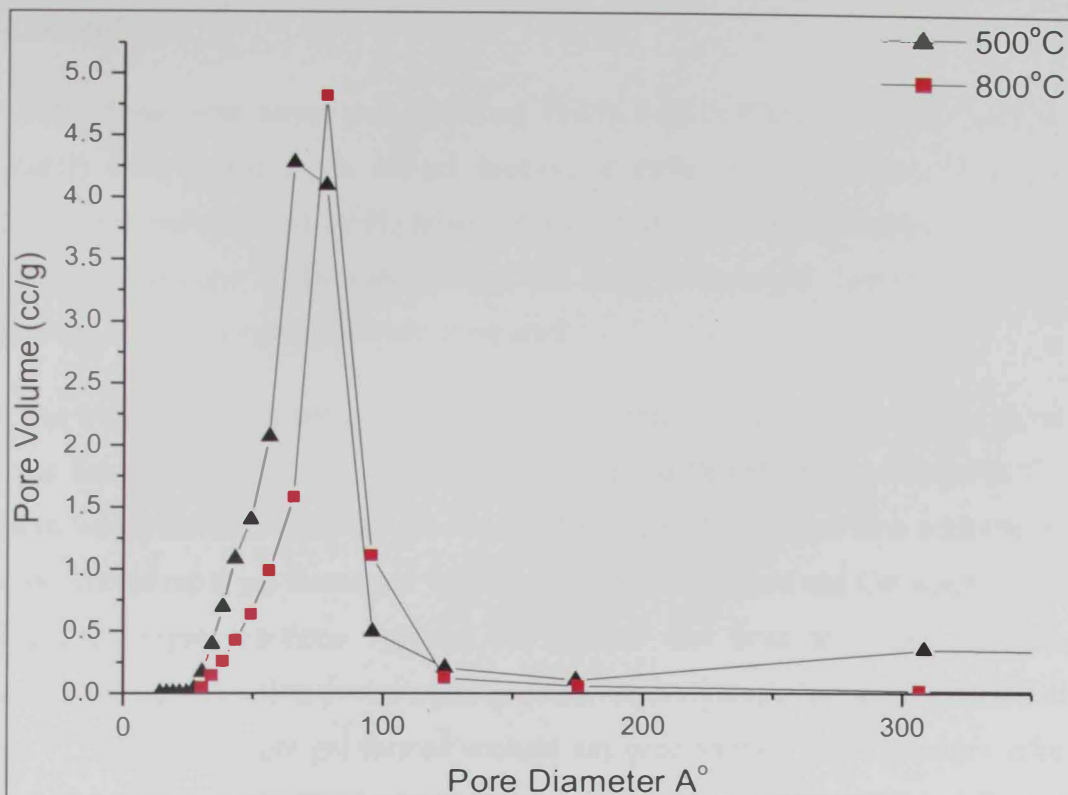


Figure 56. BJH pore size distribution of Al-Cr -0.75 prepared from Cr (acac)₃ and calcinated at different temperatures.

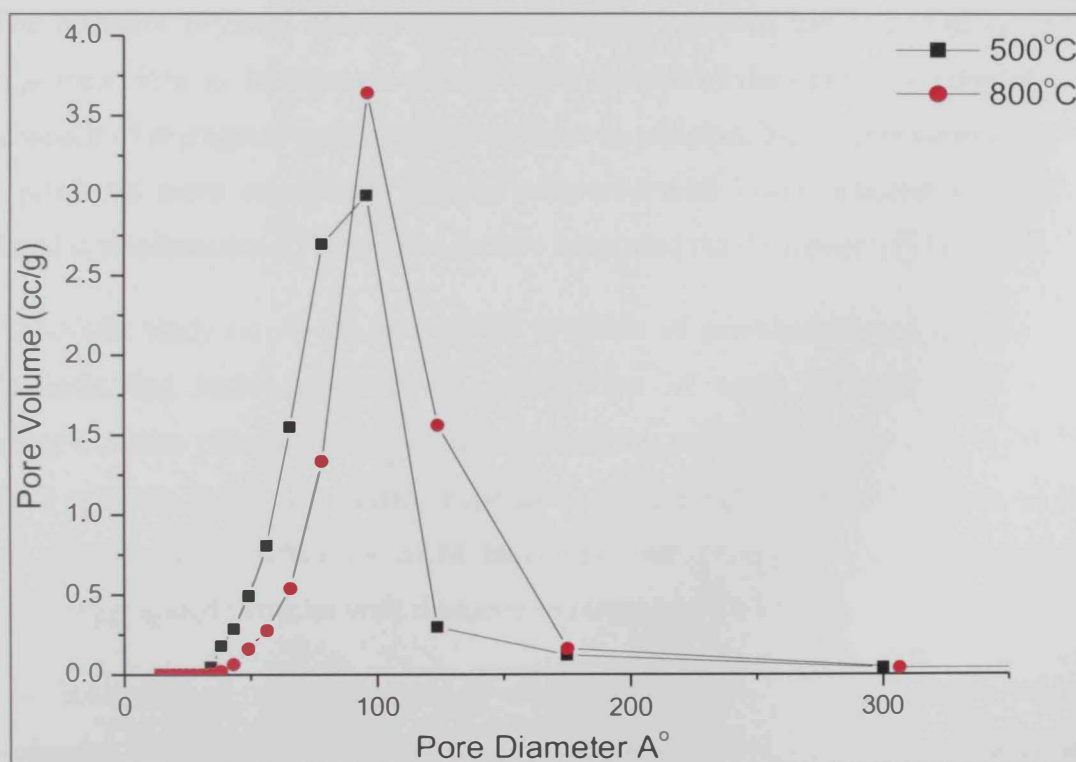


Figure 57. BJH pore size distribution of Al-Cr -5 prepared from Cr (acac)₃ and calcinated at different temperatures.

2.4. Conclusion

γ -Al₂O₃ doped with metal ions including V(III), Fe(III), Cr(III), Mn(II), Cu(II), Ce(III) and Zn(II) were prepared via sol-gel method at different compositions. The prepared samples were characterized by N₂ adsorption for textural characterization, powder XRD, Al-NMR spectroscopy, FTIR spectroscopy and SEM microscopy. The different metal ion dopants and their concentration were compared.

It was observed that various metal ions and different metal ion precursors resulted in different behaviors during the gelation process and different characteristics of the final products, which indicate different modes of interaction of the metal ions with the alumina network. Turbid rapid gel formation was observed for Zn acetate and Cu(acac)₂, which was explained by rapid reactions between the acetate and acac ions and Al precursors enhancing the condensation process and possible heterolinkage formation. In the case of Fe and V, rapid transparent gel formed without any precipitation of sol particles, a key role of the type of ion in the condensation and gel network formation. This behavior may indicate an enhanced heterolinkage formation Al-O-M (M=Fe,V) that hindered particle growth and precipitation.

The different physical characterization methods indicated the well dispersion of the foreign metal ions in the alumina matrix. XRD patterns of the studied composites showed the absence of segregated oxides of dopant ions. In addition, higher concentration of metal ions produced more amorphous powder compared with lower concentration indicating hindered crystallization. FTIR spectra further supported the dispersion of the dopant ions.

²⁷Al-NMR study on Al-Cr showed the presence of pentahedrally coordinated Al ion (Al^V) indicating lattice disorder by substitution of some Al ions with Cr ions. Thermochromism phenomenon was observed during calcinations step of Al-Cr-0.75 and Al-Cr-2 and was referred to lattice expansion. Morphology of some selected Al-doped-metals sample was studied by SEM technique. All composites showed homogenous spherical aggregated particles with diameter in range of 100-200 nm.

The final calcined products exhibited unique textural properties comparable with those of γ -alumina. N₂ adsorption study showed that final textural properties were dependent on type of metal concentration, metal precursor, solvent and acid catalyst. In general, it was found that the surface area decreased as metal concentration increased. However, metal

ions based on organic anions such as acetate and acac, resulted different behavior where high surface areas and pore volumes were generally retained when metal concentration increased. Nevertheless, the fact that doped alumina retained the desired textural properties of pure alumina was a significant achievement.

Using the acac precursors resulted in powders with high surface areas, homogeneous mesopores, and enhanced resistance to sintering. The acac precursors resulted in retaining higher surface areas of the composites at high dopant concentrations as well as at high calcination temperatures compared with the other precursors. Therefore, acac precursor of a metal dopant might be preferred over other precursors to prepare doped γ -alumina, especially with high dopant concentrations.

The surface area and pore volume decreased for composites prepared in solvents containing toluene. This behavior was referred to the high surface tension of toluene compared with 1-butanol and 2-propanol. In addition, the presence of an acid considerably decreased the surface area and total pore volume of composites prepared under acidic conditions.

Retaining the desired textural properties at elevated temperatures is of primary industrial interest. The composites studied at elevated temperatures showed no phase changes upon heating to temperatures as high as 900°C indicating an enhanced stability of the γ -phase of the doped alumina. In addition, no segregated oxide of dopant ions was observed which indicates stable dispersion of the metal ions in the alumina matrix.

Unique thermal stability was observed Cr(III)-containing composites prepared from acac precursor where high surface areas and pore volumes were obtained after calcinations at 800°C compared with their counterparts prepared from the nitrate precursor. In addition, composites with high dopant concentrations, 5% and 10% prepared from acac precursors suffered noticeably less decrease in surface areas and pore volumes upon increasing the calcination temperature from 500°C to 800°C. This behavior was referred to possible better dopant ion dispersion when using acac precursor, which eventually hinders crystallization. Furthermore, the typical increase in the pore diameter associated with elevated temperatures was generally minimized when acac precursors were used. The effect of the acac precursor on the textural properties was referred to its possible role in

controlling the condensation reactions during the gelation process or to possible formation of carbonaceous deposits on the surface of the particles.

IX. Chapter 3. Catalytic Oxidation by Transition-Metal-Doped γ -Al₂O₃: Deep Oxidation of 1,2-dichloroethane

3.1 Introduction. γ -Alumina-based Material in Applications

Nowdays, alumina exceeded silica in many applications for many reasons: it provides high surface area and possesses superior amphoteric properties. In addition, alumina is highly stable at high temperatures, over a broad range of pH values and possesses strong Lewis acid sites for superior bonding to materials. Moreover, alumina also posses many other unique properties such as: high mechanical strength and low thermal conductivity. All these properties made alumina to be one of the mostly used materials in several applications in various fields; in medical, chromatography and separations, clean energy productions , in environmental applications and catalysis.

3.1.1 Alumina in Medical Applications

Alumina is a widely used material in medical applications for its attractive properties such as hardness, stability at high temperatures and its biocompatibility. For example, alumina is used for arthroplasty applications such as total hip arthroplasty. Many studies proved that alumina ceramic possesses high resistance to wear debris which makes it a very promising material in clinical tolerance compared with metals and polymer materials [1,109,110]. Furthermore, there are many studies on utilizing alumina as a drug carrier surface in human body. As an example, Kapoor S and others [111] used mesoporous functionalized with various hydrophilic and hydrophobic surface chemical groups as the carrier for delivery of the model drug ibuprofen.

3.1.2 Alumina in Separation and Chromatographic Applications

Silica has been commonly used as a solid support in different chromatographic technologies. However, it has many deficiencies under certain experimental conditions. JJ Pesek [112] found that in HPLC techniques, silica suffer from pH instability as well as from strong affinity for strongly basic compounds. The vast majority of commercially available silica stationary phases have operating pH values between 2 and 8. At lower pH values, silica undergoes decomposition while at higher pH silica matrix begins to dissolve.

Thus, more stable material under severe pH conditions was needed, and alumina was found to serve this purpose.

3.1.3 Alumina in Clean Energy Production

Developing alternative energy resources like natural gas and electricity is gaining significant attention worldwide. Alumina based materials play a role providing these energy sources to the marketplace through their role as adsorbents and catalytic materials. As an example, alumina now is used for H₂ production as a clean energy source. Hydrogen is considered to be the most useful energy carrier due to its clean and non-polluting nature. A number of catalytic reforming technologies, such as steam reforming, partial oxidation, auto-thermal reforming, and CO₂ reforming, have been extensively investigated for the different scale of hydrogen production from various hydrocarbons and alcohols. Many studies showed that alumina can be used for H₂ production. Jeong Gil Seo and Min Hye Youn [96] prepared a series of mesoporous nickel-alumina aerogel catalysts with different second metal (Ni, Ce, La, Y, Cs, Fe, Co, and Mg) by a single-step sol-gel, and they found that all catalysts exhibited promising catalytic activity for H₂ production. Furthermore, Maria Crisan [113] prepared NiO supported over Al₂O₃ catalyst by sol-gel method and they used it for glycerol reforming to generate H₂ for fuel cell applications.

3.1.4 Alumina in Environmental Remediation

Alumina usage has been widely studied and implemented to solve many environmental issues that are of global concern. Examples of these environmental issues include: water and air purifications.

3.1.4.1 Alumina in Water Purification

A recent report from United Nations Environmental Program revealed that more people die from contaminated water and air than from all types of violence [1]. Alumina has the ability to adsorb and decompose many of toxic contaminants presents in water. Adsorption processes is one of the most important processes in water treatment technology. It was found to be the most effective treatment method (up to 100% efficiency) for the removal of many toxic materials such as: Arsenic, Lead, Fluoride, Pesticides and Dyes [2].

Activated carbon was the most popular adsorbent used for water purification. However, it was limited to adsorb mostly the non-polar compounds rather than polar compounds,

which are typically present in natural water and need polar surface functional groups as the ones presents on the surface of Alumina to adsorb them [1]. Several studies have shown that alumina was the most effective treatment material (up to 100% efficiency) for the removal of As(V), Se(VI) and (F⁻) from water. The other inorganic compounds or ions such as barium, cadmium, chromium, lead, mercury, nitrate, silver and radium were found to be adsorbed over alumina to a lower extent. In two recent studies [114,115] , it was found that alumina adsorb lead(II), Cd and As efficiently from drinking water and waste water . Moreover, it was found that alumina could adsorb several alkanes, cyclic hydrocarbons, aromatic hydrocarbons and chlorinated compounds [116].

In addition, alumina can effectively elute radioactive wastes from polluted sites by adsorption and filtration. For example, especially designed activated alumina captures uranium with high affinity, and the alumina particles can then be safely disposed of the radioactive hazard. In one study [117], it was found that alumina efficiently adsorbed Uranium and almost 100% of U(VI) was successfully been extracted from alumina.

3.1.4.2 Alumina in Air Purification

Volatile organic compounds (VOC) are considered to be a main source of air pollution. They are known to have high vapor pressure and low solubility in H₂O. VOCs are emitted from large variety of sources including various industries and house-hold products [118]. Non halogenated organic compounds are among the most common and toxic materials and they include aldehydes, Carbon monoxide, that is mainly produced from automobile, toluene, propylene, styrene, phenol , acetone and many others. Halogenated organic compounds such as 1,2-dichloroethane (1,2-DCE), Dichloromethane ,Trichloroethane and chlorobenzene are well known materials for their high toxicity and stability in the environment. All these harmful materials contribute to air as well as water pollution. They are also involved in destruction of ozone layer and global warming. Therefore, since their emission is increasing, stringent environmental regulations are placed and the need for new effective methods for their abatement is one of great importance [119-122]. Figure 58 shows some of the most common VOCs.

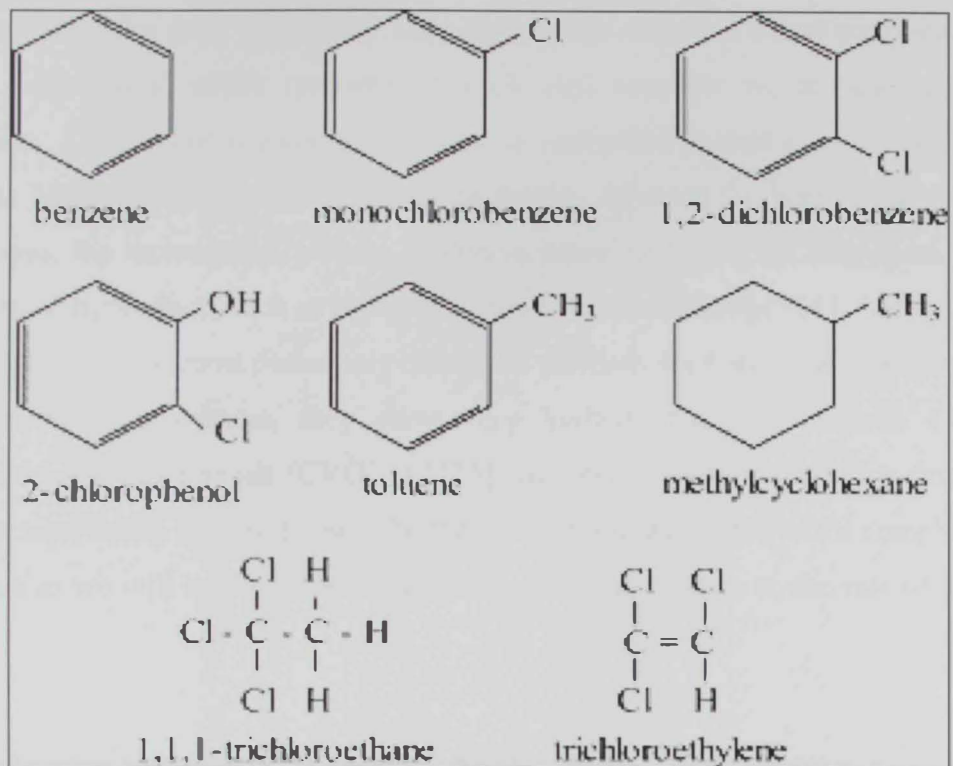


Figure 58. Chemical structure for most common VOCs [122].

Many advanced methods for the quick and economical removal of VOCs from air have been investigated. One of these methods involves Photocatalytic Oxidation which commonly uses nanosemiconductor catalysts and ultraviolet (UV) light to convert organic compounds into benign and odorless constituents, water vapor and carbon dioxide. Most Photocatalytic Oxidation reactors use nano-titania (TiO_2) as the catalyst that is activated by UV light [123]. The most commonly used method for chemical waste treatment on large scale is incineration, which typically requires high temperatures to achieve complete combustion. Chlorinated organic compounds, in particular, require elevated temperatures, as high as 1000 °C, for complete thermal oxidation. Besides the high costs, due to high temperatures, the incineration process is always associated with the formation of a wide range of toxic byproducts such as NO_x , dioxins and dibenzofurans [124]. While scrubbing and adsorption are the most commonly employed methods for removing gaseous pollutants from industrial gas streams, they show very limited efficiency towards Chlorinated Volatile Organic Compounds (CVOCs) [125]. However, catalytic oxidation that operates at lower temperatures is considered to be the most efficient alternative for complete CVOC destruction as we will be discussed in the next section in relation to the role of alumina in catalysis.

3.1.5 γ -Alumina-Supported Transition Metal Oxide for Oxidation of Chlorinated VOCs

The most common catalysts are currently studied for degradation of CVOCs are composed of noble metal particles and metal oxide supported on a high surface area support such as γ -alumina. Generally, supported noble metal catalysts exhibit higher catalytic activities as compared with metal oxide catalysts. However, disadvantages of noble metals, compared with metal oxides, include: (a) their higher costs, (b) deactivation due to their sensitivity to poisons, especially in the presence of chlorine atoms and (c) sintering at higher temperatures [126]. On the other hand, metal oxide catalysts have several advantages including higher thermal stability, lower costs, and the possibility of fabrication in high surface area porous powders. Therefore, metal oxides have been studied extensively as appropriate catalysts for the total combustion of Chlorinated Organic Compounds (COCs) [119,125-131].

Alumina by itself showed good catalytic activity toward decomposition of VOCs. As an examples, sol-gel alumina showed a promising catalytic activity in the dechlorination of carbon tetrachloride at temperature $\leq 350^{\circ}\text{C}$ [29]. In addition, alumina showed high catalytic activity for oxidation of 1,2- Dichloroethane (1,2-DCE) and trichloroethylene (TCE) , and it was found that 1,2-DCE decomposed to vinyl chloride at temperature between $250\text{-}450^{\circ}\text{C}$ and complete conversion was achieved around 350°C [132]. In addition to intrinsic catalytic activity, alumina is extensively used as catalytic supports for other catalytic materials such as noble metals and metal oxides due to its favorable textural properties and intrinsic acid-base characteristics. In particular, γ -alumina support which usually possesses high surface area, high pore volume, narrow pore size distribution and significant surface Lewis acidity can enhance the catalytic activity [132].

γ -Alumina supported Manganese oxide (MnO_3) and Chromium Oxides (Cr_2O_3) catalysts are known to have high catalytic activity for combustion of non-chlorinated and chlorinated organic compounds. Ting ke Tseng and others [133] performed catalytic destruction of 1,2-DCE over MnO_3 supported on γ -alumina ($\text{MnO}_3/\text{Al}_2\text{O}_3$), and found that 1,2-DCE decomposition started from 15% at 450 K, and rises to 100 % at temperature in the range of 700-800 K . Mc Alvares [134] performed catalytic oxidation of VOCs (Formaldehyde) over $\text{Mn}/\text{Al}_2\text{O}_3$ and found that total oxidation was achieved at 220°C over 18.2% $\text{Mn}/\text{Al}_2\text{O}_3$. Moreover, Meng Wu [135] prepared $\text{Mn}_x\text{Ce}_y/\text{Al}_2\text{O}_3$ mixed oxide catalysts with different compositions and they tested them for catalytic combustion of chlorobenzen (CB). It was found that $\text{MnCe}/\text{Al}_2\text{O}_3$ catalysts possess high catalytic activity. The literature is rich of many other examples where γ -alumina played a key role as a support for VOC degradation catalysts [118,132,136,137].

3.1.6 γ -Alumina-Based Mixed Metal Oxides and Doped Alumina

Compared with supported systems, there are few reports on γ -alumina dopes with transition metal ions and aluminum based mixed oxides. A range of transition metals such as Zn, Fe, Cr...etc are considered as catalytic promoters . As an example, Carlos J lucio and others [19] synthesized Fe-doped γ -alumina using sol-gel technique to evaluate its effect in catalytic combustion of TCE. They concluded that alumina catalyst doped with Fe was a good catalyst for abatement of VOCs. In another study, Loretta Storaro [52] found that Cr-doped alumina demonstrated high catalytic activity at low temperatures in the oxidation of chlorinated hydrocarbons.

3.1.7 Catalytic Oxidation of 1,2-Dichloroethane Over γ -Alumina

In most of the reported studies, it was found that 1,2 dichloroethane DCE, first decomposed to vinyl chloride, C_2H_3Cl , and HCl followed by direct oxidation to CO and CO_2 . However, deep oxidation took place at relatively high temperatures, around 400 °C, and, besides CO_2 , CO was a major product. In previous studies, it was found that nanostructured γ -alumina exhibited promising catalytic activity towards the adsorption and oxidation of some COCs [79,138]. It was also found that catalysts based on bulk mixed oxides can exhibit significantly enhanced catalytic activity in these reactions compared with their corresponding single metal oxides as well as their supported counterparts [119]. In the present paper work we studied the activity of several transition-metal-doped γ -alumina in the deep oxidation of DCE. Promising catalytic activities and interesting dependence on the nature of the dopant and its concentration were observed. FTIR spectroscopy was used for qualitative as well as quantitative probing of the catalytic reactions.

3.2 Objectives

In this chapter we will discuss the results of our investigation on evaluating and comparing the catalytic activity of some prepared catalysts described in chapter 2. Selected composites were studied as catalysts for the catalytic combustion of DCE. The catalytic activity and the nature of the products were evaluated and compared with those from reactions over pure γ -alumina in the same reaction.

3.3 Experimental Procedure

3.3.1 Materials and Catalysts Preparation

Materials and Catalysts preparation is described in Chapter 2. DCE (99.5% pure) was obtained from Aldrich and was used as received.

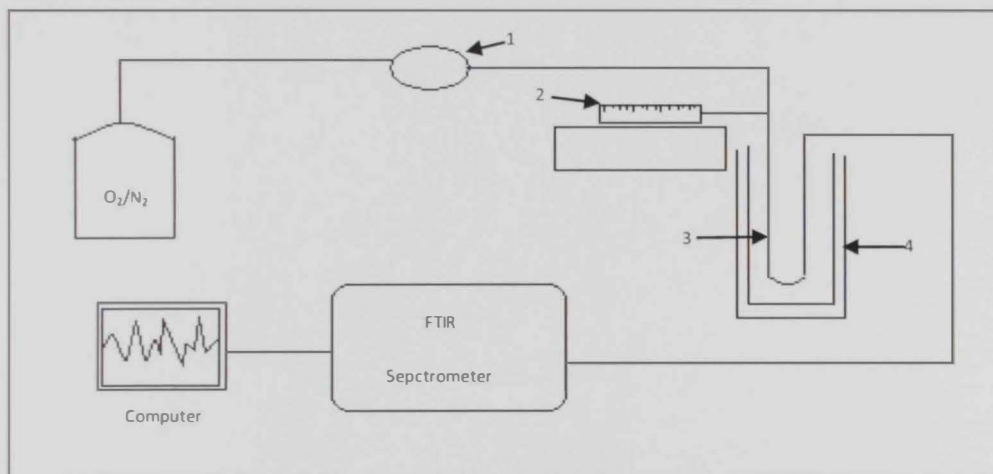
3.3.2 Catalytic Activity Study

The catalytic activity of the prepared catalysts in the oxidation of DCE vapor was investigated using fixed-bed flow reactor under atmospheric pressure (Figure 59). The reactor was coupled in-line with a continuous flow FTIR gas cell, from Pikes Technology, for continuous monitoring of the reaction products. The reactor was made of U-shape

stainless steel tube which was heated using a tube furnace equipped with a temperature controller and a K-type thermocouple. The reaction feed, monitored by mass flow controllers, was composed of O₂/N₂ mixture (20% O₂) at a flow rate of 20 ml/min and DCE vapor introduced to the feed by a syringe pump at a rate of 2.5 μl/min. The feed was preheated before entering the reactor. The catalyst (0.125 g, 180-355 mesh) was packed in the reactor between a stainless steel frit and a glass wool plug. Before each reaction, the catalyst was pretreated at 400 °C for 1 h under O₂/N₂ flow. After maintaining the desired reaction temperature (300°C) for the reactor, DCE was introduced. The eluting products were allowed to flow continuously through the heated gas cell housed in the FTIR spectrometer chamber. The transfer line and the IR cell were heated at 150 °C to prevent any condensation. FTIR spectra of the products were recorded continuously every five min during the first 30 minutes and then every 1 h for the rest of the reaction period, a total of 5 h or 36 h in selected experiments. 10 spectra were recorded continuously each time within a period of 2.5 minutes. The spectrum of the cell, with O₂/N₂ flow, was recorded before starting the reaction and was subtracted as a background from each spectrum of the products.



(a)



(b)

Figure 59a) A photograph of the Experiment setup b) Schematic diagram of Experiment setup.

- Mass flow controller (1)
- Syringe pump (2)
- Stainless Steel Tube Reactor (3)
- Furnace (4)

3.4 Results and discussion

Several studies reported that the oxidation of DCE on the surface of solid acids, including alumina and zeolites, starts at temperatures $> 200\text{ }^{\circ}\text{C}$, and in the temperature range of $200\text{-}400\text{ }^{\circ}\text{C}$ the main products were vinyl chloride ($\text{C}_2\text{H}_3\text{Cl}$) and HCl . The selectivity to the deep oxidation product, CO_2 , has been found to be relatively low [139-141]. The doped γ -alumina catalysts in the present study showed interesting results where a promising catalytic activity in the complete oxidation reaction of DCE was exhibited by certain catalysts. The employed FTIR method allowed for real-time monitoring of the reaction products and allowed for qualitative as well as quantitative comparison between the different catalysts in study.

3.4.1 Qualitative Evaluation of the Catalytic Activity

Reactions over selected prepared catalyst were conducted at 300°C . The products included mainly vinyl chloride (VC), identified by its $\lambda_{\text{C}=\text{C}}$ IR absorption around 1610 cm^{-1} , CO_2 , and HCl . Figure 60 shows FTIR spectra of the products at different reaction times at $300\text{ }^{\circ}\text{C}$ for Al-Cr-3% as an example.

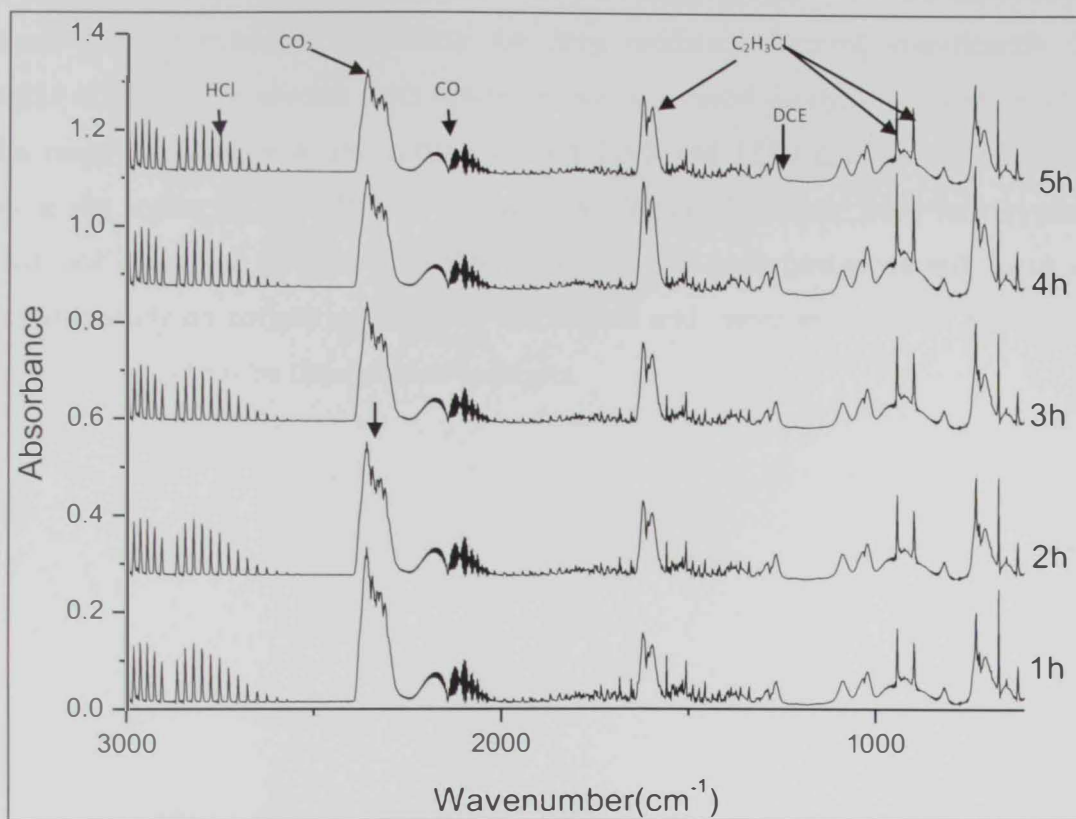


Figure 60. FTIR spectra of the products of DCE oxidation over Al-Cr-3% at 300°C at different reaction times.

Figure 61-65 present FTIR spectra recorded for reactions over Al-Cr-3, Al-V-3 , Al-Cu-3 and pure γ -alumina at 300 ° C at different reaction times for 5 hours. The % conversion as well as type of products was dependent on the type of dopant. It was found that the total conversion of DCE and the deep oxidation to CO₂ were significantly enhanced by the presence of certain dopant ions. While reactions over undoped γ -alumina produced only VC and HCl as well as very small amounts of CO₂, reactions over Cu- and Cr-doped catalysts showed enhanced capability for deep oxidation forming significantly larger amounts of CO₂. The spectra from reactions over Cu-based catalysts showed, in addition to the main products, new absorptions around 1100 and 1180 cm⁻¹ as well as multiple peaks in the region of 815-940 cm⁻¹ as shown in Figure 65. While these new byproducts are still not identified, and work for this purpose is still undergoing, we will focus in the rest of this study on comparing the total conversion and, more importantly, the ability for deep oxidation to CO₂ by the different catalysts.

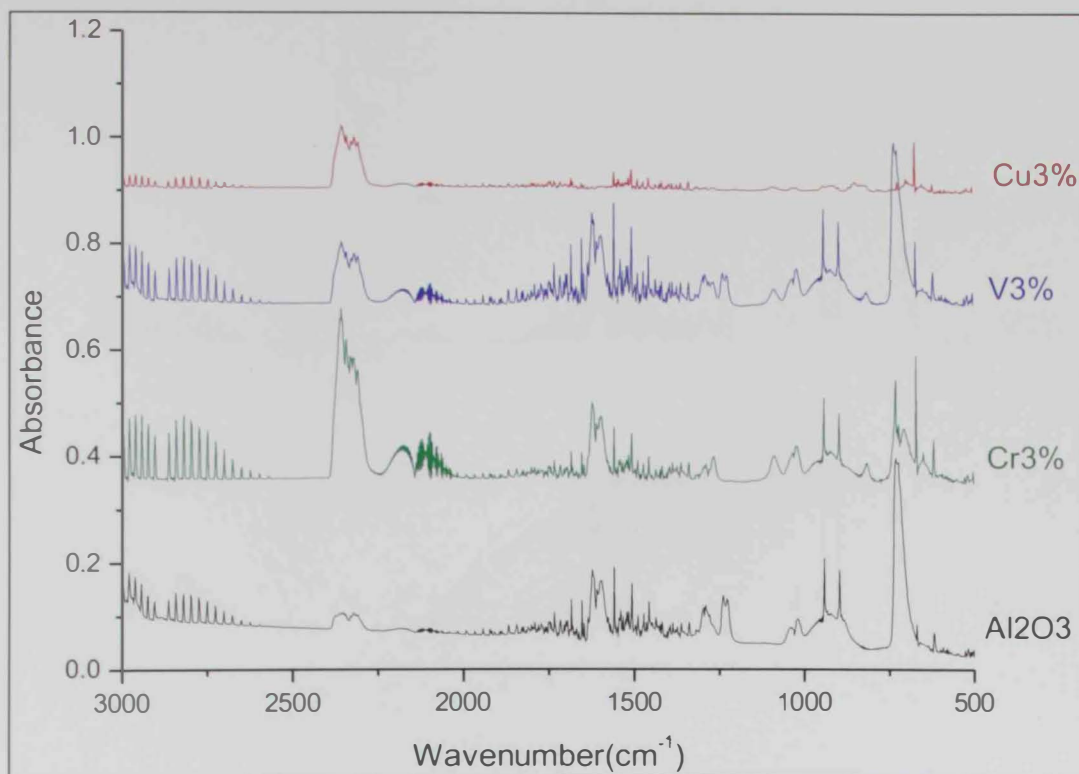


Figure 61. FTIR spectra of the products of DCE oxidation over Al-Cr-3, Al-V-3 and Al-Cu-3 at 300°C after 1hr of reaction.

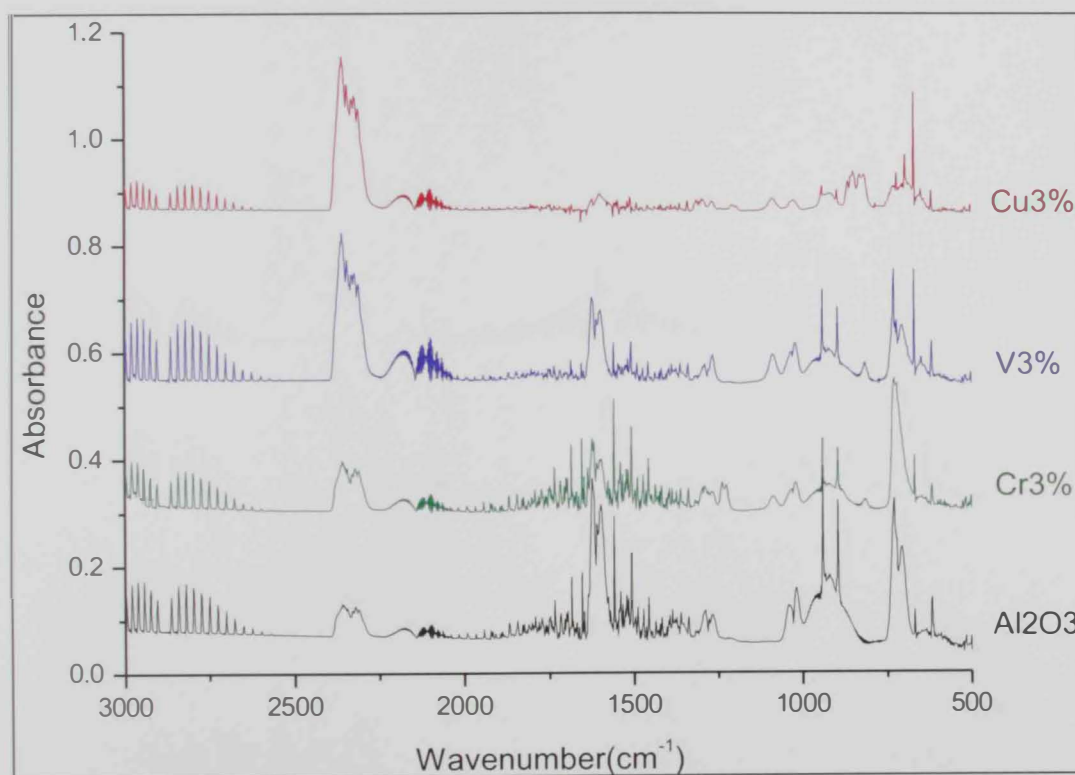


Figure 62. FTIR spectra of the products of DCE oxidation over Al-Cr-3, Al-V-3 and Al-Cu-3 at 300°C after 2hr of reaction.

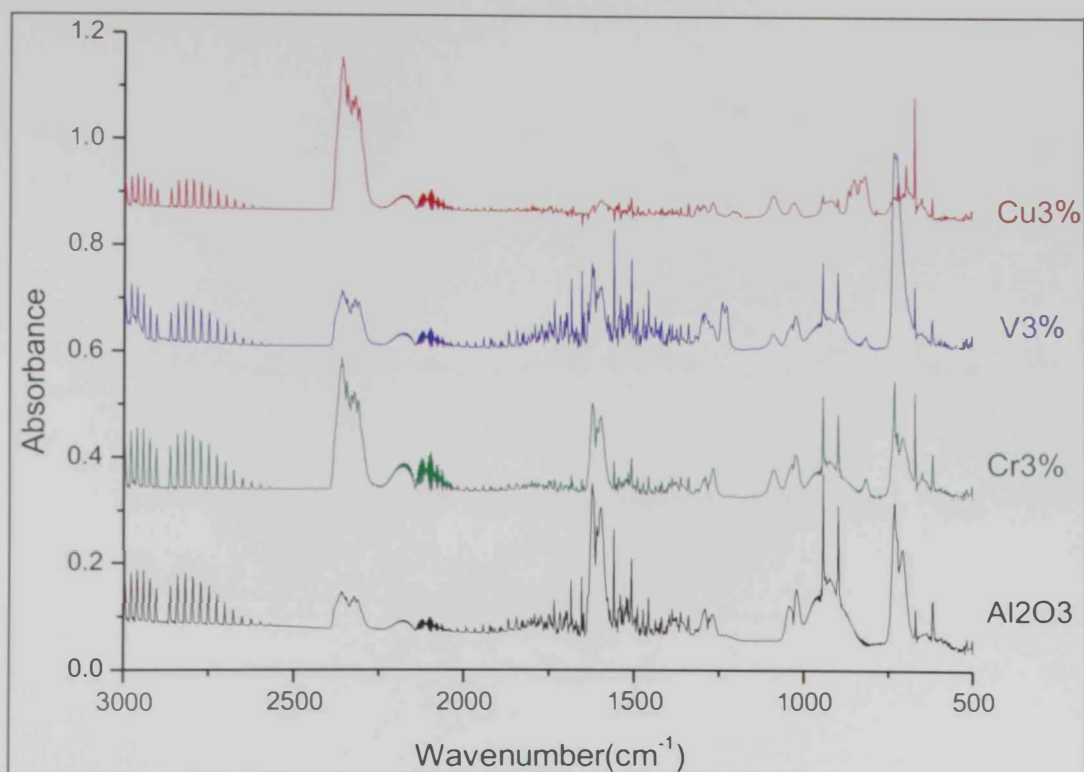


Figure 63. FTIR spectra of the products of DCE oxidation over Al-Cr-3, Al-V-3 and Al-Cu-3 at 300°C after 3hr of reaction.

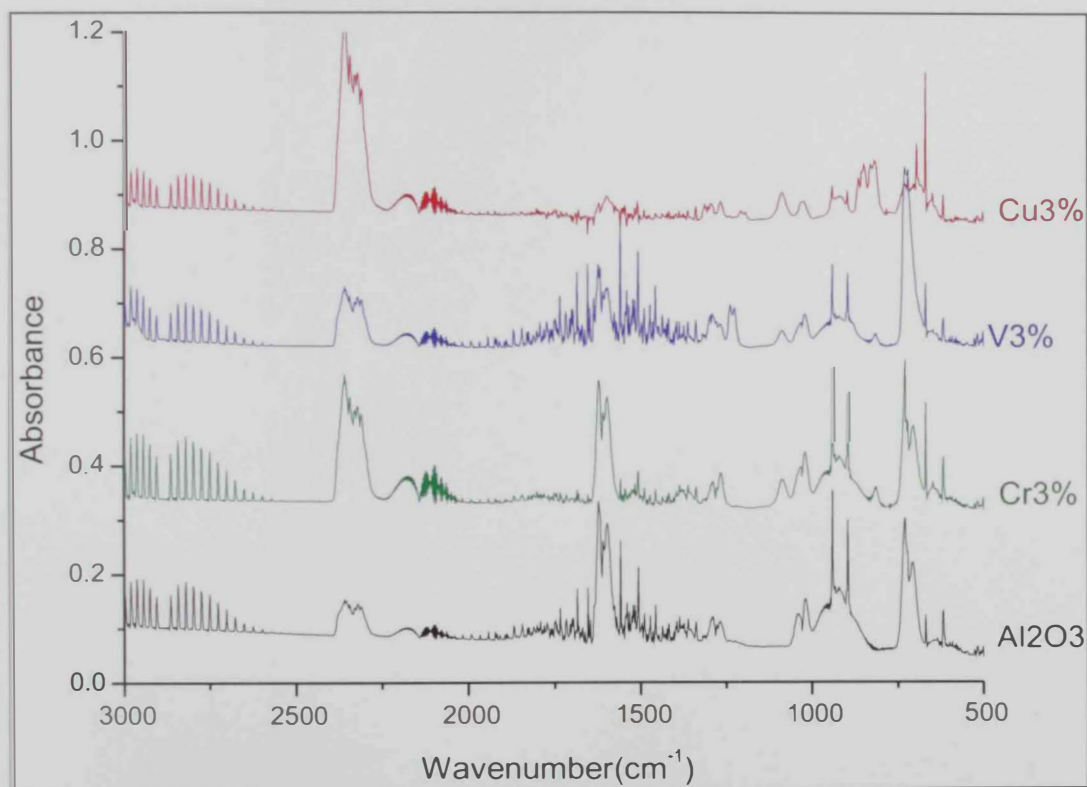


Figure 64. FTIR spectra of the products of DCE oxidation over Al-Cr-3, Al-V-3 and Al-Cu-3 at 300°C after 4hr of reaction.

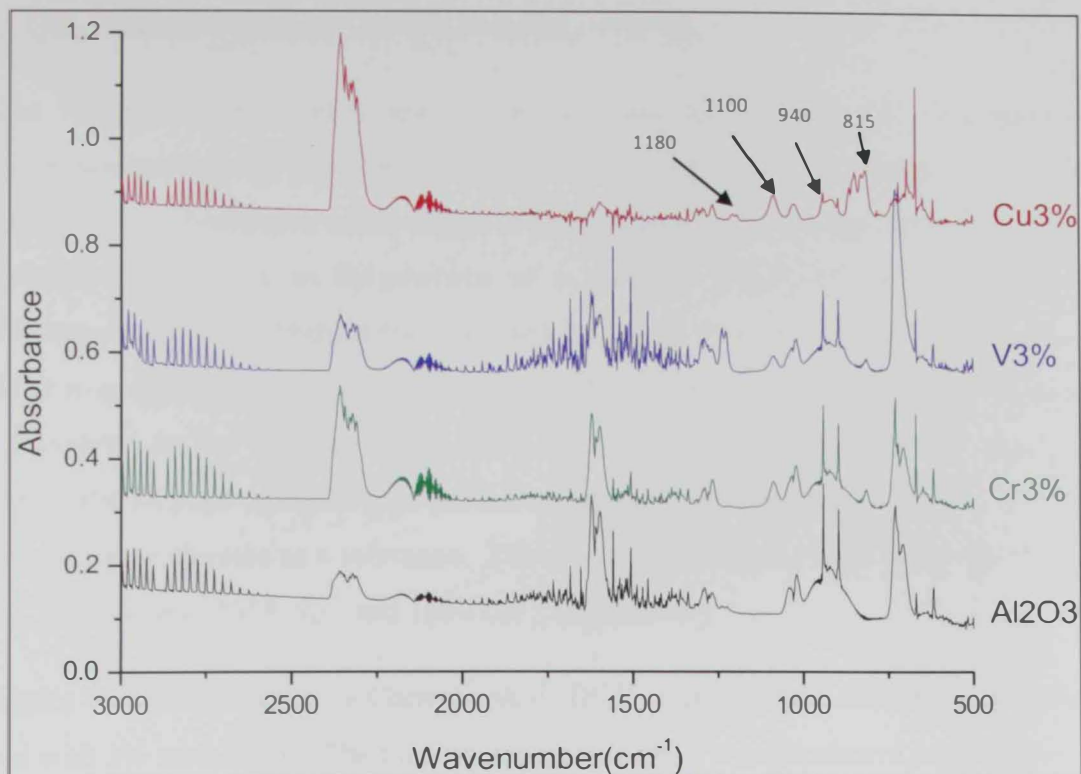


Figure 65. FTIR spectra of the products of DCE oxidation over Al-Cr-3, Al-V-3 and Al-Cu-3 at 300°C after 5hr of reaction.

3.4.2 Quantitative Evaluation of the Catalytic Activity

The % conversion of DCE was determined from the ratio of the integration of its characteristic peak at 1238 cm^{-1} to the integration of the same peak in spectra collected in a series of blank experiments where different DCE concentrations were used under the same experimental conditions in the absence of a catalyst. A calibration curve of a linear coefficient of 0.99 was obtained and was used to determine the % conversion. Since it was difficult to quantitate the different products and intermediates based on the IR study alone, the selectivity to the main products, CO_2 and $\text{C}_2\text{H}_3\text{Cl}$, was evaluated by scaling their characteristic IR peak intensities via peak integration using the same peaks in the spectra of reactions over γ -alumina as a reference. The characteristic peaks used to evaluate CO_2 and $\text{C}_2\text{H}_3\text{Cl}$ are those at 2358 cm^{-1} and 1610 cm^{-1} , respectively.

Figure 66 represents the % Conversion of DCE over undoped alumina and γ -alumina doped with 3% metal ions. The total conversion of DCE was dependent on the type of the dopant ion used. While the presence of Cr^{3+} and Cu^{2+} significantly enhanced the conversion, V^{3+} resulted in a noticeable decrease in the DCE conversion. Figure 67 represents the profile of CO_2 and VC produced from the reactions over pure alumina and 3% metal doped alumina. The VC was the major Cl-containing hydrocarbon product from reactions over Cr- and V-doped catalysts, similar to that on undoped γ -alumina, and zeolites as reported in the literature [139]. On the other hand, The Cu-doped catalyst resulted in the formation of a negligible amount of VC. More importantly, the deep oxidation to CO_2 was significantly enhanced by the Cu-doped catalyst, Figure 61-65 and Figure 67.

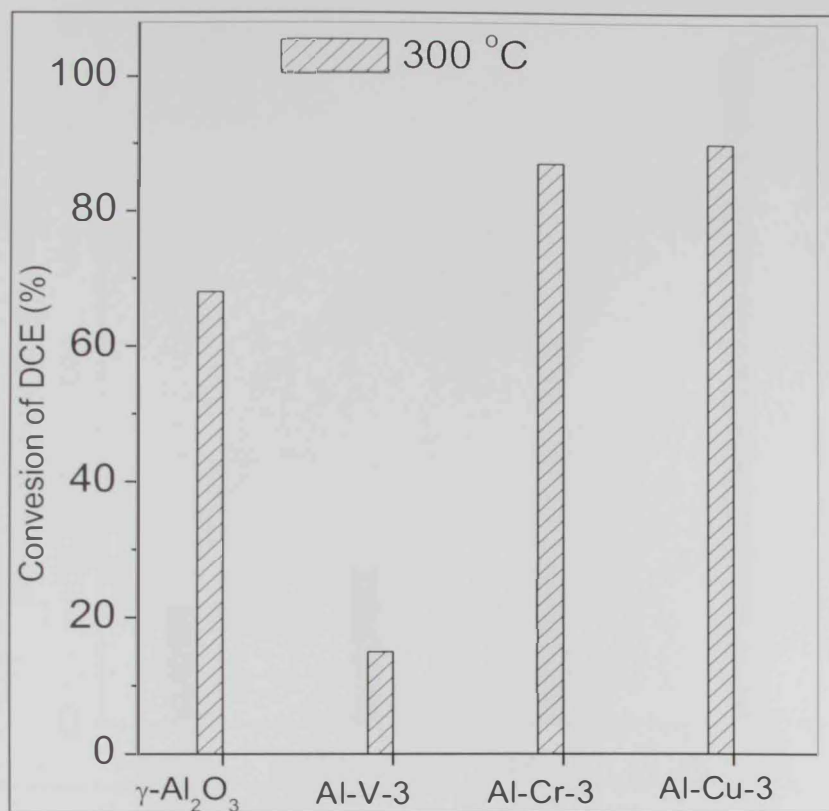


Figure 66. % Conversion of DCE over undoped and doped γ -alumina containing 3% dopants at 300°C .

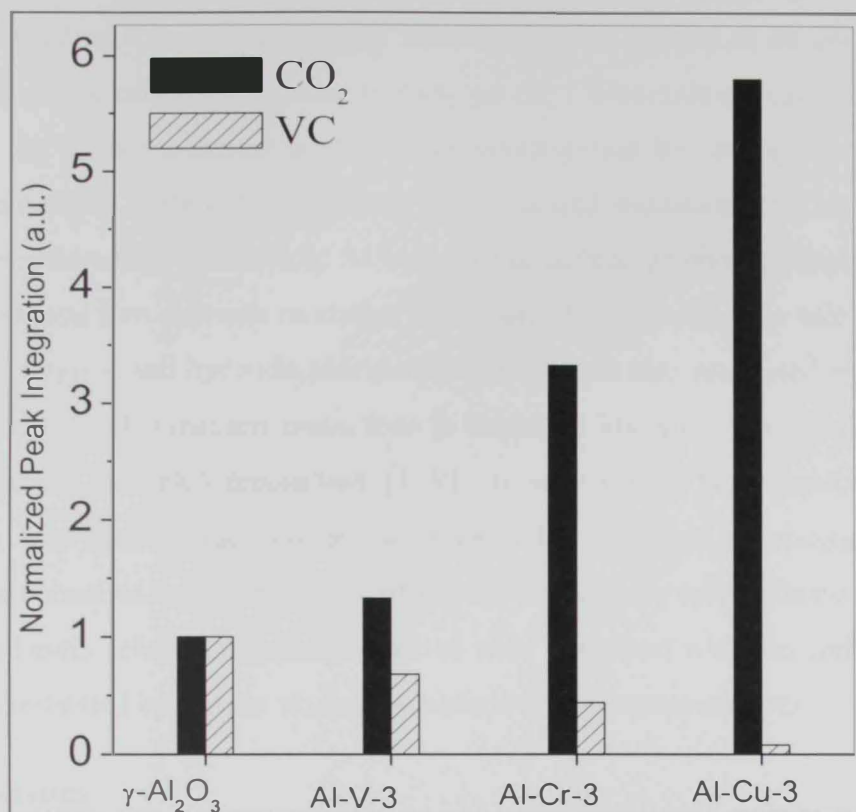


Figure 67. Carbon dioxide (CO₂) and Vinyl Chloride (VC) profiles after 5 h on stream at 300 °C over doped γ -alumina containing 3% dopants compared with undoped γ -alumina. The peak areas of both products were normalized using the area of the same peaks in the γ -alumina spectrum as a reference.

Although all metal ions enhanced the oxidation reaction compared to undoped γ -alumina, Cu^{2+} ions exhibited the highest oxidation activity resulting in significantly larger amounts of CO_2 on the account of VC. The fact that VC was the only Cl-containing hydrocarbon product over γ -alumina may indicate that VC formed as an intermediate that underwent further oxidation reactions to CO_2 on the Cu-containing catalyst. While the behavior of the different metals is still under investigation by testing a wider series of metal dopants under different conditions, the enhanced oxidation can be referred to a synergic interaction where the acidic Al ions on the surface promotes adsorption whereas the transition metal ions promote oxidation of the adsorbed species. The role of Lewis acid sites in the adsorption and hydrodechlorination of DCE was also suggested by others [142]. The suggested role of transition metal ions is based on known redox capability of these ions via Mars van Krevelen mechanism [119]. In addition, surface transition metal ions can undergo acid-base interactions besides their redox reactions enhancing the catalytic activity. The enhanced catalytic activity of the doped catalysts may indicate an increase in their surface Lewis acidity and catalytic active sites compared with the undoped catalyst. This can be confirmed by further studies on surface acidity measurements

3.5 Conclusions

Catalytic oxidation of DCE was performed over Al-Cr-3, Al-V-3 and Al-Cu-3 composites as well as on pure γ -alumina prepared by sol-gel method at 300°C . Products included $\text{C}_2\text{H}_3\text{Cl}$, CO, CO_2 and HCl. The doped catalysts showed higher % conversion and promising activity in the deep oxidation of 1,2-dichloroethane to CO_2 at relatively low temperatures compared with pure γ -alumina. The nature of the products was strongly dependent on the presence of dopant ions and on the type of dopant. Interestingly, Cu- and Cr-doped catalysts showed significantly stronger capability for deep oxidation of DCE to CO_2 . Thus they can be used to develop promising and efficient catalysts for the oxidative decomposition of chlorinated organic compounds.

X. References

1. L.D Hart. Alumina science and technology handbook chemicals, 1st ed., Westerville, Ohio: the American Ceramic Society, Inc; 1990, pg 3-5,257.
2. Barbara Kasprzyk-Hordern, Chemistry of alumina, reactions in aqueous solution and its application in water treatment, Advances in colloid and interface science: 110 (2004) 19-48.
3. H. Knozinger and P. Ratnasamy, Catalytic Aluminas: Surface Models and Characterization of Surface Site, Catal. Rev. Sci. Eng: 17(1978) 31-70.
4. Standard Transition Aluminas. Electron Microscopy Studies P. Souza Santos, H. Souza Santos, S.P. Toledo Mat. Res. vol.3 no.4 São Carlos Oct. 2000 Materials Research, Vol. 3, No. 4, 104-114, 2000.
5. Lee SK, Lee SB, Park S-Y, Yi YS, Ahn CW, Structure of amorphous aluminum oxide. Phys Rev Lett : 103(9):095501. 2009
6. M. Akia, S. Alvi, M. Rezaei, Z.F. Yan, Optimizing the sol-gel parameters on the synthesis of mesostructure nanocrystalline γ -Al₂O₃ , Micropr. Mesopor. Mater. 122 (2009) 72-78.
7. J.C. Ray, K.-S. You, J.W. Ahn, W.S. Ahn, Mesoporous alumina (I): Comparison of synthesis schemes using anionic, cationic, and non-ionic surfactants, Micropor. Mesopor. Mater. 100 (2007) 183-190.
8. Y. Tokudome, K. Nakanishi, K. Kanamori, K. Fujita, H. Akamatsu, T. Hanada, J., Structural characterization of hierarchically porous alumina aerogel and xerogel monoliths ,Colloids Interface Sci. 338 (2009) 506-513.
9. A.A. Khaleel, K.J. Klabunde, "Characterization of aerogel prepared high-surface-area alumina: In situ FTIR study of dehydroxylation and pyridine adsorption", Chemistry, vol. 8: pp. 3991-8, 2002.
10. K.M. Parida, A.C. Pradhan, J. Das, N. Sahu, Synthesis and characterization of nano-sized porous gamma-alumina by control precipitation method, Mater. Chem. Phys. 113 (2009) 244-248.
11. S.A. Hassanzadeh-Tabrizi, E. Taheri-Nassaj, Economical synthesis of Al₂O₃ nanopowder using a precipitation method , Mater. Letters 63 (2009) 2274-2276.
12. M.Riad, Influence of magnesium and chromium oxides on the physicochemical properties of γ -alumina,Applied Catalysis A:General 327(2007)13-21

13. J. Sanchez Valente, X.Boxhimi, J.A. Toledo, Synthesis and catalytic properties of nanostructured aluminas obtained by sol-gel method. *Applied Catalysis A: General* 264(2004)175-181
14. J. B. Peri , Infrared Study of the Reaction of Hydrogen Chloride with the Surface of γ -Alumina and Its Effect on Surface "Acid" Sites, *J. Phys. Chem.*:70(1965) 1482–1491.
15. Alexey A. Tsyganenko and Peter P. Mardilovich, Structure of alumina surfaces *J. Chem. Soc., Faraday Trans.*: 92(23)(1996) 4843-4852.
16. Andrei Ionescu, Alain Allouche, Jean-Pierre Aycard, and Michel Rajzmann, Study of γ -Alumina Surface Reactivity: Adsorption of Water and Hydrogen Sulfide on Octahedral Aluminum Sites, *J. Phys. Chem. B* :106(2002) 9359-9366.
17. Xiaohong Wang, Yun Guo, Guanzhong Lu, Yu Hu, Liangzhu Jiang, Yanglong Guo, Zhigang Zhang, An excellent support of Pd catalyst for methane combustion: Thermal-stable Si-doped alumina, *Catalysis Today*: 126(2007)369-374.
18. J. A. Wang, X. Bokhimi, A. Morales, and O. Novaro ,T. López and R. Gómez, Aluminum Local Enviroment and Defects in the Crystalline Structure of Sol-Gel Alumina Catalyst, *J. Phys. Chem. B*: 103 (2)(1999) 299–303.
19. Carlos J. Lucio-Ortiz ,Javier Rivera De la Rosa ,Aracely Hernandez Ramirez,Jose A. De los Reyes Heredia , Paz del Angel ,Severino Mun˜oz-Aguirre ,Lina M. De Leo'n-Covia'n, Synthesis and characterization of Fe doped mesoporous Al₂O₃ by sol-gel method and its use in trichloroethylene combustion, *J Sol-Gel Sci Technol* :58(2011) 374–384.
20. B. Xu, J. Long, H. Tian, Y. Zhu, X. Sun, Synthesis and characterization of mesoporous γ -alumina templated by saccharide molecules, *Catal. Today* 147 (2009) S46-S50.
21. Yu-Liang Zhang, Hui-Ling Li, Yu Yu, Yan-Lin Song, Wei-Guo Song, γ -Alumina with hierarchically ordered mesopore/macropore from dual templates, *Micropor. Mesopor. Mater.* 131 (2010) 289-293.
22. A. Khaleel, S. Al-Mansouri, Meso-macroporous γ -alumina by template-free sol-gel synthesis: The effect of the solvent and acid catalyst on the microstructure and

- textural properties, *Colloids and Surfaces A: Physicochemical and Engineering Aspects* 369 (2010) 272-280.
23. Synthesis and Characterization of alumina Nano-Powder obtained by sol-gel method. Rodica Rogojan, Ecaterina Andronescu, Cristina Ghitulica, Bogdan Ștefan Vasile, *U.P.B. Sci. Bull., Series B*, Vol. 73, Iss. 2, 2011
 24. Larry L. Hench and Jonn K. West, *The Sol-Gel Process*, *Chem. Rev.*:90 (1990) 33-72.
 25. Phaik Yee Looi, Ching Thian Tye, Abdul Rahman Mohamed and Subhash Bhatia, *Synthesis of Mesoporous Alumina: Effect of Preparation Variables on the Textural Properties*, *Recent Patents on Corrosion Science* 2011, 1, 156-172
 26. Rajan Bosco, B.V. Kamath, K.V. Rao, G.S. Rao, K.R. Krishnamurthy, *Alumina through sol-gel route: Influence of preparation parameters*, *Studies in surface analysis and catalysis*:113(1998) 591–598.
 27. Alain C. Pierre and Gerard M. Pajonk , *Chemistry of Aerogels and Their Applications*,*Chem.Rev.*:102(2002)4243-4265.
 28. G. Poelz and R. Riethmuller, *Preparation of silica aerogel for Cherenkov counters*, *Nucl. Instr. and Meth.*,195 (1982) 491.
 29. D.L. Trimm and A. Stanislaus, *The control of Pore size in alumina catalyst supports: A review*, *Applied Catalysis*: 21 (1986) 215-238.
 30. H.H. Kung, E.I. Ko, *Preparation of oxide catalysts and catalyst supports — a review of recent advances*, *The Chem. Eng. J.* 64 (1996) 203-214.
 31. J.A. Schwarz, C. Contescu, A. Contescu, *Methods for Preparation of Catalytic Materials*, *Chem. Rev.* 95 (1995) 477-510.
 32. R.D. Gonzalez, T. Lopez, R. Gomez, *Sol—Gel preparation of supported metal catalysts*, *Catal. Today* 35 (1997) 293-317.
 33. M.V. Landau, *Sol-gel processing*, in: K.P de Jong, KP (Edr). *Synthesis of Solid Catalysts*, Wiley-VCH, Weinheim, 2009.
 34. Jagadish C. Ray, Kwang-Seok You, Ji-Whan Ahn, Wha-Seung Ahn, *Mesoporous alumina (I): Comparison of synthesis schemes using anionic, cationic and non-ionic surfactants*, *Microporous and Mesoporous Materials*: 100(2007)183-190.
 35. Qian liu, Ai qin Wang, Xuehai Wang, Peng Gao, Xiaodong Wang, Tao Zhang, *Synthesis, characterization and catalytic applications of mesoporous γ -alumina from boehmite sol*, *Microporous and Mesoporous Materials*: 111(2008)323-333.

36. F. Vaudry, S. Khodabandeh, M.E. Davis, "Synthesis of pure alumina mesoporous materials", *Chem Mater.*, vol. 8: pp. 1451-64, 1996
37. Y. Kim, B. Lee, J. Yi, "Synthesis of mesoporous γ -alumina through pre- and post-hydrolysis methods", *Kor. J. Chem. Eng.*, vol. 19: pp. 908-10, 2002.
38. J. Aguado, J.M. Escola, M.C. Castro, B. Paredes, "Sol-gel synthesis of mesostructured γ -alumina templated by cationic surfactants", *Microporous Mesoporous Mater.*, vol. 83: pp. 181-92, 2005.
39. Carlos Marquez-Alvarez, Nadezda Zilkova, Joaquin Perez-Pariente, Jiri Cejka, *ChemInform Abstract: Synthesis, Characterization and Catalytic Applications of Organized Mesoporous Aluminas*, *Catalysis Reviews*:50(2008)222–286.
40. S. Valange, J.L. Guth, F. Kolenda, S. Lacombe, Z. Gabelica, "Synthesis strategies leading to surfactant-assisted aluminas with controlled mesoporosity in aqueous media", *Microporous Mesoporous Mater.*, vol. 35-6: pp. 597-607, 2000.
41. H.C. Lee, H.J. Kim, C.H. Rhee, K.H. Lee, J.S. Lee, S.H. Chung, "Synthesis of nanostructured γ -alumina with a cationic surfactant and controlled amounts of water", *Microporous Mesoporous Mater.*, vol. 79: pp. 61-8, 2005
42. N. Suzuki, Y. Yamauchi, "One-step synthesis of hierarchical porous γ -alumina with high surface area", *J. Sol-Gel Technol.*, vol.53: pp. 428-33, 2010.
43. Z.X. Sun, T.T. Zheng, Q.B. Bo, M. Du, W. Forsling, "Effects of calcination temperature on the pore size and wall crystalline structure of mesoporous alumina", *J. Colloid. Interface. Sci.*, vol. 319: pp. 247-51, 2008
44. F. Huang, Y. Zheng, G. Cai, Y. Zheng, Y. Xiao, K. Wei, "A new synthetic procedure for ordered mesoporous γ -alumina with a large surface area", *Scripta. Mater.*, vol. 63: pp. 339-42, 2010.
45. M. Akia, S.M. Alavi, M. Rezaei, Z.F. Yan, "Synthesis of high surface area γ -Al₂O₃ as an efficient catalyst support for dehydrogenation of n-dodecane", *J Porous Mater.*, vol. 17: pp. 85-90, 2010.
46. J. Aguado, J.M. Escola, M.C. Castro, "Influence of the thermal treatment upon the textural properties of sol-gel mesoporous γ -alumina synthesized with cationic surfactants", *Microporous Mesoporous Mater.*, vol. 128: pp. 48-55, 2010.
47. I. Levin, D. Brandon, "Metastable alumina polymorphs: Crystal structures and transition sequences", *J. Am. Ceram. Soc.*, vol. 81:pp. 1995-2012, 1998.

48. M. Ozawa, Y. Nishio, "Thermal stabilization of γ -alumina with modification of lanthanum through homogeneous precipitation", *J Alloys Compounds.*, vol. 374: pp. 397-400, 2004
49. Joseph J. Pesek, Maria T. Matyska, Modified aluminas as chromatographic supports for high-performance liquid chromatography, *Journal of Chromatography A*: 952(2002)1-11.
50. Aivaras Kareiva, C. Jeff Harlan, D. Brent Macqueen, Ronald L. Cook, and Andrew R. Barron, Carboxylate-Substituted Alumoxanes As Processable precursors to Transition Metal/Aluminum and Lanthanide/Aluminum Mixed-Metal Oxides: Atomic Scale Mixing Via A New Transmetalation Reaction, *Chem. of Mater.* 8 (1996) 2331-2340.
51. A. Vazquez, T. Lopez, R. Gomez, X. Bokhimi, J., Synthesis, characterization and catalytic properties of Pt/CeO₂-Al₂O₃ and Pt/La₂O₃-Al₂O₃ sol-gel derived catalysts, *Molec. Catal. A: Chemical* 167 (2001) 91-99.
52. L. Storaro, R. Ganzerla, M. Lenarda, R. Zanoni, A. Jimenez Lopez, P. Olivera-Pastra, E. Rodriguez Castellon, Catalytic behavior of Chromia and Chromkum-doped alumina pillared clay materials for the vapor phase deep oxidation of chlorinated hydrocarbons, *Journal of Molecular Catalysis A: Chemical* 115(1997)329-338.
53. A.P. Ferreira, D. Zanchet, R. Rinaldi, U. Schuchardt, S. Damyanova, J.M.C. Bueno, Effect Of the CeO₂ content on the surface and structural properties of CeO₂-Al₂O₃ mixed oxides prepared by sol-gel method, *Applied Catalysis A: General* 388 (2010)45-56.
54. M. Crisan, M. Railenu, S. Preda, A.M. Valen, E.J. Popvici, V.S. Teodorescu, V. Matejec, J. Mrazek, Manganese doped sol-gel materials with catalytic properties, *Journal of Optoelectronics and Advanced Materials*: 8(2)(2006) 815 – 819.
55. C. Pflitsch, R.A. Siddiqui, C. Eckert and B. Atakan, Sol-Gel Deposition of Chromium doped aluminium oxide films(ruby) for surface temperature sensor application, *Chem. Materials* : 20(2008)2773-2778.
56. Ilyes Khedher, Abdelhamid Ghorbel , Jose' Maria Fraile ,Jose' Antonio Mayoral , Physicochemical characterization of vanadium-doped alumina-pillared

- montmorillonite catalyst: Epoxidation of trans-2-hexen-1-ol, C. R. Chimie :12 (2009) 787-792.
57. J. Sanchez Valente, R. Quintana Solorzano, F. Hernandez, Role of Zinc on Zn/Alumina additives and their effects on Gazoline sulfur reduction in FCC Process.
58. H. Huang, N. Young, B. Peter Williams, Stuart H. Taylor and Craham Hutchings, COS Hydrolysis using zinc-promoted alumina catalysts, Catalysis letter: 104(2005)17-21.
59. Y. Torikai, H. Yahiro, N. Mizuno and M. Iwamoto, Enhancement of catalytic activity of alumina by copper addition for selective reduction of nitrogen monoxide by ethane in oxidizing atmosphere, Catalytic letters:9 (1991) 91-96.
60. X. Bokhimi, A. Morales and J. s. Valente, Sulfate ions and boehmite crystallization in a sol made with aluminum tri-sec-butoxide and 2-propanol, Journal of Physical chemistry: 111(2007)103-107.
61. M. Y. Samirnova, G. A. Urguntsev, A. B. Ayupov, A. A. Vedyagin, G.V. Echevsky, isobutene/butane alkylation on sulfated alumina:L influence of sulfation condition on textural , structural and catalytic properties, Applied Catalysis A: General 344 (2008) 107-113.
62. J. Xia, D. Mao, B. Zhang, Q. Chen, Y. Zhang, Y. Tang, Catalytic properties of fluorinated alumina for the production of dimethyl ether, Catalysis Communications : 7(2006)362-366.
63. J. Wang, Y. Wang, J. Wen, M. Shen, W. Wang, Effect of phosphorus introduction strategy on the surface texture and structure of modified alumina, Microporous and Mesoporous Materials: 121(2009)208-218.
64. W. Gu, M. Shen, X. Chang, Y. Wang, J. Wang, Gelification process to prepare phosphate modified alumina; study on structure and surface properties, Journal of Alloys and Compounds: 441(2007) 311-316.
65. G. Clet, J.M. Goupil, G. Szobo, D. Cornet, Chlorinated alumina as an alkylation catalyst: influence of superficial HCl, Journal of Molecular Catalysis A: Chemical 148(1999)253-264.
66. X. Chen. Y. Liu, G. Niu, Z. Yang, M. Bian, A. He, High temperature thermal stabilization of alumina modified by lanthanum species, Appl. Catal. A: General 205 (2001) 159-172.
67. M. Scheithauer, H. Knözinger, M.A. Vannice, Raman Spectra of La₂O₃ Dispersed on γ -Al₂O₃, J. Catal. 178 (1998) 701-705.

68. N. Al-Yassir, R. Le Van Mao, Thermal stability of alumina aerogel doped with yttrium oxide, used as a catalyst support for the thermocatalytic cracking (TCC) process: An investigation of its textural and structural properties, *Appl. Catal. A: general* 317 (2007) 275-283.
69. J.g. Seo, M.H. Youn, Y. Bang, I.K. Song, Hydrogen production by steam reforming of simulated liquefied natural gas (LNG) over mesoporous nickel–M–alumina (M = Ni, Ce, La, Y, Cs, Fe, Co, and Mg) aerogel catalysts, *Intern. J. of Hydrogen Energy* 36 (2011) 3505-3514.
70. M.T. Hernandez, M. Gonza´lez, A. De Pablos, C-diffusion during hot press in the $\text{Al}_2\text{O}_3\text{-Cr}_2\text{O}_3$ system, *Acta Materialia* 51 (2003) 217-228.
71. Q. Tang, X. Huang, C. Wu, P. Zhao, Y. Chen, Y. Yang, structure and catalytic properties of K-doped mangangese oxide supported on alumina, *Journal of Molecular Catalysis A: Chemical* 306(2009)48-53.
72. Sylvie Rossignol, Charles Kappenstein, Effect of doping elements on the thermal stability of transition alumina, *International Journal of Inorganic Materials* : 3(2001)51-58.
73. T. Montanari, L. Castoldi, L. Lietti, G. Busca, Basic catalysis and catalysis assisted by basicity: FTIR and TPD characterization of potassium-doped alumina, *Applied Catalysis A: General* 400 (2011) 61-69.
74. S. Srinivasan, C. R. Narayanan, A. Biaglow, R. Gorte, A.K.Datye, The role of sodium and structure and structure on the catalytic behavior of alumina: 1-Isopropanol dehydration activity, *Applied Catalysis A: General* 132(1995)271-287
75. W. Cai, J. Yu, C. Anand, A. Vinu, M. Jaroniec, Facile Synthesis of Ordered Mesoporous Alumina and Alumina-Supported Metal Oxides with Tailored Adsorption and Framework Properties, *Chem. Mater.* 23 (2011) 1147-1157.
76. J. Cejka, Organized mesoporous alumina: synthesis, structure and potential in catalysis, *Appl. Catal. A: General* 254 (2003) 327-338.
77. F. Raouf, M. Taghizadeh, A. Eliassi, F. Yaripour, Effects of temperature and feed composition on catalytic dehydration of methanol to dimethyl ether over γ -alumina, *Fuel* 87 (2008) 2967-2971.
78. S.-M Kim, Y. Lee, J.W. Bae, H.S. Potdar, K.-W Jun, Synthesis and characterization of a highly active alumina catalyst for methanol dehydration to dimethyl ether, *Appl. Catal. A: General* 348 (2008) 113-120.

79. Abbas Khaleel, Catalytic activity of mesoporous alumina for the hydrolysis and dechlorination of carbon tetrachloride, *Microporous and Mesoporous Materials*: 91 (2006) 53–58.
80. M. Akia, S. Alvi, M. Rezaei, Z.F. Yan, Optimizing the sol–gel parameters on the synthesis of mesostructure nanocrystalline γ - Al_2O_3 , *Micropr. Mesopor. Mater.* 122 (2009) 72-78..
81. K.M. Parida, A.C. Pradhan, J. Das, N. Sahu, Synthesis and characterization of nano-sized porous gamma-alumina by control precipitation method, *Mater. Chem. Phys.* 113 (2009) 244-248.
82. S.A.Hassanzadeh-Tabrizi, E. Taheri-Nassaj, Economical synthesis of Al_2O_3 nanopowder using a precipitation method, *Mater. Letters* 63 (2009) 2274-2276.
83. H.S. Potdar, K.-W. Jun, J.W. Bae, S.-M. Kim, Y.-J. Lee, Synthesis of nano-sized porous γ -alumina powder via a precipitation/digestion route, *Appl. Catal. A: General* 321 (2007) 109-116.
84. Y. Tokudome, K. Nakanishi, K. Kanamori, K. Fujita, H. Akamatsu, T. Hanada, Structural characterization of hierarchically porous alumina aerogel and xerogel monoliths, *J. Colloids Interface Sci.* 338 (2009) 506-513.
85. H.H. Kung, E.I. Ko, Preparation of oxide catalysts and catalyst supports - A review of recent advances, *The Chem. Eng. J.* 64 (1996) 203-214.
86. J.A. Schwarz, C. Contescu, A. Contescu, Methods for preparation of catalytic materials, *Chem. Rev.* 95 (1995) 477-510.
87. R.D. Gonzalez, T. Lopez, R. Gomez, Sol—Gel preparation of supported metal catalysts, *Catal. Today* 35 (1997) 293-317.
88. M.V. Landau, Sol-gel processing, in: K.P de Jong, KP (Edr). *Synthesis of Solid Catalysts*, Wiley-VCH, Weinheim, 2009.
89. Z. Shan. J.C. Jansen, W. Zhou, Th. Maschmeyer, Al-TUD-1, stable mesoporous aluminas with high surface areas, *Appl. Catal. A: General* 254 (2003) 339-343.
90. B. Xu, J. Long, H. Tian, Y. Zhu, X. Sun, Synthesis and characterization of mesoporous γ -alumina templated by saccharide molecules, *Catal. Today* 147S (2009) S46-S50.
91. S.-W. Bian, Y.-L. Zhang, H.-L. Li, Y. Yu, Y.-L. Song, W.-G. Song, γ -Alumina with hierarchically ordered mesopore/macropore from dual templates, *Micropor. Mesopor. Mater.* 131 (2010) 289-293.

92. A. Kareiva, C. J. Harlan, D. B. MacQueen, R. Cook and A. R. Barron, Carboxylate substituted alumoxanes as processable precursors to transition metal-aluminum and lanthanide-aluminum mixed metal oxides: atomic scale mixing via a new transmetalation reaction, *Chem. Mater.* 8 (1996) 2331-2340.
93. Bernard Beguin et al, Stabilization of alumina by addition of lanthanum, *Applied Catalysis A: General* 138 (1996) 161-176
94. N. Al-Yassir, R. Le Van Mao, Thermal stability of alumina aerogel doped with yttrium oxide, used as a catalyst support for the thermocatalytic cracking (TCC) process: An investigation of its textural and structural properties, *Applied Catalysis A: General* 317(2007)275-283.
95. M.A. Vannice, M. Scheithauer, H. Knözinger, Raman Spectra of La_2O_3 Dispersed on $\gamma\text{-Al}_2\text{O}_3$, *Journal of catalyst* :10 (1998) 701-705
96. Jeong Gil Seo a, Min Hye Youn, Yongju Bang, In Kyu Song, Hydrogen production by steam reforming of simulated liquefied gas (LNG) over mesoporous nickel-M-alumina ($\text{M}=\text{Ni}, \text{Ce}, \text{La}, \text{Cs}, \text{Fe}, \text{Co}$ and Mg) aerogel catalysts, *International Journal of Hydrogen Energy* :36(2011)3505-3514.
97. Hernandez M.T.; Gonzalez M.; De Pablos A.C-diffusion during hot press in the $\text{Al}_2\text{O}_3\text{-Cr}_2\text{O}_3$ system, *Acta Materialia*:51(1) (2003) 217-228 (12)
98. J.D.S. Lisboa, D.C.R.M. Santos, F.B. Passos, F.B. Noronha, Influence of the addition of promoters to steam reforming catalysts, *Catal. Today* 101 (2005) 15-21.
99. S.P. Feofilov, A.A. Kaplyanskii, R.I. Zakharchenya, Optical generation of nonequilibrium terahertz resonant vibrational excitations in highly porous aluminium oxide, *J. Lumin.* (1996), 66-67, 349-357
100. A. Khaleel, Nanostructured Pure $\gamma\text{-Fe}_2\text{O}_3$ via Forced Precipitation in an Organic Solvent, *Chem. Eu. J.*, 10 (2004) 925-932.
101. Jun Wang, Andrew G. Haerle, Chemical mechanical planarization of copper using transition alumina nanoparticles, *Thin Solid Film*:516 (2008) 7648-7652.
102. Q. Yu, X. Wu, C. Tang, L. Qi, F. Gao, K. Sun, L. Dong, Y. Chen, Textural, structural, and morphological characterizations and catalytic activity of nanosized $\text{CeO}_2\text{-MO}_x$ ($\text{M} = \text{Mg}^{2+}, \text{Al}^{3+}, \text{Si}^{4+}$) mixed oxides for CO oxidation, *J. Colloid Interface Sci.* 354 (2011) 341-352.

103. N. Kaneko, T. Horie, S. Ueno, J. Yano, T. Katsuragi, K. Sato, Impurity effects on crystallization rates of n-hexadecane in oil-in-water emulsions, *J. Crystal Growth* 197 (1999) 263-270.
104. B. Pal and M. Sharon and G. Nogami, Preparation and characterisation of $\text{TiO}_2/\text{Fe}_2\text{O}_3$ binary mixed oxides and its photocatalytic properties, *Mater. Chem. and Phys.* 59(1999) 254-261.
105. A. Vazquez, T. Lopez, R. Gomez, X. Bokhimi, Synthesis, characterization and catalytic properties of $\text{Pt/CeO}_2\text{-Al}_2\text{O}_3$ and $\text{Pt/La}_2\text{O}_3\text{-Al}_2\text{O}_3$ sol-gel derived catalysts, *J. Molec. Catal. A: Chemical* 167 (2001) 91-99.
106. S. Rossignol, C. Kappenstein, Effect of doping elements on the thermal stability of transition alumina, *International J. Inorg. Mater.* 3 (2001) 51-58
107. Xiaoyin Chen, Yong Liu, Guoxing Niu, Zhuxian Yang, Maiying Bian, Adi He, High temperature thermal stabilization of alumina modified by lanthanum species, *Applied Catalysis A: General* 205 (2001) 159-172.
108. K. Balakrishnan, R.D. Gonzalez, Preparation of Pt/Alumina Catalysts by the Sol-Gel Method, *J. Catal.* 144 (1993) 395-413
109. Olivier Roulades, Marie-Eve Duclos, Dan Gutknecht, Lucien Frappart, Jerome Chevalier, Daniel J. Hartmann, In vitro and in vivo evaluation of alumina-zirconia composite for arthroplasty applications, *Biomaterials*: 31(2010)2043-2054
110. Jonathan Garino, Mohamed N. Rahaman and B. Sonny Bal, The Reliability of Modern Alumina Bearings in total Hip arthroplasty, *Seminars in Arthroplasty*: 17(2006)113-119.
111. Kapoor S, Hegde R, Bhattacharyya AJ, Influence of surface chemistry of mesoporous alumina with wide pore distribution on controlled drug release, *J Control Release*. 2009 Nov 16;140(1):34-9. Epub 2009 Aug 3.
112. Joseph J. Pesek, Maria T. Matyska, Modified aluminas as chromatographic supports for high-performance liquid chromatography, *Journal of Chromatography A*: 952(2002)1-11.
113. Maria Crisan, Maria Zahrescu, Valluri Durga Kumari, Machiraju Subrahmanyam, Dorel Crizan, Nicolae Dragan, Malina Raileanu, Mihaela Jitianu, Adriana Rusu, Gullapelli Sadanandam, Sol-gel based alumina powders with catalytic applications, *Applied Surface Science*: 258(2011)448-455

114. Mohamed E. Mahmoud, Maher M. Osman, Osama F. Hafez, Abdelrahman H. Hegazi, Essam Elmelegy, Removal and preconcentration of lead (II) and other heavy metals from water by alumina adsorbents developed by surface-adsorbed-dithione, *Desalination*:251 (2010) 123-130.
115. Cesar Lucio Lopes de Faria Jr, Tania Keli Resende De Oliveira, Vera Lucia dos Santos, Carlos Augusto Rosa, Jose Domingos Ardisson, Waldemar Augusto de Almeida Macedo, Usage of the sol-gel process on the fabrication of macroporous adsorbent activated-gamma alumina spheres, *Microporous and Mesoporous Materials* :120(2009)228-238.
116. Eva Dias, Salvador Ordonez, Aurelio Vega, Jose Coca, Adsorption characterization of different volatile organic compounds over alumina, zeolites and activated carbon using inverse gas chromatography, *Journal of Chromatography A*:1049(2004)139-146
117. Yubing Sun , Shitong Yang , Guodong Sheng , Zhiqiang Guo , Xiaoli Tan , Jinzhang Xu , Xiangke Wang, Comparison of U(VI) removal from contaminated groundwater by nanoporous alumina and non-nanoporous alumina, *Separation and Purification Technology*: 83 (2011) 196–203
118. L.F. Liotta, Catalytic oxidation of volatile organic compounds on supported noble metals, *Applied Catalysis B: Environmental* 100 (2010) 403-412.
119. Abbas Khaleel , Aysha al- Nayli, Supported and mixed oxide catalysts based on iron and titanium for the oxidation decomposition of chlorobenzene, *Applied Catalysis B: Environmental* 80(2008)176-184.
120. Xingyi Wang , Qian Kang, Dao Li, Low-temperature catalytic combustion of chlorobenzene over MnO_x-CeO₂ mixed oxide catalysts. *Catalysis Communications*: 9(2008)2158-2162.
121. R.M. Lago, M.L.H. Green, S.C. Tsang, M. Odlyha. Catalytic decomposition of chlorinated organics in air by copper chloride based catalysts. *Applied Catalysis B: Environmental* 8(1996)107-124.
122. K. Everaert , J. Baeyens, Catalytic combustion of volatile organic compounds. *Journal of Hazardous Materials B*:109(2004)113-139.
123. Qiujian Xu a, Jennifer Joaquin Lamson a,b, Rongyi Zhao , a Photocatalytic purification of volatile organic compounds in indoor air: A literature review *Jinhan Moa*, Yinping Zhang a, , *Atmospheric Environment* 43 (2009) 2229–2246.

124. S.P. Decker, J.S. Klabunde, A. Khaleel, K.J. Klabunde, Catalyzed Destructive Adsorption of Environmental Toxins with Nanocrystalline Metal Oxides. Fluoro-, Chloro-, Bromocarbons, Sulfur, and Organophosphorus Compounds, *Environ. Sci. Technol.* 36, 4 (2002) 762-768.
125. E. Finocchio, G. Busca, M. Notaro, A review of catalytic processes for the destruction of PCDD and PCDF from waste gases, *Appl. Catal. B: Environ.* 62 (2006) 12-20
126. S. Scire, S. Minico, C. Crisafulli, Pt catalysts supported on H-type zeolites for the catalytic combustion of chlorobenzene, *Appl. Catal. B: Environ.* 45 (2003) 117-125.
127. D. Döbber, D. Kießling, W. Schmitz, G. Wendt, MnO_x/ZrO₂ catalysts for the total oxidation of methane and chloromethane, *Appl. Catal. B: Environ.* 52 (2004) 135-143.
128. J. Lichtenberger, M. D. Amiridis, Catalytic oxidation of chlorinated benzenes over V₂O₅/TiO₂ catalysts, *J. Catal.* 223 (2004) 296-308.
129. M.A. Larrubia, G. Busca, An FT-IR study of the conversion of 2-chloropropane, *o*-dichlorobenzene and dibenzofuran on V₂O₅-MoO₃-TiO₂ SCR-DeNO_x catalysts, *Appl. Catal. B: Environ.* 39 (2002) 343-352.
130. L. Forni, I. Rossetti, Catalytic combustion of hydrocarbons over perovskites, *Appl. Catal. B: Environ.* 38 (2002) 29-37.
131. S. Krishnamoorthy, J. A. Rivas, M. Amiridis, Catalytic Oxidation of 1,2-Dichlorobenzene over Supported Transition Metal Oxides, *J. Catal.* 193 (2000) 264-272.
132. Manon M.R. Feijen-Jeurissen, Jelle J. Jorna, Bernard E. Nieuwenhuys, Gills Siquin, Corinne Petit, Jean-Paul Hindermann, Mechanism of Catalytic destruction of 1,2-dichloroethane and trichloroethylene over γ -Al₂O₃ and γ -Al₂O₃ supported chromium and palladium catalysts. *Catalysis Today*: 54 (1999) 65-79.
133. T. Ke Tseng, L. Wang, C. The Ho, H. Chu, The destruction of dichloroethane over a γ -alumina supported manganese oxide catalyst, *Journal of Hazardous Materials* : 178(2010)1035-1040.
134. M.C. Alvarez-Galvan, V.A. de la Pena O'Shea, J.L.G. Fierro, P.L. Arias, Alumina-supported manganese and manganese-palladium oxide catalysts ofr VOCs combustion, *Catalysis Communications* : 4 (2003) 223-228.

135. M. Wu, X. Wang, Q. Dai, Y. Gu, D. Li, Low temperature catalytic combustion of chlorobenzene over Mn-Ce-O/ γ -Al₂O₃ mixed oxides catalyst, *Catalysis Today*: 158(2010)336-342.
136. Beatriz Miranda, Eva Diaz, Salvador Ordonez, Aurelio Vega, Fernando V. Diez. Oxidation of trichloroethene over metal oxide catalysts: Kinetic studies and correlation with adsorption properties. *Chemosphere* : 66 (2007) 1706-1715.
137. Sung Dae Yim, Dong Jun Koh, In-Sik Nam, Young Gul Kim. Effect of the catalyst supports on the removal of perchloroethylene (PCE) over chromium oxide catalysts. *Catalysis Letters*: 64 (2000) 201-207.
138. A. Khaleel, B. Dellinger, FTIR Investigation of Adsorption and Chemical Decomposition of CCl₄ by High Surface-Area Aluminum Oxide, *Environ. Sci. Technol.* 36 (2002) 1620-1624.
139. R. López-Fonseca, A. Aranzabal, P. Steltenpohl, J.I. Gutiérrez-Ortiz, J.R. González-Velasco, Performance of zeolites and product selectivity in the gas-phase oxidation of 1,2-dichloroethane *Catal. Today* 62 (2000) 367-377.
140. A. Aranzabal, J.A. González-Marcos, J.L. Ayastuy, J.R. González-Velasco, Kinetics of Pd/alumina catalysed 1,2-dichloroethane gas-phase oxidation, *Chem. Eng. Sci.* 61 (2006) 3564 – 3576.
141. Q. Huang, X. Xue, R. Zhou, Decomposition of 1,2-dichloroethane over CeO₂ modified USY zeolite catalysts: Effect of acidity and redox property on the catalytic behavior, *J. Hazard. Mater.* 183 (2010) 694-700.
142. B. de Rivas, R. López-Fonseca, J.R. González-Velasco, J.I. Gutiérrez-Ortiz, On the mechanism of the catalytic destruction of 1,2-dichloroethane over Ce/Zr mixed oxide catalysts, *J. Molec. Catal. A: Chem.* 278 (2007) 181-188

اهداء

الحمد لله الذي علم بالقلم، علم الأنسان ما لم يعلم، و الصلاة و السلام على من بعثه الله رحمة للبشرية و هاديا إلى الطريق السوية، و على آله و صحبه و من بعثه إلى يوم الدين. و بعد

فإن الانسان من خلال رحلة حياته يمر بمحطات ... منها ما يشكل علامات فارقة و منعطفات هامة يطبع آثارها البالغة على مسيرته... و تحقق له تميزا على مختلف الصعد لعل من اهمها الشعور بالرضا.

و هو بذلك يدين بأهل الفضل ممن أعانوه على بلوغ نتيجة و تحقيق غايه... و من ثم ملامسة النجاح...و في هذا فإن و دأبي يسير تجاه الإقرار بالفضل و تأكيد الشكر و التقدير إلى من كان لهم أياد بيضاء فيما تحقق لي من إنجاز لهذه الدراسة و التي تشرفت بآتمامها و هم أساتذتي الدكتور عباس خليل، المشرف على رسالتي، و مساعد المشرف الدكتور ياسر غريش...و الأستاذ بسام هنداوي و الدكتور نواز.

و على صعيد أشمل...لكل من اسهم في تقديم العون لي من أهلي ابتداء من والدي و زوجي و أطفالي.

و آخر دعوانا أن الحمد لله رب العالمين

الملخص باللغة العربية

لقد تم تحضير - الأيونات المعدنية - المعالجة بمركبات (γ -alumina) بمختلف تركيزات (Cr^{3+} , Fe^{3+} , Ce^{3+}) من خلال أسلوب ترسيب المحلول الكيميائي المباشر (sol-gel)، و تم تحليل المركبات المحضرة بالتقنيات التالية: (XRD, FTIR, SEM, NMR and N_2 -adsorption-desorption) إن وجود أيونات المعدنية المعالجة بوجه عام أدى إلى تعزيز تشكيل الجل (الهلام) وسلوكها يعتمد على طبيعة الأيون المعدني وتركيزه. إن بعض الأيونات، على وجه الخصوص (Fe^{3+}) أدت إلى تكوين سريع لجل شفاف عند التحلل المائي. هذا بالإضافة، أدى وجود أيونات (Acetylacetone) إلى تعزيز تفاعلات التكثيف في عملية ترسيب المحلول الكيميائي (sol-gel) مما نجم عنه في نهاية المطاف خصائص تكوينية فريدة من نوعها للمنتجات المكلسة بما في ذلك مساحات عالية السطح، وجزيئات صغيرة الحجم ومواد متجانسة محتوية على مسامات وتعزيز مقاومة التكتل خاصة عند التركيزات العالية المعالجة و درجات حرارة التكليل العالية.

يتم بلورة مساحيق (γ -alumina) المعالجة التي تم إعدادها تحت تركيزات أيون مادة معالجة منخفضة 3%، وأصبحت غير متبلورة تماماً عند تركيز 10%، ويعتمد تشكل الجزيئات أيضاً على تركيز المادة المعالجة. بينما أدى تركيز المادة المعالجة عند 2% إلى جزء من ألف مليون من الجزيئات مع كمية كبيرة فيما بين جزيئات المادة المحتوية على مسامات، وقد أدت نسبة 10% من تركيزات التجمع الكبير إلى جزيئات كبيرة. وقد أظهرت (γ -alumina) المعالجة التي تم إعدادها و (γ -alumina) غير المعالجة مساحات سطحية عالية (377 م²/جرام) وأحجام مسام (65 و 1 سم/جرام) والتي تعتمد إلى حد كبير على طبيعة أيونات المادة المعالجة وعلى تركيزاتها.

أظهرت المركبات ذات تركيز أيون (Cr^{3+}) المنخفض، 75 و 2% قدرة عكسية لتغير اللون نتيجة لتغير الحرارة حيث تغير لونها الأصفر المخضر إلى اللون الأحمر عند التكليل في درجات حرارة تتراوح ما بين 500 و 700 درجة مئوية، واستناداً على نتائج (NMR) يفضل شغل (احتلال) المواقع الرباعية السطوح بأيونات (Cr^{3+}) على المواقع الثمانية السطوح عند تركيزات (Cr^{3+}) المنخفضة. أظهرت المركبات خصائص تكوينية فريدة من نوعها مقارنة مع تلك (γ -alumina) العالية المساحة السطحية المسامية، خاصة عند تركيزات (Cr^{3+}) المنخفضة.

تم دراسة النشاط المحفز للمادة الحفازة المعالجة وكذلك تلك (γ -alumina) غير المعالجة من خلال (1,2-dichloroethane) (DCE) عند درجة حرارة 300 درجة مئوية باستخدام تحليل طيفي (FTIR) لرصد منتجات التفاعل. أظهر محفز (γ -alumina) المعالجة مع أيونات النحاس ((II)) والكروم ((III)) تحول عالي مقارنة مع (γ -alumina) غير المعالج. و طبيعة المنتجات تعتمد بشدة على وجود أيونات المادة المعالجة وعلى نوعية المادة المعالجة. بينما نجم عن (γ -alumina) النقية، بشكل رئيسي، تكوين ($\text{C}_2\text{H}_3\text{Cl}$)، وأظهرت محفزات النحاس والكروم المعالجة قدرة قوية بشكل ملحوظ على الأكسدة العميقة ل (DCE) إلى ثاني أكسيد الكربون (CO_2) على حساب ($\text{C}_2\text{H}_3\text{Cl}$).

تحضير، تحليل و دراسة مواد حفازة معدلة مبنية على أكسيد الألمنيوم

اعداد

سهام ناصر سالم ناصر الحضرمي

قسم هندسة و علوم المواد

كلية الهندسة

جامعة الإمارات العربية المتحدة

رسالة مقدمة لإستكمال متطلبات الحصول على درجة الماجستير في هندسة و علوم المواد

برنامج الماجستير في هندسة و علوم المواد

قسم هندسة و علوم المواد

كلية الهندسة

جامعة الإمارات العربية المتحدة

يناير ٢٠١٣